Impurity Effects In High Strength Steel Weld Deposits.

IMPURITY EFFECTS IN HIGH STRENGTH STEEL WELD DEPOSITS

By

Robert Quattrone

A DISSERTATION

PRESENTED TO THE GRADUATE COMMITTEE

OF LEHIGH UNIVERSITY

IN CANDIDACY FOR THE DEGREE OF

DOCTOR OF PHILOSOPHY

IN

METALLURGY AND MATERIAL SCIENCES

Lehigh University
1969

CERTIFICATE OF APPROVAL

Approved and recommended for acceptance as a dissertation in partial fulfillment of the requirements for the degree of Doctor of Philosophy.

8 September 1969
(date)

R S Stout
Professor in Charge

Accepted, 8 September 1969
(date)

Special committee directing the doctoral work of Mr. Robert Quattrone

Alan W. Reuse
Chairman

R S Stout

George Krauss

J. K. Grass

Dedication...

To my family with whom I now hope to

spend much more time.

ACKNOWLEDGEMENTS

Although only one person is acknowledged as the producer of a document such as this, in truth it is the result of the labors of many people. The author would like to take this opportunity to thank the following persons whose efforts made the completion of this dissertation possible:

Dr. R. D. Stout who served as thesis advisor and was responsible for originating and guiding the research.

Dr. A. W. Pense who served as Chairman of the special committee which also included Dr. G. Krauss and Dr. J. Gross.

The personnel of the United States Steel Corp. Applied Research Laboratory, especially Dr. L. Connor, for material and chemical analyses.

The personnel of the Naval Applied Science Laboratory especially Messrs. F. D'Oria, G. Di Giacomo, and M. Green and Mrs. J. Morton for their technical assistance, Messrs. J. Alfano and J. Menichino, machinists, "Sandy" Raichelle, photographer, and Mrs. C. Fernandez and Miss D. Andrzejewska, typists.

The support staff at Lehigh University especially Messrs. W. Mohylsky, machinist, and D. Busch, electrical technician.

Special thanks to Mrs. S. Montague who converted my

chicken scratching into legible type, and to Mrs. R. Super for her immeasurable aid and pleasant smile.

Most of all, to Anita, my wife, for her unwaivering faith and unbelievable tolerance of me during the period of our lives in which the completion of this dissertation ranked paramount in my mind.

TABLE OF CONTENTS

LIST OF FIGURES

LIST OF TABLES

ABSTRACT

The effect of additions of oxygen and hydrogen, alone or in combination, on the strength, toughness and crack susceptibility of weld metals made from 3% Ni and 5% Ni HY 130 type welding wires was studied. High purity vacuum induction heats of welding wire were used and controlled impurity additions were made through the weld shielding gas in an atmosphere chamber.

Oxygen effects on strength were complicated by the competitive processes of partial decarburization and dispersed phase strengthening. The loss in strength by decarburization appeared to be the more significant of the two effects.

When decarburization did not occur, a steady rise of approximately $3^{o}F$/ppm oxygen in the weld deposit was observed for the Charpy V-notch 50 ft-lb transition temperature. Severe reduction of shelf energy occurred above 60 ppm oxygen; above 200 ppm oxygen, 50 ft-lbs was not attained. This embrittlement was attributed to the formation of silicon dioxide particles.

Susceptibility to hydrogen induced cracking was evaluated using the Keyhole slotted plate restraint specimen. GTA welds were found to be more resistant to cracking than GMA

welds and 5% Ni welds more resistant than 3% Ni welds. Oxygen addition to the shielding gas of GTA welds further increased the hydrogen crack resistance, however, oxygen addition to the shielding gas of GMA welds made these welds more susceptible to hydrogen cracking. Possible mechanisms for the observed results are presented.

INTRODUCTION

1. Development of HY 130 (T) Steel

There exists a need for deep diving undersea vessels capable of exploring and/or protecting the greatest depths of the ocean. The severe limitation which exists in the depth capability of current undersea vessels was graphically shown by the difficulties attending the recovery of the lost hydrogen bomb off the coast of Spain and the inability of the Navy to rescue the crew of the submarine Thresher or even to locate the Scorpion. In addition, the discovery of natural gas fields on continental shelves and important underwater mineral deposits in various marine sites offer great promise for undersea exploitation.[1]*

It is generally agreed [1]-[4] that the crucial element in the design of a deep submersible is the capacity of the hull to resist failure at the high hydrostatic pressures associated with ocean depths. On the basis of strength/density ratio alone, is has been shown[2][4] that submersibles with hulls fabricated from materials such as aluminum, titanium and glass can achieve greater depths than steel hulled submersibles. However, Gross[2] and others[5][6] have stated that factors other than strength/density are important in hull design. When consideration is given to toughness,

---

*Numbers in parenthesis refer to references at the conclusion of this paper.

designability, fabricability, producibility and economy, steel is far superior to other materials for hull use. Therefore, to be useful for hulls in new deep diving vessels, steels must be developed with higher strengths than those currently in use without sacrificing toughness, corrosion resistance, fatigue strength, designability, fabricability, producibility and economy.[2]

In 1963, Naval Ship Systems Command contract NObs - 88540 was let to develop a new hull steel with a yield strength of 130 to 150 Ksi to replace the current HY 80 hull steel in future submersibles. The contract was unique in material development because in addition to requiring a new base metal with suitable strength, hardenability, toughness, fatigue life and corrosion resistance, it also required (a) satisfactory weldability of the base metal, (b) the development of compatible filler metals and joining techniques and (c) demonstration of the structural suitability of the weldment[7]. To meet these goals, the prime contractor (the United States Steel Corporation) was aided by various weld metal manufacturers (Linde Division, Union Carbide Corporation, Air Reduction Company, Arcos Corporation, McKay Company), universities (Lehigh University, University of Illinois), and government laboratories (NASL, NRL, NSRDC Anna.Div.)[8]. As a result of this effort, HY 130

(T) steel was developed.

HY 130 (T) steel is a quenched and tempered 5% Ni-Cr-Mo-V steel with a minimum tensile yield strength of 130,000 psi. Typical chemical composition and properties are listed in Table 1[9]. The fact that this 5% Ni plate has the required mechanical and weldability properties for an HY 130 hull steel has been shown in many papers[8][10]-[15].

The high degree of reliability in properties obtained with this plate is due in no small part to the extensive statistical studies conducted on the effects of composition on mechanical and weldability properties[8][11]. These studies led to the development of optimum levels of the major alloying elements and the need for reducing the amount of "tramp" elements (such as P and S) in high strength steels to improve consistency of properties.

Concomitant with the development of HY 130 (T) steel, several filler metals for joining this steel were investigated. However, these welding wires and electrodes have not yet been developed to the same degree of reliability as the 5% Ni base plate. Early work indicated that high levels of toughness could be achieved with GMA welds but that the toughness varied from heat to heat of wire[16] and among the various compositions[17]. Tensile properties also exhibited inconsistencies between and among heats of

these wires[16]. In addition to these problems, weld deposits made with these wires and electrodes generally exhibited a greater tendency to cracking than did the 5% Ni base plate[7][13][15]-[19].

Many of these variations have been explained in terms of minor differences in composition or welding procedures. As examples, several investigators have shown yield strengths of these weld deposits to be an extremely sensitive function of cooling rate and, therefore, of variations in welding heat input, preheat and interpass temperatures[7][8][17][20]-[23]. Toughness inconsistencies have been attributed to minor differences in weld deposit chemistry[7][16]. Hot cracking was found in one weld deposit with a high (0.30%) copper content[13][16][18]. Cold cracking was attributed to a generally low tolerance of the weld deposits to hydrogen in the filler metal[8][13][15][18][19].

These findings serve to indicate that there is still a significant amount of work required before the HY 130 filler metals are certified for use in hulls of deep diving submersibles. Of high importance on this list is the quantitative investigation of the effects of minor or "tramp" elements on the strength, ductility, toughness and crack susceptibility of HY 130 weld deposits. To this end, studies on the effects of oxygen, nitrogen, hydrogen and

various metallic elements on the strength, ductility, toughness and crack susceptibility of the HY 130 weld deposits have been initiated. This paper deals with the effects of oxygen and hydrogen additions to the weld shielding gas on these properties.

2. The Problem of Oxygen in Steel Welds

Of the major electric arc welding processes for large section steel fabrication (GMA,GTA, SMA, submerged arc) only the GTA process is usually shielded from the atmosphere with a purely inert gas. Oxygen or an oxygen compound is usually a part of the shielding gas in the other processes. Oxygen may also be present in the filler metal itself. The entry of this oxygen into the weld deposit has been shown to influence adversely the properties of weld deposits. Yield/tensile ratio increased as the oxygen content increased in high purity iron base weld metals[24]. However, the greatest problem of oxygen in weld deposits appears to be its effect on notch toughness. Above a critical level of oxygen, the Charpy test transition temperature of iron weld deposits increases rapidly with small increase in oxygen[25][26]. Deoxidation of filler wires or use of strongly deoxidizing flux in submerged arc welds has greatly improved weld deposit toughness[25]. Heuschkel[27]-[30]

has studied the effects of many impurities on the toughness of a 150,000 psi yield strength weld deposit. Among his findings was that for vacuum induction heats of steel, GTA welds fabricated in a chamber had toughness superior to those fabricated in open air. This was again attributed to the detrimental effect of oxygen in the presence of other minor impurities.

3. The Problem of Hydrogen in Steel Welds

Sources of hydrogen in weld deposits can be the base plate, weld atmosphere or the filler metal. The solubility of hydrogen in molten steel is high but decreases rapidly upon solidification and further cooling of the steel. If cooling of the steel is rapid enough, the weld deposit becomes supersaturated in hydrogen. If enough hydrogen is present in the steel, a decrease in the tensile strength and ductility may occur in smooth tensile specimens or fracture of notched tensiles will occur (after a period of time) at a stress level below the notched tensile strength of a specimen without hydrogen[31][32]. Hydrogen can also cause cracking in steels[32]-[36] which may be delayed, i.e., occurring minutes to weeks after completion of welding. The embrittlement due to hydrogen requires the following[36]:

A. A susceptible microstructure

B. Tensile stress

C. A hydrogen concentration "critical" for the applied stress

D. Time

The critical stress, time and amount of hydrogen required for embrittlement are inversely related to each other. The susceptibility of steel microstructures has been listed in the following order[32]:

A. Martensite with appreciable internal twinning formed in medium carbon, low alloy steels

B. Martensite with no internal twins formed in low carbon, low alloy steels

C. Mixtures of martensite and other softer phases

D. Non-martensitic structures

The time required for hydrogen embrittlement and the fact that low temperatures and high strain rates inhibit embrittlement have suggested a diffusion mechanism. Troiano[31] has presented a theory of stress induced diffusion to the region of high triaxial stress in front of internal defects. Cracks form when the concentration of hydrogen at the region of maximum triaxial stress near a defect reaches a critical value. The crack grows a short distance and further growth must await diffusion of hydrogen to the new crack tip.

Factors important in susceptibility to hydrogen embrittle-

ment include composition (generally expressed as a carbon equivalent) and cooling rate, which determine the microstructure and degree of hydrogen retention, ambient temperature (which affects the rates of diffusion or elimination of hydrogen) and the nature and magnitude of the applied stress.

In addition to embrittlement by hydrogen alone, there has been an indication that the presence of oxygen may increase the susceptibility of a steel weld deposit to hydrogen cracking[18]. Also, moist hydrogen has been found to be chemically more detrimental in steel than dry hydrogen[44]. However, little has been done to evaluate the difference in cracking tendency between atmospheres containing hydrogen with or without oxygen.

II. OBJECTIVE

The purpose of this investigation was to develop quantitative information on the following:

1. The effect of oxygen on the strength, ductility and notch toughness of HY 130 (T) weld deposits.

2. The effect of hydrogen, alone and in the presence of oxygen, on the crack susceptibility of HY 130 (T) weld deposits.

3. The mechanisms by which these effects are produced.

III. EXPERIMENTAL PROCEDURE

1. Materials

The materials used in this investigation consisted of two different grades of HY 130 type filler metals. The first, designated herein as 5% Ni wire, was introduced into the Navy HY 130 program in 1966, but has undergone limited work. The second, designated as 3% Ni wire, was a special composition the major element analysis of which is representative of the type of HY 130 filler metal undergoing extensive study in the Navy program. Both wires were made from low residual vacuum induction melts. Three hundred pounds of each material were supplied as 1/16 inch diameter wire on 25 to 30 pound reels by the United States Steel Corporation. In order to minimize base plate dilution effects during welding, U.S. Steel also supplied 1 inch thick plates matching the composition of each of the filler wires. Compositions of base plates and filler wires are given in Table 2.

Filler wires were protected from contamination before use by sealing in a moisture proof bag along with a supply of dessicant. The wires were kept in this package until immediately before they were to be used, and were repackaged immediately after the completion of each weld.

2. Welding Chamber

Since it was desired to fabricate weldments with controlled levels of gaseous impurities, the welding chamber shown in Figures 1 and 2 was fabricated. In this apparatus, the welding torch is fixed and the plate being welded is moved. This is accomplished by mounting the plate on a "slave" carriage which is connected by a pull rod to a cutting torch carriage outside the chamber. Both carriages move on tracks. Since the plate was to be moved, it was grounded electrically by means of a battery cable (Figure 3). Permanent seals required for the chamber (i.e. for the windows) were made with General Electric silicone rubber sealant. The moveable seal required for the connecting rod between the carriages was made from a polyethylene bag which could be compressed or expanded in an accordian fashion depending on the direction of motion of the carriage.

Prior to welding, the chamber was purged with the gas to be used for welding. The gas entered the chamber through the welding torch. Purging was continued for 5 to 10 minutes at flow rates of from 100 to 150 cubic feet per hour (cfh). In order to determine the effectiveness of the purge in removing atmospheric air from the chamber, oxygen readings were made by both Orsat analysis and Beckman gage after purging with pure argon. No oxygen was

detected in the chamber by either measuring technique. In order to maintain the desired chamber atmosphere between weld passes, welding gas was fed through the torch at 20 cfh between passes to maintain a positive gas pressure. Check analysis with Beckman gage or Orsat analysis demonstrated that this "holding" technique was effective.

3. Welding Equipment

Power supplies used included a Linde SVI 300 DC arc welder and a Vickers Controllarc MIG-TIG DC arc welder. The control and wire feed unit was a Linde SWM-11A. Controls for arc start, wire feed, carriage travel, etc. were on a hand held remote unit to facilitate operation.

GTA welds were made with a Linde HW-13 MIG-TIG torch using a number 6 nozzle, a 1/8 inch tungsten - 2% thoriated electrode and DC straight polarity. Cold wire feed was 20 to 25 inches per minute (ipm) and welding gas flow rate was 100 cfh. Arc starting was aided by the use of a high frequency arc starter unit.

GMA welds were made with both a Linde HW-13 MIG-TIG torch and a Linde ST-5 MIG torch, using a number 8 nozzle and DC reverse polarity. Wire feed was 180 to 200 ipm and welding gas flow rate was 60 cfh.

For both processes, gas flow was controlled and measured

by constant pressure (30 psig), dual range flow meters.

4. Welding Procedure - Oxygen Series

Both GTA and GMA processes were used to produce weldments in the atmosphere chamber. In addition, two hot wire GTA welds were fabricated with the 5% Ni wire by the Linde Division, Union Carbide Corporation. The latter two welds were fabricated out of chamber.

Joint design for these welds was a 60° U groove in a plate 16" X 6" X 1" as shown in Figure 4. The plate was ground to clean metal on the top surface and cleaned in either acetone or methyl butane. A chromel-alumel thermocouple was attached 1" from the groove wall for monitoring preheat and interpass temperature.

Preheating to $250^{\circ}F \pm 25^{\circ}F$ was done in chamber after purging by running weld arcs on the top surface of the plate on both sides of the groove a minimum of 2 inches from the groove wall. Plate temperature was allowed to rise to about $300^{\circ}F$ and to cool to $250^{\circ}F$ to obtain an even temperature distribution. Beads were deposited using the tempering bead technique. All beads were deposited at $250^{\circ}F \pm 25^{\circ}F$. Heat input calculated from

$$\frac{EI}{S} \times 60$$

where

E = welding voltage (volts)

I = welding current (amps)

S = welding speed (ipm),

was held at 46,000 $\pm$ 6,000 joules/inch for the GTA and GMA welds.

5. Welding Procedure - Hydrogen Series

In order to determine the hydrogen level required to cause cold cracking, Keyhole slotted plate restraint tests[13] [37]-[40] were conducted. The Keyhole test specimen is shown in Figures 6 and 7. Direction of welding is from the open end toward the closed end. As the weld cools, contraction is hindered by the test plate resulting in a transverse separating force on the weld. Because of the specimen geometry, the magnitude of this separating force is a minimum at the open end and increases rapidly along the weld length to a maximum at the closed end. If the combination of separating force and weld deposit hydrogen level reaches a critical value, a crack will appear at the closed end after a period of time and grow in length toward the free end.

An analysis of the forces in the Keyhole specimen can be found in reference 39.

Prior to testing, the specimen was ground to clean metal to at least 1 inch from the groove, cleaned in acetone

and wire brushed. Both GTA and GMA welds were made in chamber using the same conditions as in the oxygen series except that no preheat was used and only one bead was deposited. The weld crater was not filled. After welding, the weld was examined for cracking for 72 hours using magnetic particle inspection techniques.

6. Specimen Preparation - Oxygen Series

Specimens were removed from completed weldments as shown in Figure 4. Charpy V-notch impact specimens were made according to standard specifications[41] and were removed so that the top of the specimen was 1/8" below the surface of the plate. Notching was perpendicular to the weld surface. A minimum of 2 specimens were conditioned at each test temperature for 20 minutes in a medium of either acetone, methyl butane or freon 12 for temperatures below room temperature, or in water for temperatures above room temperature. Dry ice or liquid nitrogen was used as a coolant. Specimens were fractured 3 to 5 seconds after removal from the bath. After fracturing, specimens were immediately placed in acetone to prevent rusting. After heating back to room temperature, fractures were removed from the acetone and sprayed with a commercial lacquer for corrosion protection during storage.

Tensile specimens were removed from each weldment as shown in Figure 4. In order to test only weld deposit, the tensile specimen was reduced in cross section across the weld as shown in Figure 5. Testing was done on an Instron tensile tester at a speed of 0.05 inches/minute. Strain was measured over a 1/2 inch gage length.

7. Metallographic Examination

Macrosections were removed from each weldment in the oxygen series and from representative weldments in the hydrogen series and polished through 1 micron diamond paste for metallographic examination. Macro examination was conducted at 2 to 5 diameters on specimens etched in either a saturated solution of ammonium persulphate or 2% nital. Micro examination was conducted at 500 and 750 diameters using unetched specimens and specimens etched in 2% nital.

8. Electron Microscopy

A. Replication Fractography

Charpy specimens fractured at $-80^{\circ}F$ and $-100^{\circ}F$ were replicated to study fracture appearance. A double replica[42] technique was used as follows:

1) The protective coating on the Charpy specimens was removed by immersion in trichloroethylene.

2) Specimen was washed with acetone and dried with Effa Duster, a commercial, dry freon aerosol spray.

3) Fracture surface was covered with a solution of 3% cellulose acetate in acetone and allowed to dry.

4) Two or 3 drops of acetone were placed on a 3/4 inch square of 5 mil thick cellulose acetate tape and allowed to partially evaporate before the tape was pressed onto the fracture surface.

5) The specimen was allowed to stand overnight before the plastic was mechanically stripped.

6) The plastic was placed upright in a vacuum evaporator and shadowed at a 30° angle with platinum and then at 90° with carbon until a light brown film was developed.

7) The replica was cut into 1/16 inch squares and placed in acetone to dissolve the cellulose acetate tape.

8) When the films floated free, they were removed with 1/16" diameter 200 mesh copper or stainless steel support grids for examination at 50 KV in an RCA EMU 3H electron microscope.

B. Extraction Fractography

After replication fractography, the Charpy specimens were examined by an extraction fractography technique[43] to extract particles from the surface of the fractures for examination and identification. The procedure was as

follows:

1) A relatively thick carbon film was deposited at 90° to the surface.

2) The specimen was placed in a solution of 5% bromine in methyl alcohol for 1 to 2 minutes.

3) Traces of bromine were removed by placing the specimen in methyl alcohol for one hour.

4) The entire specimen (except the fracture surface) was coated with Unichrome stripable vinyl lacquer, immersed in a solution of 775 ml glacial acetic acid, 150 grams sodium chromate, 75 grams chromic oxide in 1 liter of water for etching to loosen the carbon film. The specimen was etched for 40-80 seconds at 0.4 amps using a stainless steel cathode.

5) The etching solution was rinsed off in methyl alcohol.

6) The carbon film was floated off in methyl alcohol and removed with 1/16 inch diameter 200 mesh stainless steel support grids for examination at 100 KV in an RCA EMU 3H electron microscope.

Electron diffraction patterns were used to identify particles. The camera constant for diffraction was obtained from a gold standard.

9. Electron Microprobe Analysis

To aid in the identification of particles on the Charpy fracture surface, grids prepared for extraction fractography were analyzed on an Acton electron probe microanalyzer.

IV. RESULTS AND DISCUSSION

1. Effects of Oxygen

A. Structure - The combinations of process and atmosphere used for the welds fabricated in the oxygen series are listed in Table 3. The welding conditions used for each weld are given in Table 4. Figure 8 shows macro sections representative of GTA, GMA, and hot wire GTA welds. The effective refinement obtained from the large number of passes in the GTA weld is readily seen in comparison to the coarser structure in the GMA and hot wire GTA welds. Micrographs of 3% Ni and 5% Ni welds are presented in Figures 9 through 12, Figures 9 and 11 showing the structure in the last bead deposited with each process (with and without oxygen) and Figures 10 and 12 showing the structure typical of the remaining beads in the weldments. The structure in the last bead appears similar in each weld although the grain sizes of the 5% Ni welds are larger than those of the 3% Ni welds. Structure in each case appears to be massive martensite[45]. Because of refinement by subsequent beads, the interior weld beads are finer grained than the last bead. Again the high degree of refinement obtained from the large number of GTA beads can be seen.

Oxygen additions to the shielding gas do not appear to have affected the microstructure of weld deposits, but, as can be seen in unetched microsections (Figure 13) the amount of non-metallic (oxide) inclusions increased with increasing oxygen in the shielding gas.

B. Bead Appearance and Welding Conditions - GTA and GMA welds made under pure argon were bright and slag free after completion. A heavy smoke of fine dark brown to black particles formed during the GMA welding in pure argon and settled heavily on the weld plate and chamber floor and walls. The addition of 1/4% oxygen to the shielding gas eliminated this smoke and resulted in islands of slag on the final weld. Slag increased with oxygen content in GMA welds until at 2% oxygen, a thick slag coating similar to that developed in SMA welding was found (Figure 14). This slag was a cumulative buildup from each bead since it was not possible to remove slag after each bead. Qualitative identification of the slag by electron probe revealed it to be high in Si and Mn.

GTA welds made under pure argon exhibited smooth arcs. However, the addition of 1/4% oxygen resulted in significant changes in arc characteristics. Oxidation of the tungsten electrode resulted in the electrode shape and

coloration shown in Figure 15. Arc starting was easier in argon-oxygen than in argon. The arc in argon - 1/4% oxygen was more forceful, developed higher voltage and lower current for the same machine setting, and resulted in more undercut than comparable welds in pure argon. Porosity was noted in some beads of welds made in argon - 1/4% oxygen.

GMA welding in pure argon exhibited high voltage, erratic, unstable arcs with the major mode of transfer globular. Undercut was noted. The addition of 1/4% oxygen tended to stabilize the arc by lowering the transition current for axial spray[46] and the lower ionization potential of oxygen[46] lowered the voltage. However, 1% oxygen was required before complete arc stability and axial spray were obtained. Lack of fusion was a problem in all low oxygen GMA welds but was more serious in the 5% Ni welds because of the more limited flow characteristics of this wire.

Shielding gas had a major effect on the shape of GMA weld beads as shown in Figure 16. Welds deposited under pure argon were wider and had less penetration than those deposited under argon-oxygen. In addition, the penetration finger present in 1% and 2% oxygen welds was absent in welds made under pure argon and was only slightly apparent in welds made with 1/4% oxygen.

C. Oxygen Content of Weld Deposit - Weld metal oxygen content as a function of shielding gas oxygen content is shown in Figure 17. As can be seen, data for in-chamber welds generally fall into a broad band regardless of wire or process. The low oxygen content of the hot wire GTA weld made with 1/2% oxygen in the shielding gas may be due to the fact that the tungsten electrode was reground after each pass exposing a fresh tip to the shielding gas for each bead. The subsequent oxidation of the tungsten by the shielding gas may have resulted in the low oxygen content of the weld deposit. The importance of the condition of the tungsten electrode can be seen in the results of the in-chamber GTA welds made with 1/4% oxygen. For these welds, the tungsten was not ground clean after each bead and the resulting oxygen content of the weld deposit was higher than the hot wire GTA welds.

D. Weld Deposit Properties - The following weld characteristics were affected by oxygen additions to the weld shielding gas:

1) Chemistry
2) Strength and ductility
3) Toughness

1) Chemistry - Total analysis was made on one weldment from each type of process. In addition, analyses of

C, O, H and N were made for each in-chamber weldment fabricated (Table 5). With the exception of the oxygen content, the major chemical change associated with the presence of oxygen was a change in carbon content. The carbon content of GTA welds was reduced from 0.11% to 0.08% for both 3 and 5% Ni welds as the oxygen increased from 0 to 1/4% of the weld atmosphere. Carbon decreased from 0.12 to 0.10% as oxygen increased from 0 to 1% for the 5% Ni GMA welds, however, no noticeable change in carbon content attended the increase in oxygen from 0 to 2% in the 3% Ni GMA welds. The decarburization is caused by the reaction of carbon and oxygen with the evolution of CO gas[47]. The effect may be more pronounced in GTA rather than in GMA welds because of the following:

a. GTA welds were made under a higher gas flow rate.

b. The wire feed in GTA welds is much slower than in GMA welds.

Therefore, for a given oxygen content of the shielding gas and the conditions used, a GTA weld should absorb significantly more oxygen than a GMA weld. Since the oxygen content of GTA welds made under 1/4% oxygen is in fact less than that of GMA welds, oxygen is being

lost. This loss is divided among the oxygen used to oxidize the tungsten and the oxygen lost in decarburization.

2) Strength and Ductility - Results of tensile tests are presented in Table 6. Figures 18 and 19 show yield strength, ultimate tensile strength and reduction in area as a function of weld metal oxygen content for 3 and 5% Ni weld deposits respectively. Yield strengths of GTA welds made under pure argon are higher than comparable GMA and hot wire GTA welds because of the finer grain size[24][48]. Strengths of 5% Ni welds are higher than 3% Ni due to the additional solid solution strengthening.

Results indicate slight decreases of the tensile strength in GTA welds and the 5% Ni GMA welds and a slight increase in the 3% Ni GMA welds. Yield strength of 5% Ni GMA welds showed a slight decrease as oxygen content increased and the yield strength of 3% Ni GMA welds increased as oxygen increased to 60 ppm and then remained constant with increasing oxygen. Large decreases in yield strength were observed for both 3% and 5% Ni GTA welds as oxygen increased. Reduction in area decreased 15% to a minimum level of 60% for 3%

Ni welds as oxygen increased, and 10% for 5% Ni GTA welds, however, ductility increased 15% for 5% Ni GMA welds. Because of the close proximity in oxygen content for the 5% Ni hot wire GTA welds, data on trends are limited.

It is possible to explain the effects of oxygen on strength and ductility in terms of the competitive oxygen effects of decarburization and dispersion strengthening by the formation of particles such as iron silicate, the presence of which will be shown later. Many investigators have shown that the strength of low carbon martensite is directly proportional to the carbon content[10][25][49]-[51]. For steels with a base composition similar to the 3% Ni, Telford[16] reported a yield strength decrease of 16,000 psi as carbon decreased from 0.115 to 0.095%. Therefore, in specimens where decarburization has occurred, it is expected that the strength will decrease. However, the formation of particles in the matrix can increase the strength by impeding dislocation movement [25][48][52]. Consequently, if the particle content is sufficient, the effect of carbon loss can be lessened. This is apparently the case for the 5% Ni GMA welds and the result is a slight loss in strength. For the GTA welds, the oxygen content is apparently insufficient to overcome the large carbon loss and the strength decreases sharply. For the 3% Ni GMA welds, which

exhibited no decarburization, the effect of the oxygen strengthening can be seen to be a rapid early rise in yield strength tapering off after approximately a 9 ksi increase. The slight tensile strength increase compared to the yield strength increase is similar to that reported by others[24][53].

Except for the GTA welds, reduction in area followed the often observed inverse relationship to yield strength [48][54][55]. The decrease in the reduction in area of GTA welds as oxygen increased may be due to porosity in the weldments.

3) Toughness - Results of weld metal Charpy V notch impact tests are presented in Figures 20 through 39. Figures 20 through 32 show the Charpy energy vs temperature curves for each weldment, Figures 33, 34 and 35 show the Charpy data for the 3% Ni GMA and GTA, 5% Ni GMA and GTA, and 5% Ni hot wire GTA series respectively as affected by the oxygen content of the shielding gas. Charpy 50 ft - lb transition temperature and energy at 75°F are plotted as a function of weld metal oxygen content in Figures 36 and 37 for the 3% Ni welds and in Figures 38 and 39 for the 5% Ni welds.

The superior toughness of the GTA welds when compared to the GMA welds is evident in each figure. This

superiority is due to the very fine grain size of the GTA welds. Many investigators have reported similar toughness, grain size relationships[25][26][54][56].

As shown in Figures 33 and 36, oxygen consistently increases the 50 ft - lb transition temperature of 3% Ni GTA and GMA welds approximately 3°F per ppm oxygen for values below 200 ppm oxygen (GMA, A - 2%O_2). With 214 ppm oxygen, 50 ft - lbs was not obtained for temperatures as high as +212°F. These data agree well with that of Rees and Hopkins[53] who reported a rise of approximately 4°F per ppm oxygen for high purity iron-oxygen alloys for values less than 110 ppm oxygen.

Charpy energy at 75°F is shown in Figure 37 for 3% Ni GTA and GMA welds. The energy of the GTA welds increases slightly over the range from 6 to 55 ppm oxygen. The energy of the GMA welds remains constant at approximately 125 ft - lbs from 24 to 60 ppm oxygen then drops sharply to 52 ft - lbs at 105 ppm oxygen. Further addition of oxygen to 214 ppm results in only a slight change in this lower level of energy.

In contrast to the marked dependency of toughness on oxygen content displayed by the 3% Ni welds, 5% Ni weld deposit toughness was not markedly affected by

oxygen content (Figures 34, 35, 38 and 39). The only exception was in the case of the energy at 75°F for 5% Ni GTA welds which increased markedly with oxygen content.

The fact that oxygen increases the Charpy energy at 75°F for GTA welds appears to be due to decarburization. On the other hand, the immunity to toughness embrittlement of the 5% Nickel GMA welds may be due to a balance between the embrittling effects of oxygen and the decarburization which it produces. Since decarburization did not occur in the 3% Ni GMA welds, the constant increase in 50 ft - lb transition temperature with increasing oxygen content is to be expected[53]. The appearance of a critical oxygen level beyond which the shelf energy drops precipitously rather than steadily decreasing, however, suggests a change in the fracture process at this level of oxygen.

To examine the fractures of the Charpy specimens, electron fractographs were made of specimens fractured at either -80°F or -100°F. The high energy associated with the majority of the fractures at these temperatures was indicative of fracture by the mechanism of microvoid coalescence[57][58]. By this mechanism, small particles (as inclusions or precipitates) present in the matrix act as sites for initiation of fracture[57][59]-[61]. Under load, the deformation of the matrix results in a stress

concentration at particles because of the difference in flow strengths. Upon continued application of load, there will result either a separation of the particle from the matrix (if the bonding is weak) or fracture of the particle, forming a microvoid. Similar microvoids form at other particles. As loading continues, the voids grow by tearing of the matrix until they join to form a continuous fracture surface. The fracture surface exhibits cup-like depressions, called dimples, that are a direct result of the microvoid growth. The shape of the dimples is a function of the type of load applied[59]. Under tensile load, dimples will be equiaxed; under bending or tearing (as in a Charpy fracture) dimples will be elongated. The size of the dimple is related to the distribution of fracture initiating sites. If the number of sites is high, void growth would be limited by rapid intersection with voids from other sites and dimples will be fine. If sites are few, voids must grow rather large before intersecting other voids and dimples will be large.

Results of fractographic examination are shown in Figures 40, 41 and 42 and in Table 7. All specimens exhibited only elongated dimples except for the 3% Ni GMA argon - 2% oxygen specimen in which some flat areas were noted. Dimple size appears to be much the same

for both filler metals and only slightly changed by welding process, however, size is extremely dependent upon the oxygen content of the weld deposit. Welds containing less than 20 ppm O_2 exhibited very fine dimples with a mean size of approximately 1 micron. Welds with oxygen contents of between 40 and 105 ppm exhibited large dimples ranging in size from 3 to 10 microns. Welds with oxygen contents of 105 ppm or greater exhibited dimples of an intermediate size ranging from approximately 2 to 3 microns.

The change in dimple size indicates a change in density of particles initiating fracture. However, since the oxygen content constantly increases while the dimples change from fine to coarse to intermediate in size, there is a suggestion that particles involved in the fracture may differ as oxygen content changes. To examine this possibility, extraction replicas were made of each of the Charpy fractures examined to remove the particles associated with the formation of the dimples so that their identity could be determined. The results of this study are given in Table 7 and Figure 43.

Particles extracted from the Charpy specimens were of three general types:

a. Type A - These particles appeared short and "feathery". Distribution was general over the surface of the replica and occasionally they were agglomerated into groups. All were less than 1 micron (about 1/2 - 3/4 microns) in length.

b. Type B - These particles were irregular or geometric. Hexagonal, triangular, sector and "near-square" shapes were noted. Distribution was limited and they were found only on large dimples. The size of these particles measured from 3/4 to 2 microns, most being of the order of 1 to 1 1/2 microns.

c. Type C - These particles were nominally round although examination at very high magnification showed that they were actually faceted. One particle was found on each dimple. The size of these particles ranged from 1/4 to 1 1/2 microns, most being from 1/2 to 1 micron.

Type A particles were found on the fracture surface of all specimens examined and, except for a rare type B particle, were the only particles extracted from the low oxygen (less than 20 ppm) weldments. The general distribution of these particles accounts for the presence of very fine dimples in the low oxygen weldments.

Type B particles were found mainly on the fracture surface of the intermediate oxygen (40 to 105 ppm)

weldments. Since these particles were large and limited in distribution, they may have triggered the very large dimples observed in these weldments at a lower level of flow than that required for the type A particles to act.

Type C particles were in predominance only in the high oxygen (greater than 105 ppm) weldments. Their number was not as great as the type A particle but it was greater than the type B, therefore, these particles could account for the dimples of intermediate size noted in the high oxygen weldments.

Identification of these particles was made by the technique of selected area diffraction[42]. Because of the large number of particles of type A in any one area, random orientation is assured and the diffraction pattern is a ring pattern as shown in Figure 44. Because types B and C particles are larger than type A particles, it was possible to single each particle out and obtain single crystal spot patterns for the particular orientation of the particle. Such spot patterns for types B and C particles are shown in Figure 44.

The results of electron diffraction analysis of types A, B and C particles are shown in Tables 8, 9 and 10 respectively. As can be seen, the diffraction data obtained from these particles agree well with

calculated d_{hkl} spacings as follows:

a. Type A - Iron silicate (Fe_2SiO_4)

b. Type B - Silicon dioxide (beta quartz) (SiO_2)

c. Type C - Silicon dioxide (beta quartz) (SiO_2).

Because of the excellent pattern shown in Figure 44 for a type B particle, it is possible to further verify that this is indeed SiO_2 (beta quartz) by calculation of the lattice constant, a_o. Figure 45 shows the hexagonal lattice for the (001) plane and the resulting reciprocal lattice[42][64]. For electron diffraction, it has been shown[42] that

$$r_{hkl}d_{hkl} = \lambda\ell$$

where r_{hkl} = radius of ring (or distance from center to spot) for the (hkl) reflection,

d_{hkl} = interplaner (hkl) spacing,

$\lambda\ell$ = camera constant,

or,

$$\frac{1}{d_{hkl}} = \frac{r_{hkl}}{\lambda\ell} = d^*_{hkl},$$

therefore,

$$\frac{1}{d_{100}} = \frac{r_{100}}{\lambda\ell} = d^*_{100} = a^*.$$

For this pattern, r_{100} = 0.483 cm and $\lambda\ell$ (calculated from a gold standard) = 2.141 cm Å.

Therefore,

$$a^* = \frac{0.483}{2.141} = d^*_{100} = 0.226 \text{ r.l.u.}$$

$$d_{100} = \frac{1}{0.226} = 4.425\text{Å}.$$

From the geometry of the hexagonal lattice (Figure 45),

$$a_o = \frac{d_{100}}{\sin 60} = \frac{4.425}{0.866} = 5.110 \text{ Å}.$$

This value agrees well with the published value for the lattice constant, a_o, for SiO_2 (beta quartz) of 5.11Å[63].

As a further check, specimen grids of each particle type examined on the electron microscope were examined qualitatively on the electron probe. Only iron and silicon were detected.

Thus, results indicate that in the low oxygen weldments, ductile fracture of Charpy specimens is initiated at particles of iron silicate. Because of the high number of these particles, dimple size is limited by the large number of nucleation sites. At higher levels of oxygen, fracture is initiated at silicon dioxide particles. Because these particles are larger and of lower density than the iron silicate particles, dimples formed by

void coalescence from these particles are large. As oxygen increases further, a higher density of silicon dioxide particles are formed. Initiation of fracture by these particles results in dimple size intermediate to those initiated by the types A and B particles because of their intermediate size and density.

Thus, on the basis of fractographic examination, it is possible to propose a model for the existence of a critical oxygen level beyond which the shelf energy of 3% Ni GMA welds drops rapidly. (The 3% Ni GMA welds are the only specimens in which complications from decarburization are missing). Fracture initiated by iron silicate particles (low oxygen specimens) requires high energy. Due to the low density of the type B silicon dioxide particles, fracture initiated by these particles (intermediate oxygen levels) are also tough even though the particle is brittle because of the extreme amount of matrix tearing required for void growth (witness the extremely large dimples). However, at high oxygen levels, fracture requires less energy because the density of brittle type C silicon dioxide particles is very high. Thus voids initiated by these particles grow only a short distance through the matrix before intersecting other voids resulting in a lower energy fracture. Increasing

the oxygen content beyond 110 ppm results in a continued decrease in energy as the density of type C silicon dioxide particles continues to increase.

Although this model was developed for 3% Ni GMA welds, it is important to note that as oxygen increased, the silicon dioxide particles appeared in all other welds as well (Table 7). These results indicate that a major cause of toughness embrittlement in steels by oxygen is the formation of large amounts of silicon dioxide. This is in agreement with the results of Heuschkel[27][30] showing that silicon degradation of toughness is increased markedly in the presence of oxygen.

2. Effects of Hydrogen

Hydrogen effects on cracking tendency were evaluated from Keyhole slotted plate restraint tests. The welding conditions for the tests conducted are listed in Table 11. Examples of welded Keyhole specimens are shown in Figures 46 and 47.

A. Welding Conditions - Hydrogen additions to the shielding gas had little, if any, effect on the arc characteristics or mode of transfer, but, in argon - hydrogen - oxygen GTA welds, oxidation of the electrode was not as great as in the argon - oxygen welds previously mentioned. This is probably due to the reducing action of

hydrogen on the tungsten electrode. With this exception, welding conditions under argon - hydrogen - oxygen shielding were similar to those under argon - oxygen described earlier.

Argon - hydrogen welds were bright and slag free after completion. Argon - hydrogen - oxygen welds generally exhibited a light slag cover.

B. Bead Appearance - Macrosections representative of cross sections from test welds are shown in Figure 48. As can be seen, the smaller GTA bead is much lower in the groove than the larger GMA bead. Although hydrogen did not have much effect on bead shape, the addition of oxygen to the shielding gas had a pronounced effect on the bead cross section. As in the oxygen series weldments, penetration increased and the bead narrowed when oxygen was added to the shielding gas. For GTA welds, heavy undercut is apparent when oxygen is added; for GMA welds, the presence of a penetration finger is noted as oxygen is added.

Solidification patterns evident in the finger of GMA oxygen - bearing welds are different from at the root of the welds made without oxygen. This is due to the fact that the penetration brings the finger deep into the straight walled section of the joint. Solidification and grain growth proceeds perpendicular to the parallel walls in this area and

grains meet "head on" along the bead centerline. Solidification and growth in the vee section of the groove in the oxygen - shielded GMA welds are also perpendicular to the walls but because of the 60^{o} included angle, grains meet at a 60^{o} angle along the weld centerline. Solidification in GMA welds made in oxygen - free shielding atmosphere is different from welds made in oxygen - bearing gas because of the lack of the penetration finger and the wider bead which does not conform to the original shape of the vee section. Growth is perpendicular to the weld/base metal interface but because this interface is more curved, grain growth is not as aligned as in the previously described case and intersections occur at places other than the weld centerline.

A view parallel to the bead face (along the sections a-a and b-b in Figure 48) is shown in Figure 49. This view shows that the solidification pattern is more severe in the oxygen - shielded welds than in the non-oxygen shielded welds. The implications of this difference in GMA solidification pattern will be discussed later.

C. Cracking Tendency - Results of Keyhole tests are listed in Table 11 and summarized in Table 12. The majority of the 5% Ni welds exhibited crater cracks upon the completion of welding. In the absence of a crater fill procedure, this is to be expected from the enrichment during solidification of the crater in solute elements[55][65]

which promote hot cracking (here notably nickel[7][11][25]). Welds in 3% Ni were usually free of crater cracks. When cold cracking (defined as cracking occurring at least 15 minutes after completion of welding[33]) occurred, growth of the crack was from the root of the weld (where stress concentrations are high) upward and from the closed (high stress) end of the plate to the open (low stress) end. It was possible to deduce that cracks grew from root to face, because, in many instances, the loud metallic "ping" associated with crack growth would be heard several times before the crack would appear on the surface.

Crack growth was discontinuous, growing a short distance and then stopping as was the hydrogen cracking described by Troiano and others[31][66][67]. In specimens for which crack growth was slow, it was noted that the growing crack would appear on the surface a short distance away from the front of the major crack. This too is in agreement with the stress induced diffusion theory[31] which requires that hydrogen diffuse to the region of maximum triaxial stress which is in front of a crack.

As shown in Table 12, 3% Ni welds were more susceptible to hydrogen cracking than 5% Ni welds and GMA welds were more susceptible than GTA welds.

The requirement of higher hydrogen to cause cracking in GTA welds when compared to GMA welds may be related to the difference in separating force between the two processes.

Adams[68] has shown that, for similar heat inputs, GTA welds solidifying under conditions of hindered contraction develop lower transverse separating force than GMA welds. Since it has been shown that the amount of hydrogen required to cause cracking is inversely related to the separating force [31][66][67], it is, therefore, logical that GTA welds require more hydrogen for embrittlement than GMA welds.

The superior crack resistance of the 5% Ni welds compared to the 3% Ni welds is not so readily explained. While this effect is no doubt due to the difference in chemistry of the wires, calculation of carbon equivalents from the wire analysis using the cold cracking equation developed by Rathbone, et al[11] results in a prediction that the 5% Ni wire would be more crack susceptible. It should be pointed out that this equation was developed for base plate rather than weld deposit cracking, using steels with manganese contents significantly less than the 1.7% present in the 3% Ni wire. Since the Rathbone data showed a significant increase in cold cracking tendency as manganese increased, it is possible that manganese may be more important in the cold cracking tendency of these wires than nickel.

Another, perhaps more probable, explanation for the inferior crack resistance of the 3% Ni wire may be its extremely low phosphorus and sulfur content when compared

to the 5% Ni wire. It has generally been shown that steels with high phosphorus and sulfur contents are susceptible to hot cracking and that the reduction of these impurities markedly reduces this tendency[25][47][55]. However, recent work by Smith and Bagnall[69] has indicated that if the sulfur content is too low, the cold (hydrogen) crack susceptibility of the steel may increase. This result was explained in terms of the low number of MnS inclusions in the very low sulfur steels. Hydrogen is believed to be innocuously occluded at these inclusions and, if sufficient numbers are present, the amount of harmful diffusible hydrogen can be lessened below that required for cracking. However, if the density of inclusions is low, there will be an inadequate void capacity to absorb the diffusible hydrogen and it is possible to promote cracking at lower hydrogen levels.

D. Oxygen - Hydrogen Effects - Once the critical hydrogen level to cause cold cracking was determined, the effect of oxygen on the hydrogen crack susceptibility was evaluated by fabricating weldments using shielding gases containing either the critical hydrogen level plus oxygen or half the critical level plus oxygen. As closely as possible, GTA welds were made with 1/4% oxygen and GMA welds with 1% oxygen. Results of this series are given in Tables 11 and 12. As noted, therein, addition of oxygen to GTA

welds eliminated cracking at the critical hydrogen level. This is explainable in terms of the decarburization of the GTA weld deposit by 1/4% oxygen previously mentioned in the section dealing with the effect of oxygen on strength. Since lower carbon steels are less susceptible to cold cracking[11][25][32][33][55][67], it is not surprising that the oxygen addition to the GTA atmosphere results in an increase in the hydrogen content required to cause cracking.

Addition of oxygen to the atmosphere of GMA Keyhole specimens had the opposite effect. Instead of increasing the level of hydrogen required for cracking, the addition of 1% oxygen resulted in critical hydrogen levels of at most half that required in the absence of oxygen. This result may be due to two effects:

1) The formation of an oxide film

2) The change in weld bead profile and solidification pattern as a function of atmosphere.

The formation of oxide films has been reported to hinder the escape of hydrogen[70]. If so, a weld made under argon - hydrogen - oxygen would retain a higher hydrogen content than one made under the same hydrogen content without oxygen. This condition, of course, would tend to promote cracking.

Because of the solidification pattern exhibited by

the oxygen - shielded bead (Figures 48 and 49), a line of weakness develops in the weld centerline. Fracture susceptibility along this line is high compared to other areas of the bead[16][47][55]. If any element (as C, Ni, etc.) segregates during solidification, there will be an enrichment in solute at this line. Such an enrichment would locally raise the carbon equivalent and further increase the tendency toward centerline cracking. Examination of the cracked argon - hydrogen - oxygen weldments shows that the crack does seek out this plane of weakness.

As previously mentioned such a plane of weakness was not as prevalent in GMA welds made without oxygen in the shielding gas. It is felt that the amount of hydrogen required to cause cracking in a specimen without a plane of weakness would be greater than that required for a specimen with such a plane.

On the basis of this analysis, the effect of oxygen additions on hydrogen crack susceptibility can be both chemical and catalytic. Chemically, oxygen can decarburize the steel and cause the formation of an oxide film retarding hydrogen loss. As a catalytic factor oxygen can induce a change in bead profile to one more susceptible to hydrogen embrittlement.

V. SUMMARY AND CONCLUSIONS

The composition of the weld shielding gas was found to have a marked effect on the properties of GTA and GMA welds deposited with HY 130(T) type steel filler metals. Oxygen additions to the shielding gas affected weld chemistry, strength and toughness. Decarburization was the major chemical effect of these additions. When decarburization occurred, yield strength was decreased as much as 23,000 psi and Charpy V-notch energy at 75°F increased as much as 32 ft-lbs. In the absence of decarburization, oxygen additions resulted in a yield strength increase of 9,000 psi for one filler metal tested. This increase was believed to be due to a dispersed phase strengthening mechanism.

For 3% Ni welds, oxygen additions resulted in an increase in the Charpy 50 ft-lb transition temperature of 3°F per ppm of oxygen for values up to 200 ppm. At 214 ppm oxygen (produced by argon-2% oxygen shielding gas) toughness of 3% Ni welds did not attain 50 ft-lbs at temperatures as high as 212°F. Charpy energy at 75°F for 3% Ni GMA welds was constant below 60 ppm oxygen and then decreased 70 ft-lbs at 100 ppm oxygen. On the basis of electron extraction fractography, it was concluded that the formation of large amounts of silicon dioxide was responsible for weld metal embrittlement by oxygen.

Weld deposit cracking in Keyhole slotted plate restraint specimens was observed when hydrogen additions to the shielding gas exceeded a critical value. GTA welds were more resistant to hydrogen cracking than GMA welds and 5% Ni welds were more resistant than 3% Ni welds. The difference between the GTA and GMA processes was believed to be due to the difference in separating force developed by the weld metals of the two processes. The superiority of the 5% Ni welds over the 3% Ni welds was believed to be due to one or both of the following:

1. The extremely low (<0.002%) sulphur and phosphorus content of the 3% Ni welds which result in relatively few inclusions to act as sinks for hydrogen.

2. The high manganese content of the 3% Ni welds.

The addition of oxygen to the shielding gas for GTA welding increased the critical amount of hydrogen necessary to cause cracking. This response was ascribed to decarburization. The addition of oxygen to GMA weld deposits decreased the critical amount of hydrogen necessary for cracking to a level less than or equal to half that required in the absence of oxygen. This effect was believed to be attributable to the formation of an oxide film which retards the escape of hydrogen, and to the difference in solidification pattern between welds made with and without oxygen.

Table 1

Typical Properties and Composition of HY-130(T) Steel Plate[9]

Typical Chemical Composition, percent

C	Mn	P	S	Si	Ni	Cr	Mo	V
0.10	0.75	0.010 max	0.010 max	0.30	5.00	0.55	0.55	0.06

Typical Tension Test Results

		0.2% Yield Str. (psi)	Tensile Str. (psi)	% Reduction in Area
1/2" Plate	L	143,000	152,000	65
	T	142,000	152,000	63
2" Plate	L	137,000	144,000	71
	T	137,000	145,000	70

Typical Charpy V Energy Absorption

Temp. (°F)	+80	0	-80	-160	-240
Ft-lbs	100	92	90	50	20

Table 2

Compositions of Plates and Welding Wires

Product	Heat	C	Mn	P	S	Si	Ni	Cr	Mo	V	Al
5 Ni-Cr-Mo-V Plate	50400	0.11	0.85	0.004	0.004	0.33	5.00	0.54	0.55	0.06	0.018
5 Ni-Cr-Mo-V Wire	50646	0.12	0.84	0.005	0.007	0.36	4.99	0.58	0.55	ND	0.01
Mn-Ni-Cr-Mo Plate	W8807	0.12	1.74	0.001	0.004	0.31	2.82	0.44	0.86	<0.005	0.002
	W8808	0.13	1.76	0.001	0.004	0.31	2.81	0.46	0.85	<0.005	0.002
	W8809	0.09	1.76	0.001	0.003	0.32	2.82	0.46	0.88	<0.005	0.004
	W8810	0.10	1.70	0.001	0.004	0.33	2.79	0.46	0.88	<0.005	0.003
	W8811	0.11	1.74	0.001	0.003	0.28	2.80	0.45	0.86	<0.005	0.001
Mn-Ni-Cr-Mo Wire	W8774	0.10	1.70	0.001	0.003	0.29	2.70	0.44	0.84	<0.005	0.017

Plates are one-inch thickness; wires are 1/16-inch diameter.
All materials vacuum induction melted.

Table 3

Welds Fabricated - Oxygen Series

Wire	Process	Shielding Gas
3% Ni	GTA	Argon
	GTA	A-1/4% O_2
	GMA	Argon
	GMA	A-1/4% O_2
	GMA	A-1% O_2
	GMA	A-2% O_2
5% Ni	GTA	Argon
	GTA	A-1/4% O_2
	GMA	Argon
	GMA	A-1/4% O_2
	GMA	A-1% O_2
	Hot Wire GTA	A-75% He
	Hot Wire GTA	A-75% He-1/2% O_2

Table 4

Welding Conditions - Oxygen Series

Wire	Welding Process	Shielding Gas	Amps	Volts	Travel Speed (ipm)	Heat Input (joules/in)	No. of Passes
3% Ni	GTA	Argon	300	16 1/2	6 1/2	45,700	35
	GTA	A-1/4% O_2	290	19	7	47,200	36
	GMA	Argon	325	36	13 1/2	52,000	11
	GMA	A-1/4% O_2	320	32	13	47,300	13
	GMA	A-1% O_2	330	31	13	47,200	11
	GMA	A-2% O_2	315	30	13	43,600	11
5% Ni	GTA	Argon	300	16	7	41,100	42
	GTA	A-1/4% O_2	290	17	6 1/2	45,500	37
	GMA	Argon	280	37	13	47,800	11
	GMA	A-1/4% O_2	315	33	13	48,000	11
	GMA	A-1% O_2	330	30 1/2	13	46,500	11
	Hot Wire GTA	A-75% He	515	13	12	-	13
	Hot Wire GTA	A-75% He-1/2% O_2	515	13	12	-	14

Table 5

Chemical Analysis of Test Weld Metals

Filler Wire	Process	Shielding Gas	Percent or Parts Per Million												
			C	Mn	P	S	Si	Ni	Cr	Mo	V	Al	N	O	H
3% Ni	GTA	Argon	0.11	1.75	<0.002	<0.002	0.29	2.83	0.45	0.86	N.D.	0.014	10	6	<1
	GTA	A-0.25% O_2	0.08										20	55	<1
	GMA	Argon	0.10	1.85	<0.002	<0.002	0.30	2.95	0.50	0.88	N.D.	0.018	20	24	<1
	GMA	A-0.25% O_2	0.10										40	60	<1
	GMA	A-1.0% O_2	0.10										10	105	<1
	GMA	A-2.0% O_2	0.11										20	214	N.D.
5% Ni	GTA	Argon	0.11	0.77	0.013	0.006	0.37	5.0	0.62	0.51	<0.01	0.007	30	14	<1
	GTA	A-0.25% O_2	0.08										40	42	N.D.
	GMA	Argon	0.12		0.011	0.008							30	14	<1
	GMA	A-0.25% O_2	0.10										50	107	<1
	GMA	A-1.0% O_2	0.10		0.007	0.005							40	117	<1
	Hot Wire GTA	A-75% He	0.16	0.78	0.013	0.007	0.37	5.0	0.71	0.53	<0.01	0.009	40	11	N.D.
	Hot Wire GTA	A-75% He-0.5% O_2	N.D.										50	17	N.D.

Notes:
N.D. - Not Determined
O, H, N in ppm

Table 6

Properties of Test Weld Metals

A. 3% Ni Wire

Process	Shielding Gas	Analysis O (ppm)	Analysis C (%)	Tensile Data: 0.2% Yield Str. (ksi)	Tensile Data: Ultimate Tensile Str. (ksi)	Tensile Data: % Red. in Area	Charpy V-Notch Data: 50 ft-lb Trans. Temp. (°F)	Charpy V-Notch Data: Energy at 75°F (ft-lbs)
GTA	Argon	6	0.11	139.6	146.8	75	-250	140
GTA	A-0.25% O_2	55	0.08	117.0	143.0	59	-190	150
GMA	Argon	24	0.10	118.3	142.6	68	-200	125
GMA	A-0.25% O_2	60	0.10	127.0	146.3	66	- 95	122
GMA	A-1.0% O_2	105	0.10	124.5	148.5	56	+ 40	52
GMA	A-2.0% O_2	214	0.11	125.4	146.9	59	*	43

B. 5% Ni Wire

Process	Shielding Gas	Analysis O (ppm)	Analysis C (%)	Tensile Data: 0.2% Yield Str. (ksi)	Tensile Data: Ultimate Tensile Str. (ksi)	Tensile Data: % Red. in Area	Charpy V-Notch Data: 50 ft-lb Trans. Temp. (°F)	Charpy V-Notch Data: Energy at 75°F (ft-lbs)
GTA	Argon	14	0.11	144.7	154.4	70	-250	118
GTA	A-0.25% O_2	42	0.08	129.8	152.0	62	-230	150
GMA	Argon	14	0.12	139.3	160.1	45	- 70	62
GMA	A-0.25% O_2	107	0.10	136.8	147.1	63	- 80	79
GMA	A-1.0% O_2	117	0.10	133.0	157.0	58	- 70	67
Hot Wire GTA	A-75% He^2	11	0.16	132.7	150.8	50	- 95	70
Hot Wire GTA	A-75% He-0.5% O_2	17	N.D.	130.5	151.6	56	- 75	74

Note: Tensile data are averages of duplicate or triplicate specimens
* Did not attain 50 ft-lbs in tests as high as 212 °F

Table 7

Fracture Characteristics of Charpy Test Specimens

Oxygen content of weld	3% Ni		5% Ni		
	GTA Process	GMA Process	GTA Process	GMA Process	Hot Wire GTA Process
Low, <30 ppm	Very fine dimples, mean approx. 1 micron. Few particles extracted, mainly type A.	Duplex dimples, approx. 1 to 1.5 microns. Particles mainly type A.	Very fine dimples, 1 micron or less. Few particles extracted, clusters of type A.	Dimples larger than GTA, mean approx. 1 micron some duplex. Few particles extracted, mostly clusters type A, some type B	Dimples comparable to GMA, mean 1 micron. Many particles, mostly type A, some B.
Intermediate, 30-105 ppm	Very large duplex dimples, mean 5-10 microns. Types A & B particles.	Very large dimples, mean 6-7 microns. Types A & B particles	Large dimples, mean 3-4 microns. Types A & B particles	Very large dimples with duplexing, mean 7-10 microns. Many particles types A & B.	
High (GMA welds with 1 & 2% O_2), >100 ppm		Large dimples mean 2-3 microns each containing one type C particle and groups of type A.		Large dimples mean 3 microns each containing one type C particle and groups of type A.	

Table 8

Electron Diffraction Data for Identification of "Type A" Particles as Iron Silicate

Unknown Diffraction Ring	Unknown d_{hkl} (Å)	Fe_2SiO_4 d_{hkl} (Å) Calc.*	Fe_2SiO_4 hkl
1	2.43	2.48	311
2	2.01	2.06	400
3	1.50	1.46	440
4	1.398	1.392	315
5	1.147	1.142	460
6	1.001	0.999	446, 820
7	0.896	0.899	824
8	0.825	0.824	860, 1000

Iron Silicate (Fe_2SiO_4)

System - Cubic (Face Centered)

$a_o = 8.235$ Å(62)

* d_{hkl} for Fe_2SiO_4 from calculated values in Appendix A

Note: Lines lower than 311 not measurable due to high background noise from the central spot and the diffuse carbon ring.

Table 9

Electron Diffraction Data for Identification of "Type B" Particles as Silicon Dioxide (Beta Quartz)

Unkown d_{hkl} (Å) (spot pattern)	SiO_2 d_{hkl} (Å) Calc.*	SiO_2 hkl
4.46	4.43	100
2.59	2.56	110
2.22	2.21	200
1.64	1.67	210
1.49	1.48	300
1.30	1.28	220
1.26	1.23	310
1.12	1.11	400
1.03	1.02	320
0.977	0.966	410
0.873	0.885	500

Silicon Dioxide (SiO_2) Beta Quartz

System - Hexagonal

$a_o = 5.11$ Å, $c_o = 5.37$ Å(63)

Zone axis for pattern above is [001]

*d_{hkl} for SiO_2 (beta quartz) from calculated values in Appendix B

Table 10

Electron Diffraction Data for Identification of "Type C" Particles as Silicon Dioxide (Beta Quartz)

Unknown d_{hkl} (Å) (spot pattern)	SiO_2 d_{hkl} (Å) Calc.*	SiO_2 hkl
2.33	2.31	111
2.14	2.21	200
2.06	2.05	201
1.86	1.85	112
1.62	1.60	211
1.24	1.24	221
1.15	1.15	222

Silicon Dioxide (SiO_2) Beta Quartz

System - Hexagonal

$a_o = 5.11$ Å, $c_o = 5.37$ Å[63]

* d_{hkl} for SiO_2 (beta quartz) from calculated values in Appendix B

Table 11

Keyhole Tests Conducted

Filler Wire	Process	Shielding Gas	Amps	Volts	Travel Speed (ipm)	Heat Input (joules/in)	Result
3% Ni	GTA	A	290	17	6	49,300	No Crack
		A-3.1 ppm H_2	304	16	6	48,600	No Crack
		A-6.2 ppm H_2	296	16	6	47,400	No Crack
		A-470 ppm H_2	300	16	6	48,000	No Crack
		A-835 ppm H_2	295	17	6	50,100	No Crack
		A-1140 ppm H_2	298	16	6	47,700	No Crack
		A-2280 ppm H_2	300	16	6	48,000	No Crack
		A-3565 ppm H_2	304	16	6	48,600	No Crack
		A-4850 ppm H_2	304	16	6	48,600	Cracked - 25 minutes
		A-1% H_2	300	16	6	48,000	Cracked - 2 hours
		A-2425 ppm H_2-0.26% O_2	304	18	6	54,700	No Crack
		A-5100 ppm H_2-0.21% O_2	296	17	6	50,300	No Crack
3% Ni	GMA	A	300	32	13	44,400	No Crack
		A-835 ppm H_2	280	32	13	41,400	No Crack
		A-1140 ppm H_2	320	32	13	47,300	Cracked - 22 minutes
		A-1140 ppm H_2-1% O_2	340	30	13	47,100	Cracked - > 4 hours
		A-500 ppm H_2-0.8% O_2	320	27	13	39,900	Cracked - 10 hours

(Continued)

Table 11 (Continued)

Keyhole Tests Conducted

Filler Wire	Process	Shielding Gas	Amps	Volts	Travel Speed (ipm)	Heat Input (joules/in)	Result
5% Ni	GTA	A	298	17	6	50,700	No Crack
		A-470 ppm H_2	300	16	6	48,000	No Crack
		A-835 ppm H_2	296	17	6	50,700	No Crack
		A-1% H_2	300	16	6	48,000	No Crack
		A-1.4% H_2	296	16	6	47,400	No Crack
		A-2% H_2	296	16	6	47,400	Cracked - 1 hour
		A-1% H_2-0.26% O_2	300	18	6	54,000	No Crack
		A-2% H_2-0.25% O_2	300	18	6	54,000	No Crack
5% Ni	GMA	A-835 ppm H_2	280	34	13	44,000	No Crack
		A-1140 ppm H_2	280	32	13	41,400	No Crack
		A-2280 ppm H_2	260	36	13	43,200	No Crack
		A-4850 ppm H_2	265	34	13	41,600	No Crack
		A-8000 ppm H_2	300	35	13	48,500	Cracked - 2 hours, 15 min
		A-1% H_2	275	36	13	45,400	Cracked - 5 hours, 30 min
		A-2% H_2	275	37	13	47,000	Cracked - 2 hours
		A-4300 ppm H_2-1% O_2	355	32	13	52,500	Cracked - 18 minutes

Table 12

Summary of Keyhole Test Results

Process	Highest Hydrogen Content Welded Without Cracking	Lowest Hydrogen Level at which Cracking Occurred	Effect of Oxygen Additions (GTA-1/4% O_2; GMA-1% O_2)
		3% Ni Wire	
GTA	3565 ppm	4850 ppm	No crack at 5100 ppm H_2
GMA	835 ppm	1140 ppm	Cracked at 500 ppm H_2
		5% Ni Wire	
GTA	1.4%	2%	No crack at 2% H_2
GMA	4850 ppm	8000 ppm	Cracked at 4300 ppm H_2

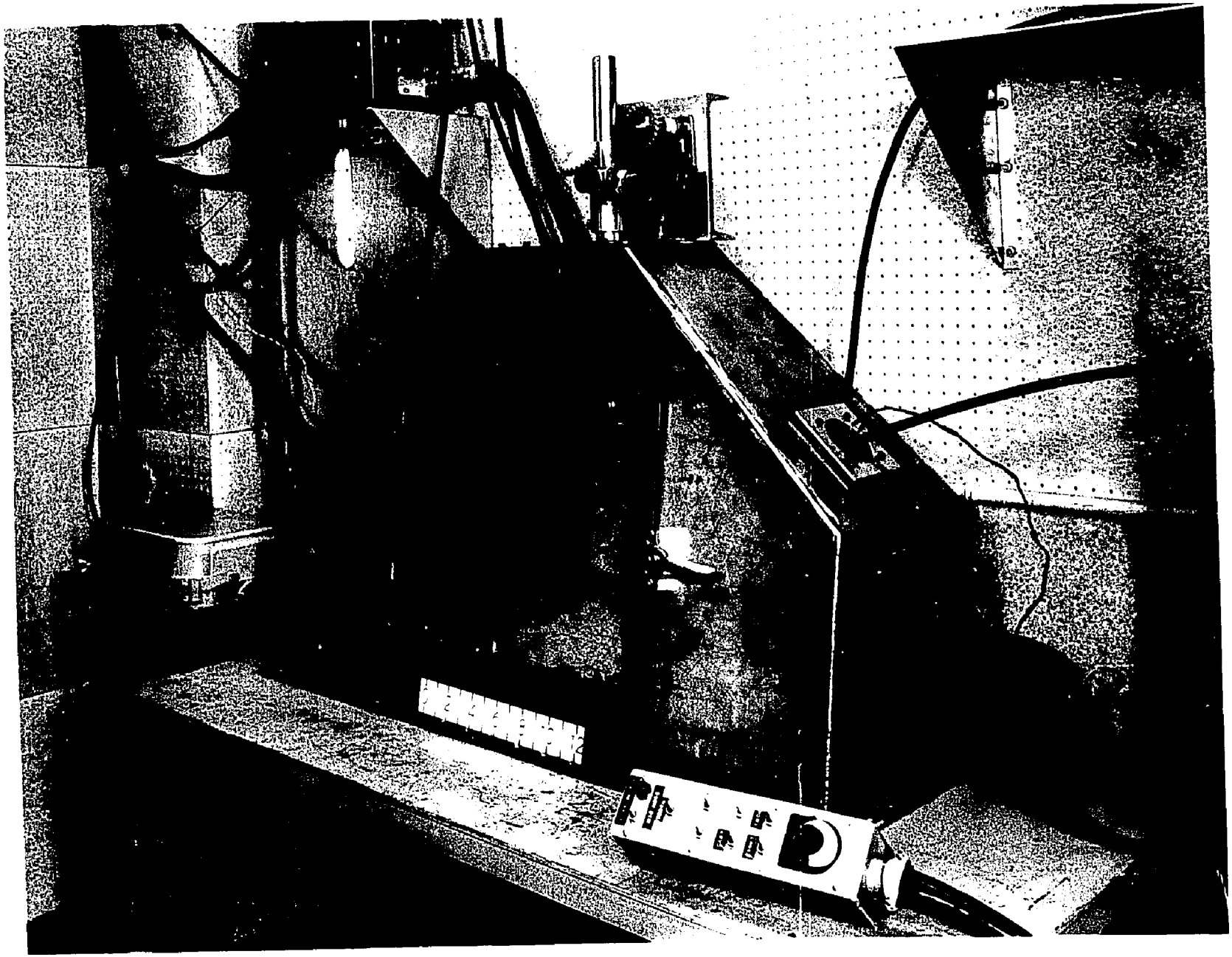

Figure 1 - Overall view of welding chamber.

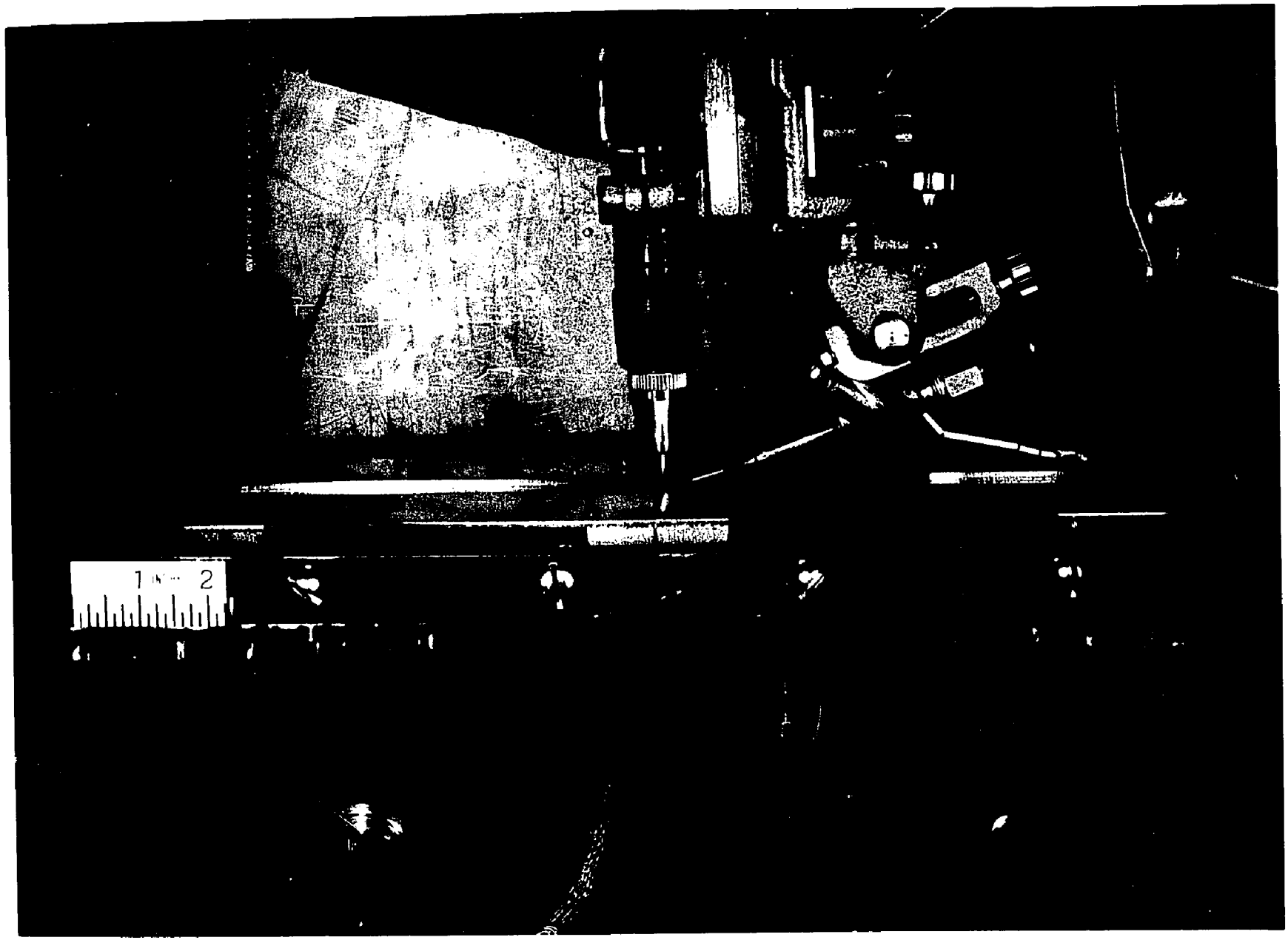

Figure 2 - View of interior of welding chamber.

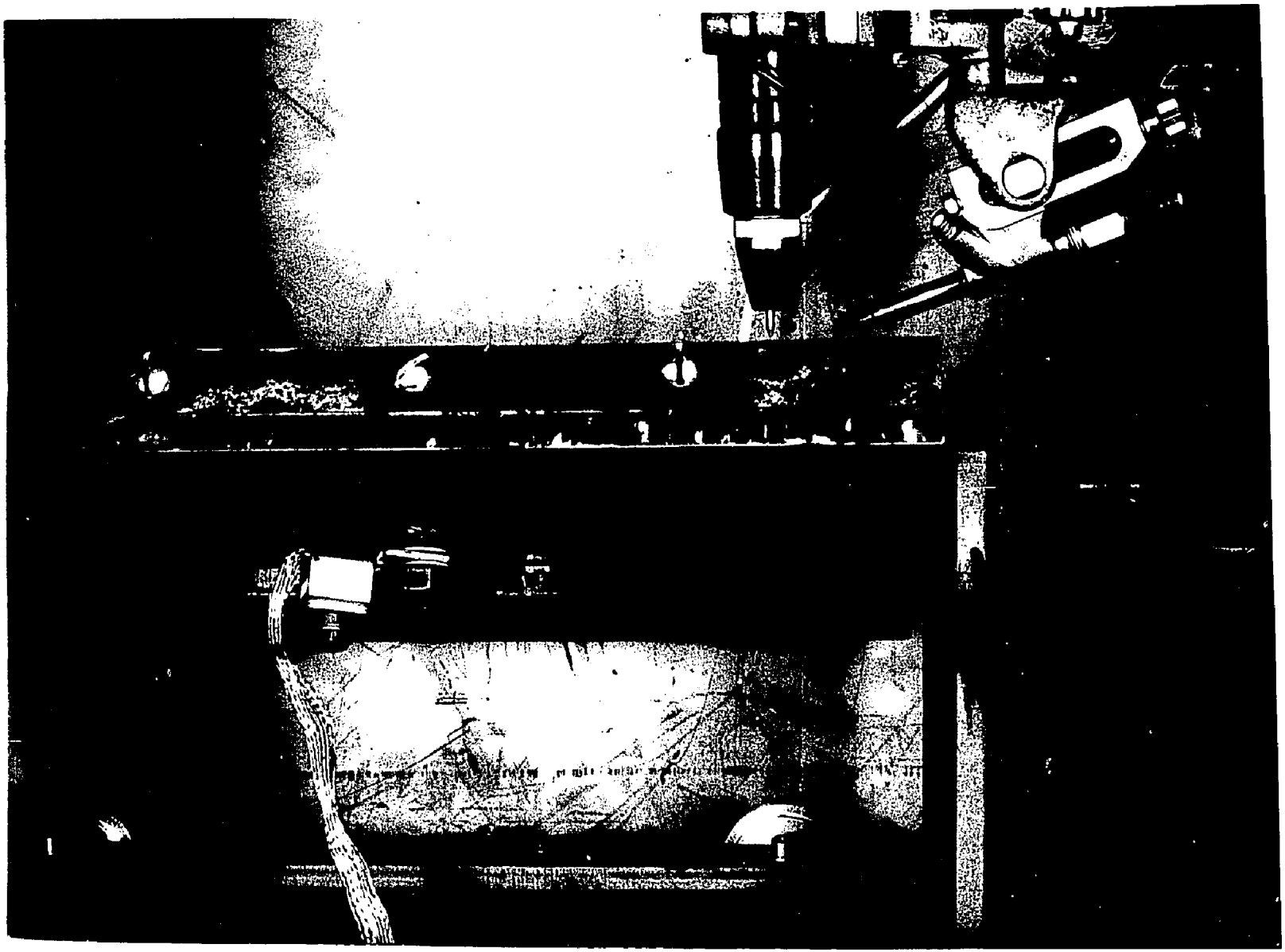

Figure 3 - View of carriage in chamber showing movable ground arrangement.

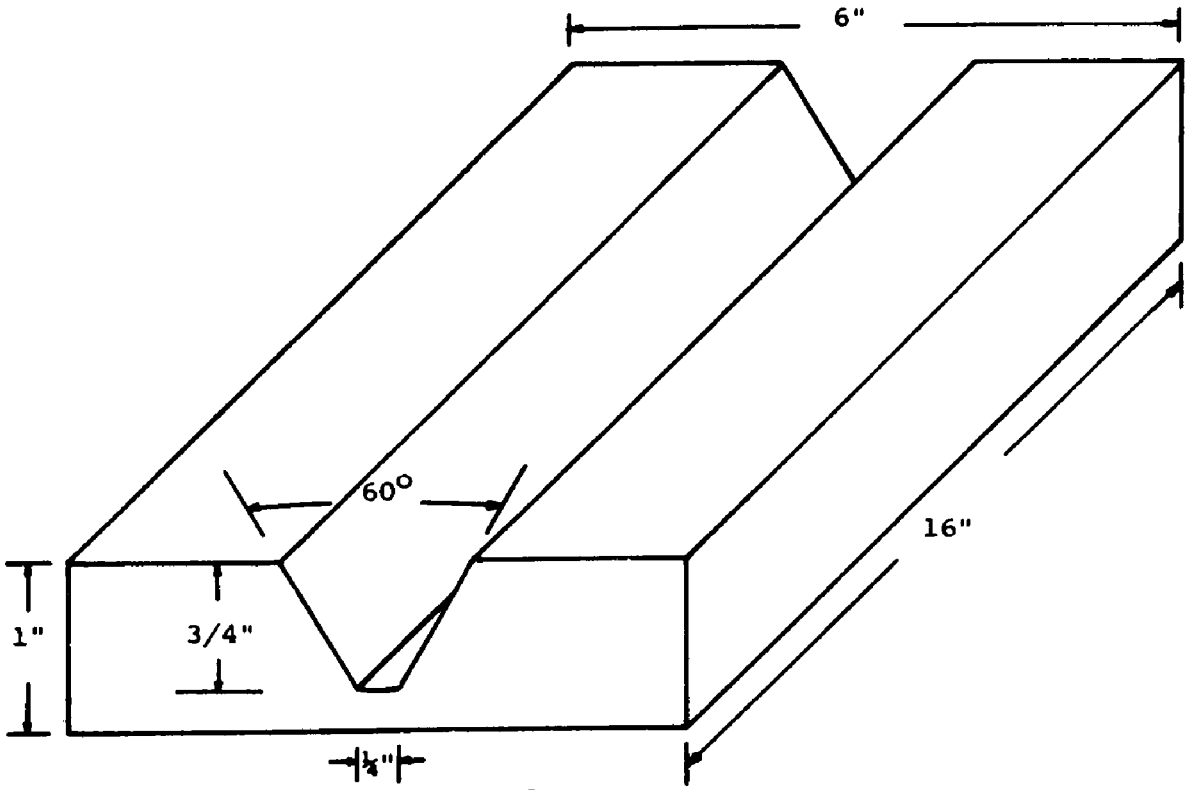

a. Details of test plate and welding groove

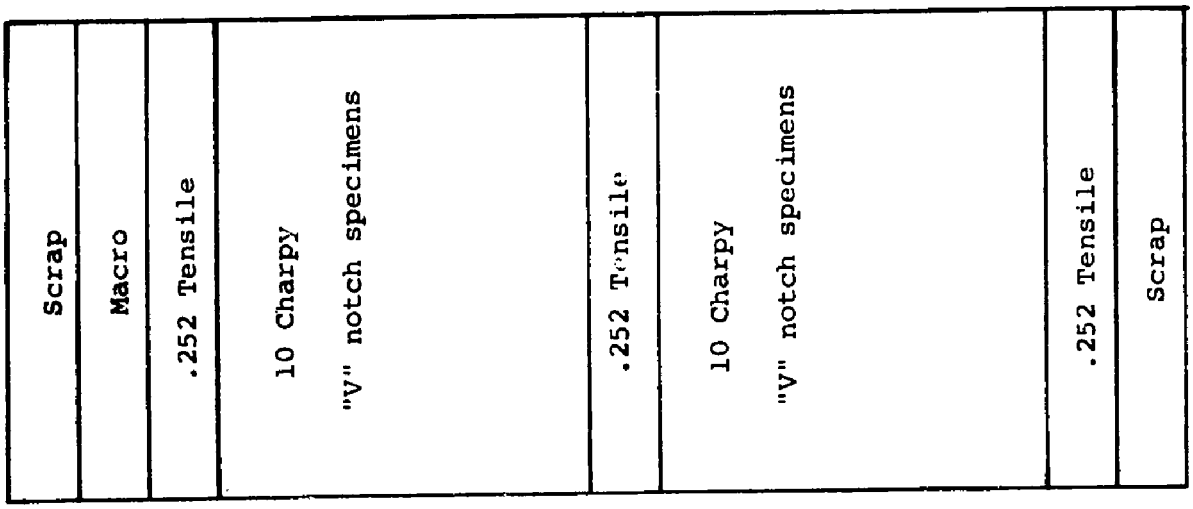

b. Selection of specimens

Figure 4 - Joint design and selection of specimens.

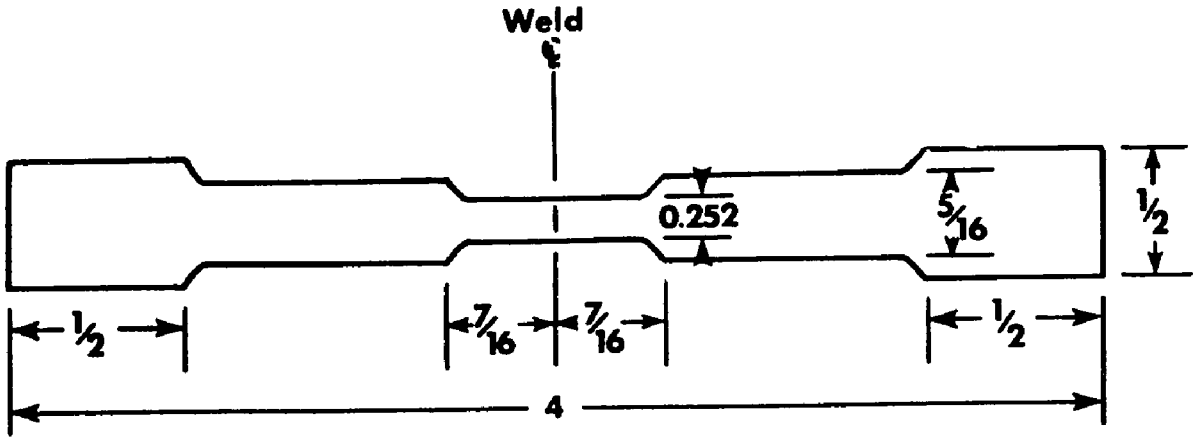

Figure 5- Details of tensile specimen (Dimensions in inches)

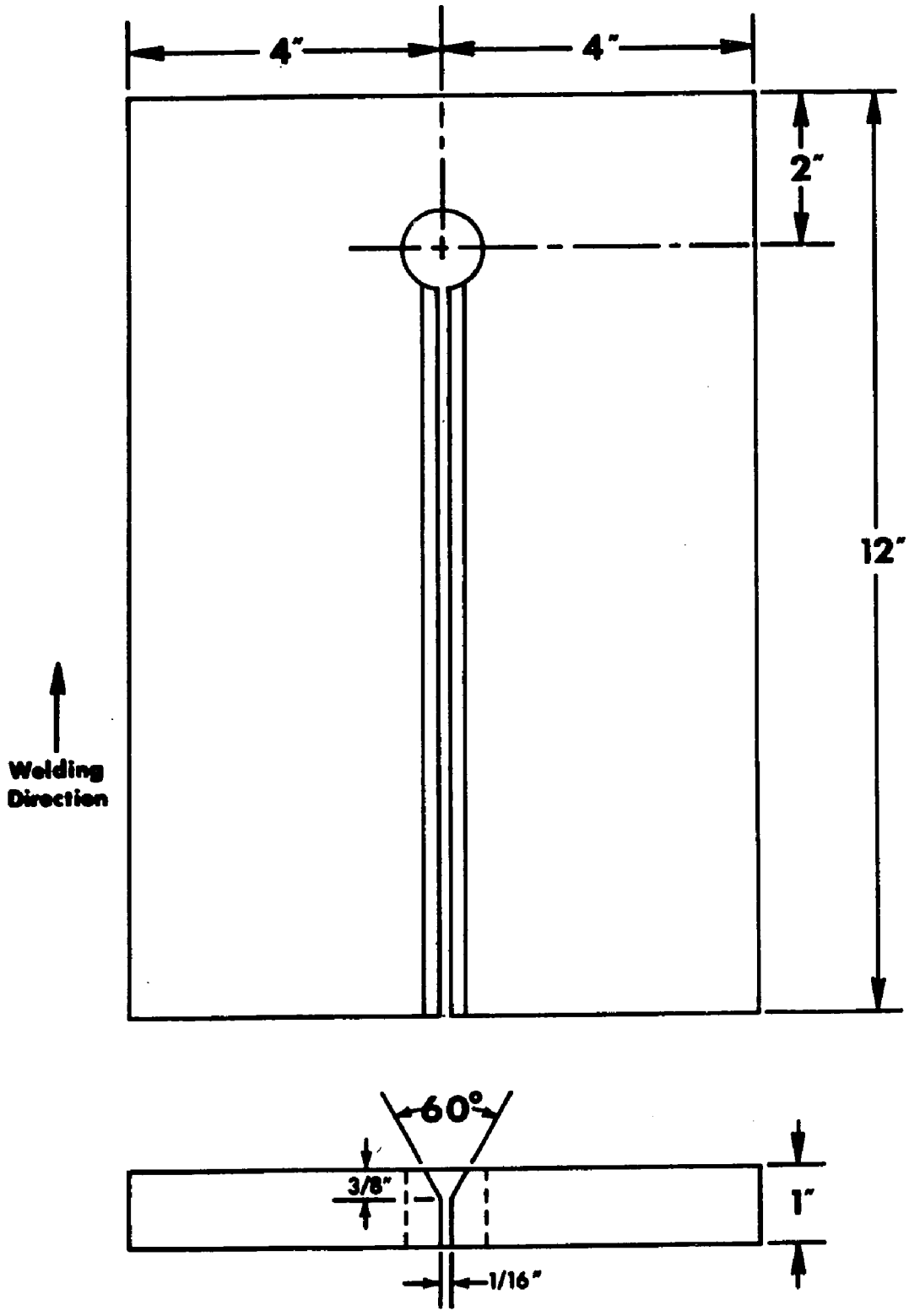

Figure 6 - Dimensions of Keyhole slotted plate restraint specimen.

Figure 7 - Keyhole specimen ready for welding.

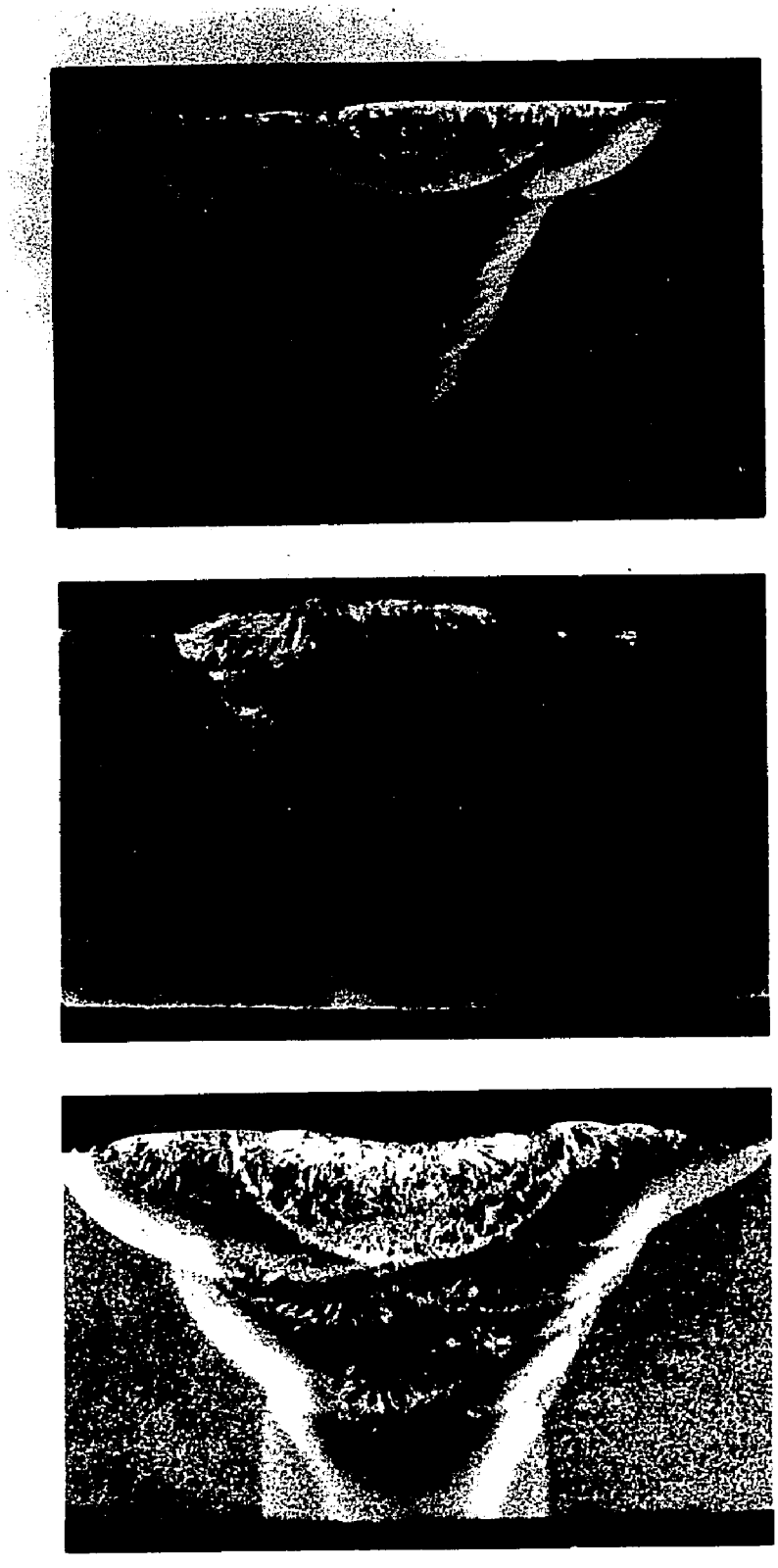

Figure 8 - Macrographs of weld cross sections-pure inert gas shielding. Ammonium persulfate etch, 2 diameters.

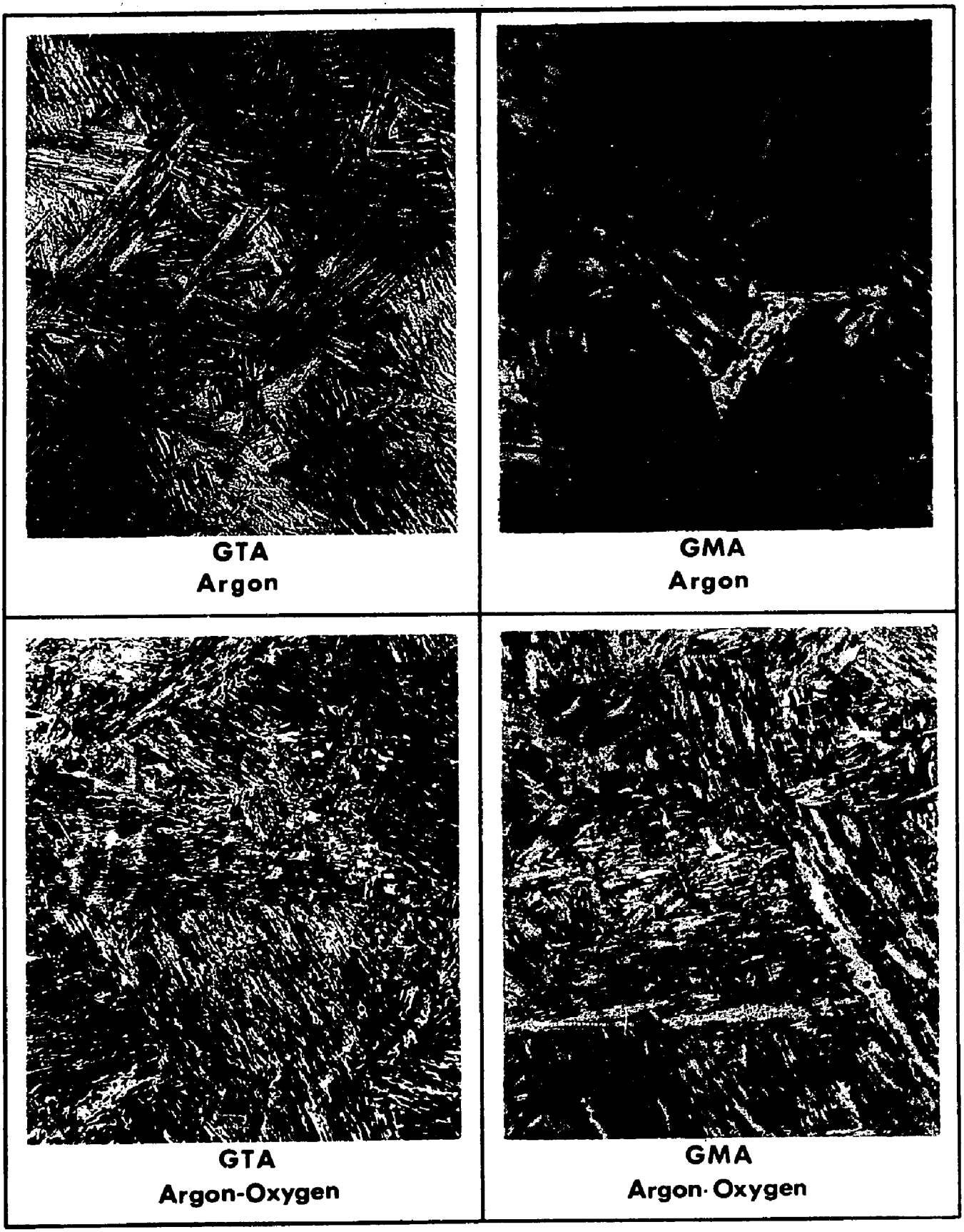

Figure 9 - Representative microstructures of 3% Ni welds-last bead deposited. 2% Nital etch, 500 diameters (reduced 22% by reproduction).

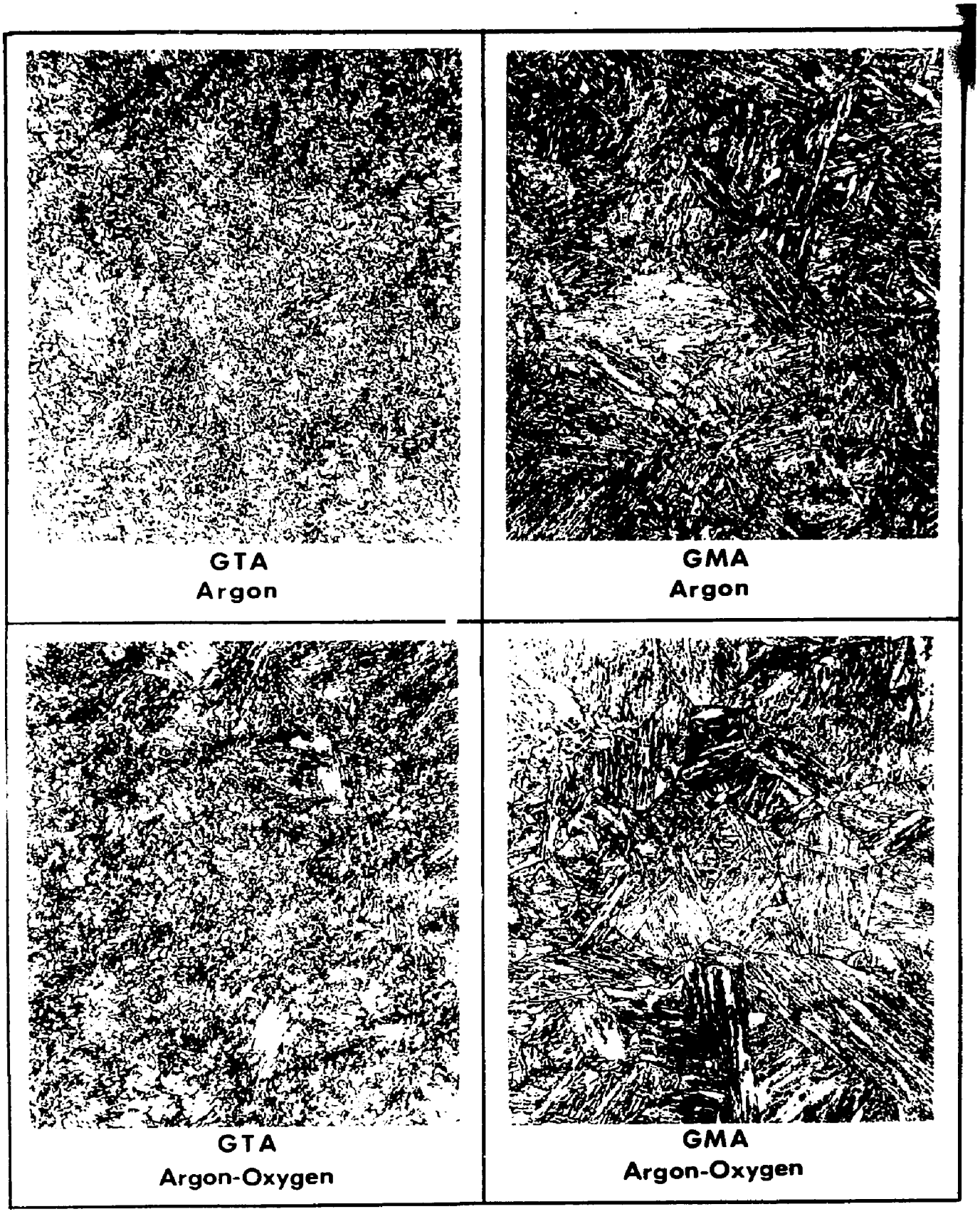

Figure 10 - Representative microstructures of 3% Ni welds-interior weld beads. 2% Nital etch, 500 diameters (reduced 22% by reproduction).

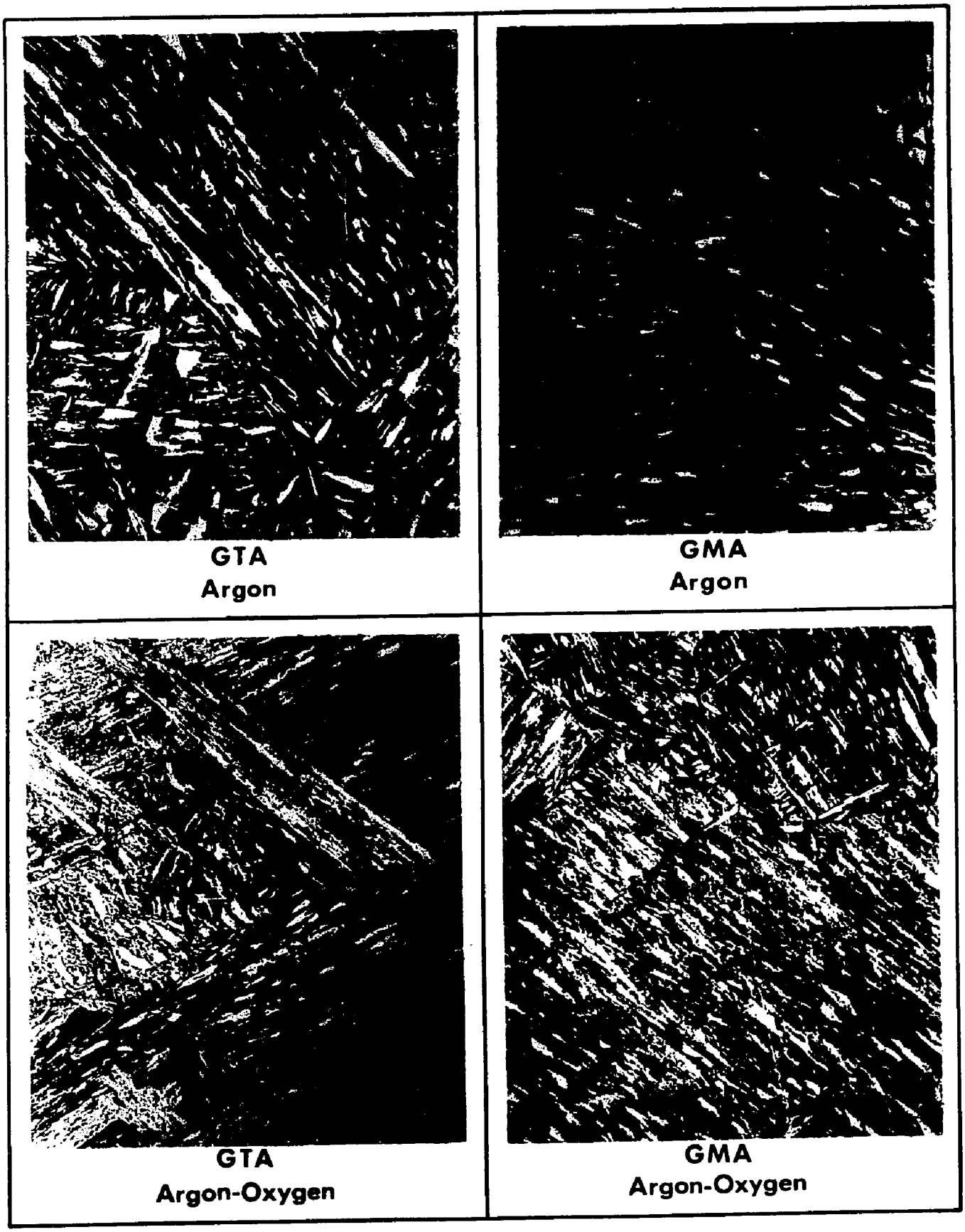

Figure 11 - Representative microstructures of 5% Ni welds-last bead deposited. 2% Nital etch, 500 diameters (reduced 22% by reproduction).

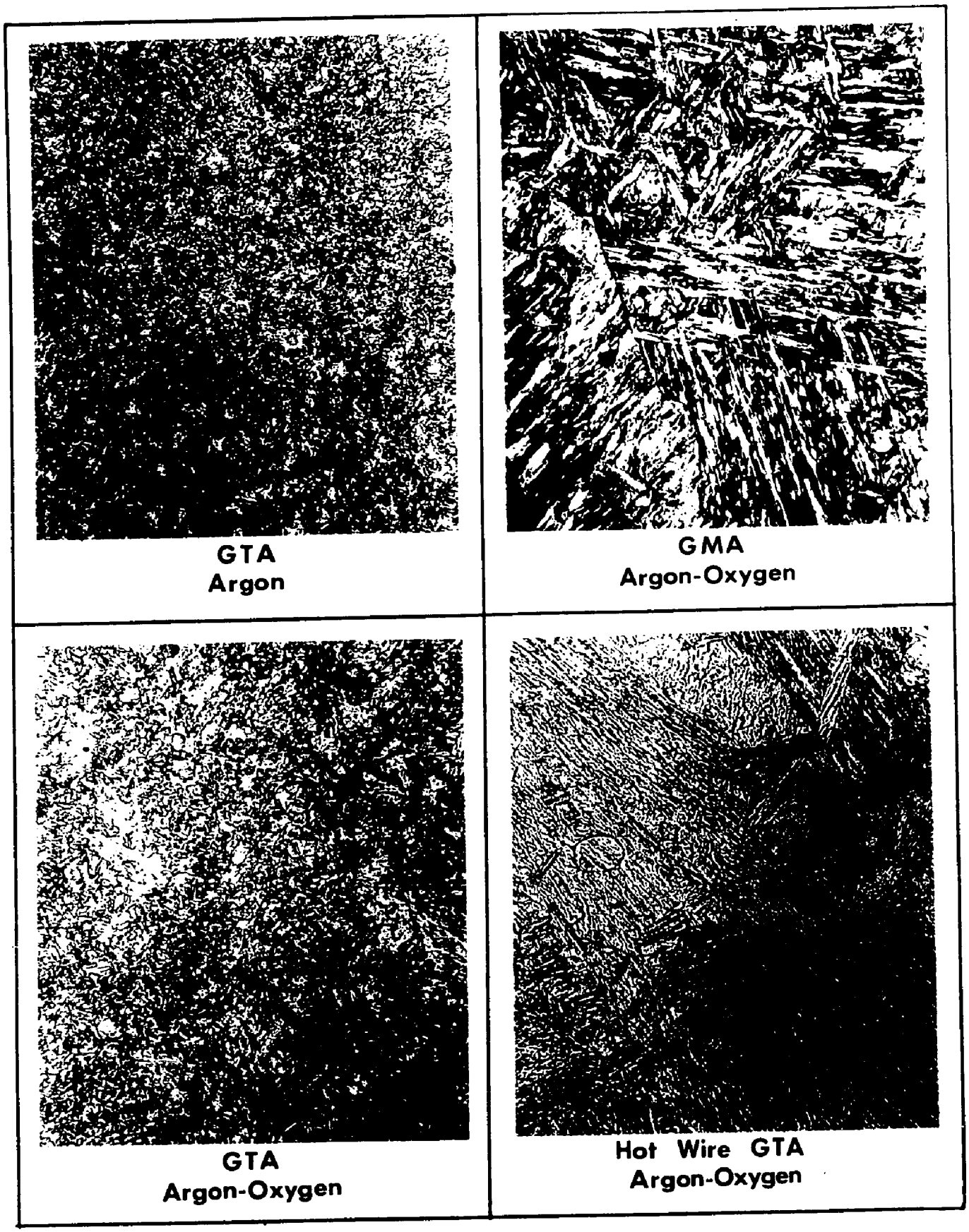

Figure 12 - Representative microstructures of 5% Ni welds-interior weld beads. 2% Nital etch, 500 diameters (reduced 22% by reproduction).

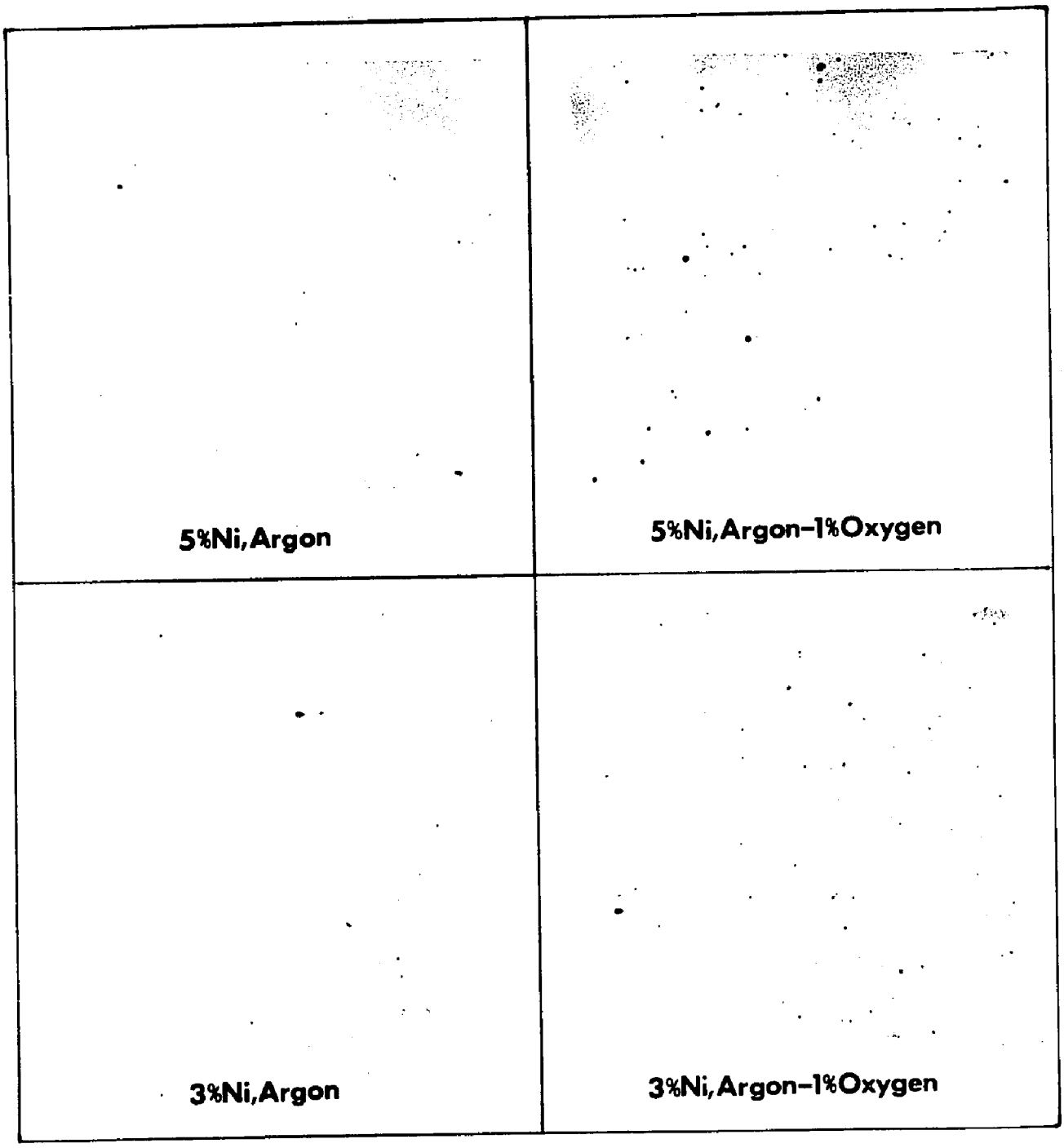

Figure 13 - Relative cleanliness of GMA weld metals deposited in argon and argon-1% oxygen.
Unetched, 750 diameters (reduced 26% by reproduction).

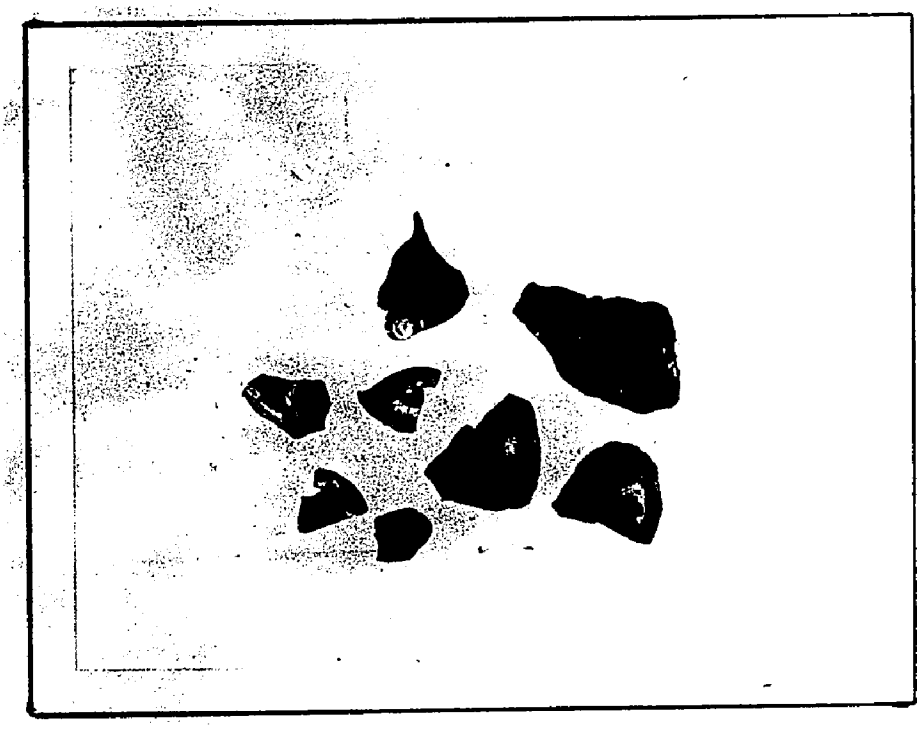

Figure 14 - Example of slag on 3% Ni, argon-2% oxygen weld. 2.5 diameters.

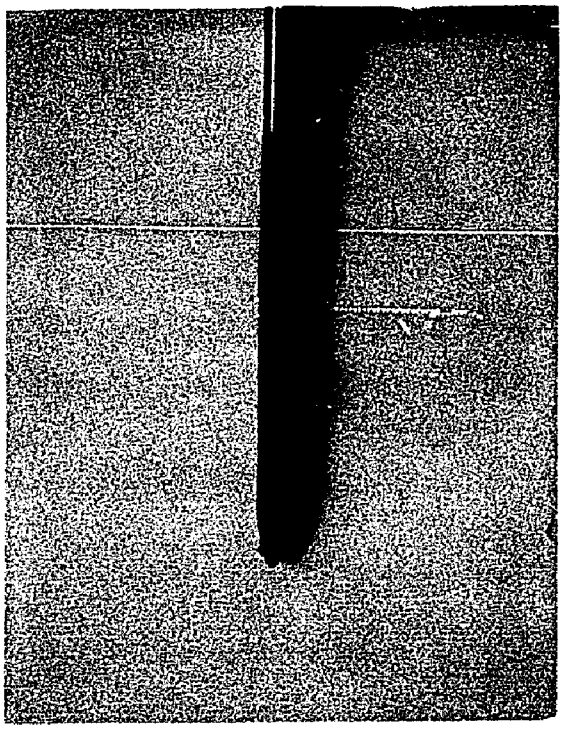

Figure 15- Appearance of tungsten electrode after welding under argon- 0.25% oxygen.

Argon

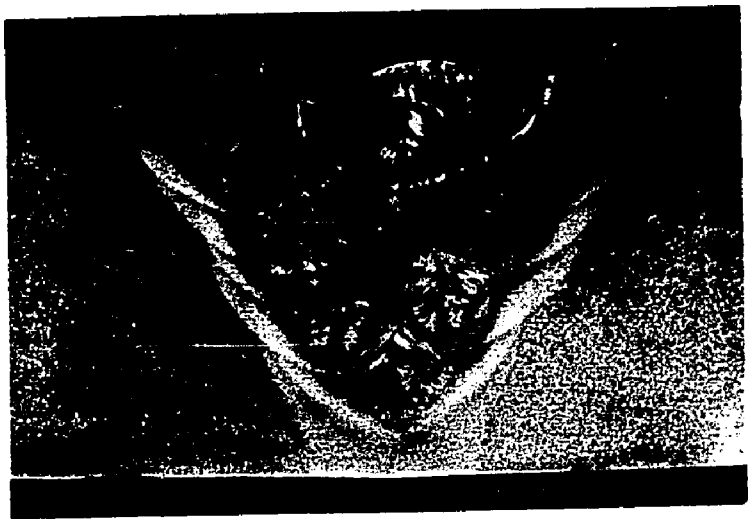

Argon–1%Oxygen

Figure 16 - Appearance of GMA welds deposited under pure argon and argon-1% oxygen.
Ammonium persulfate etch, 2 diameters.

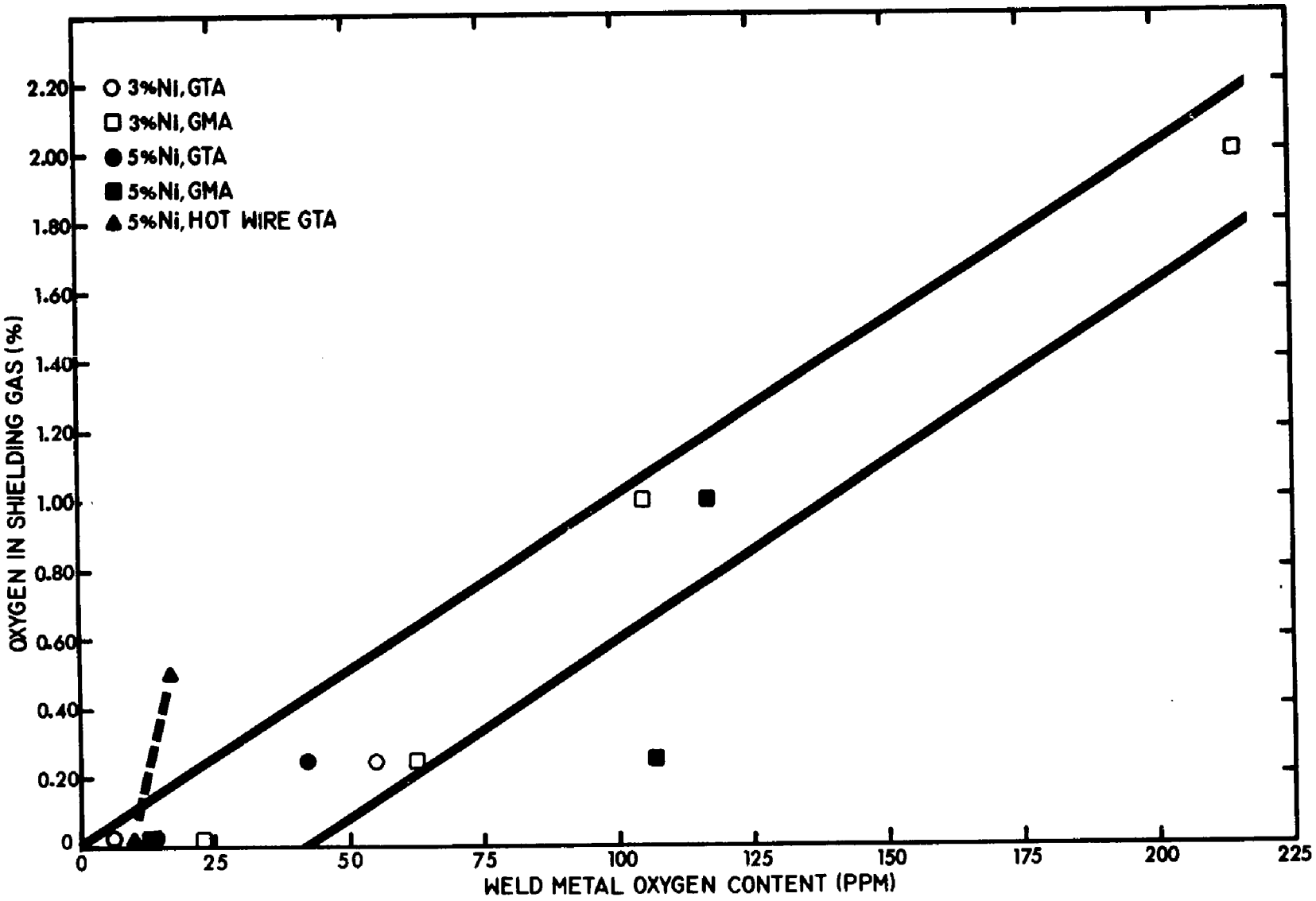

Figure 17 - Variation of weld metal oxygen content as a function of weld shielding gas.

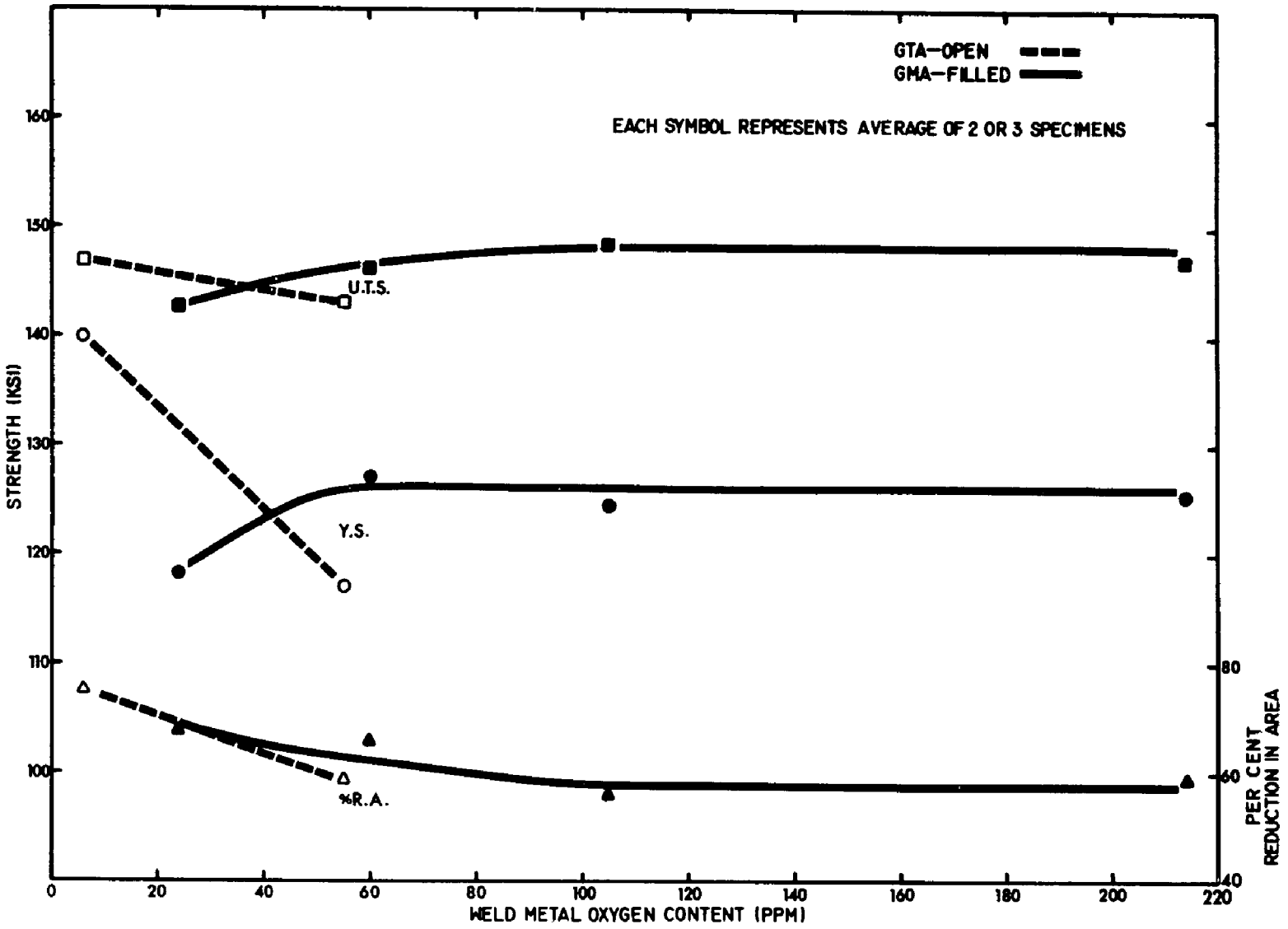

Figure 18 - Variation of tensile properties as a function of weld metal oxygen content. 3% Ni welds.

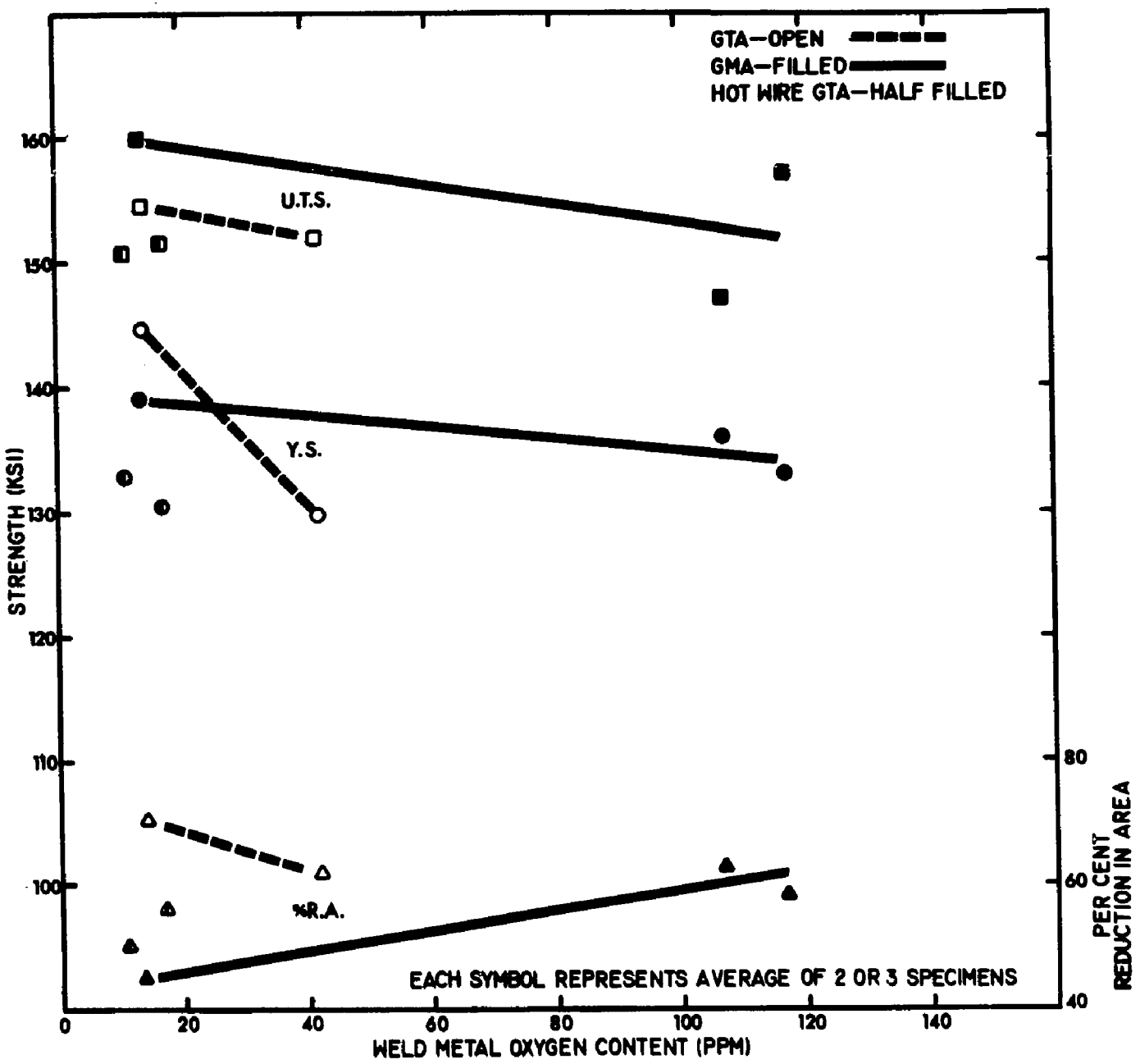

Figure 19 - Variation of tensile properties as a function of weld metal oxygen content. 5% Ni welds.

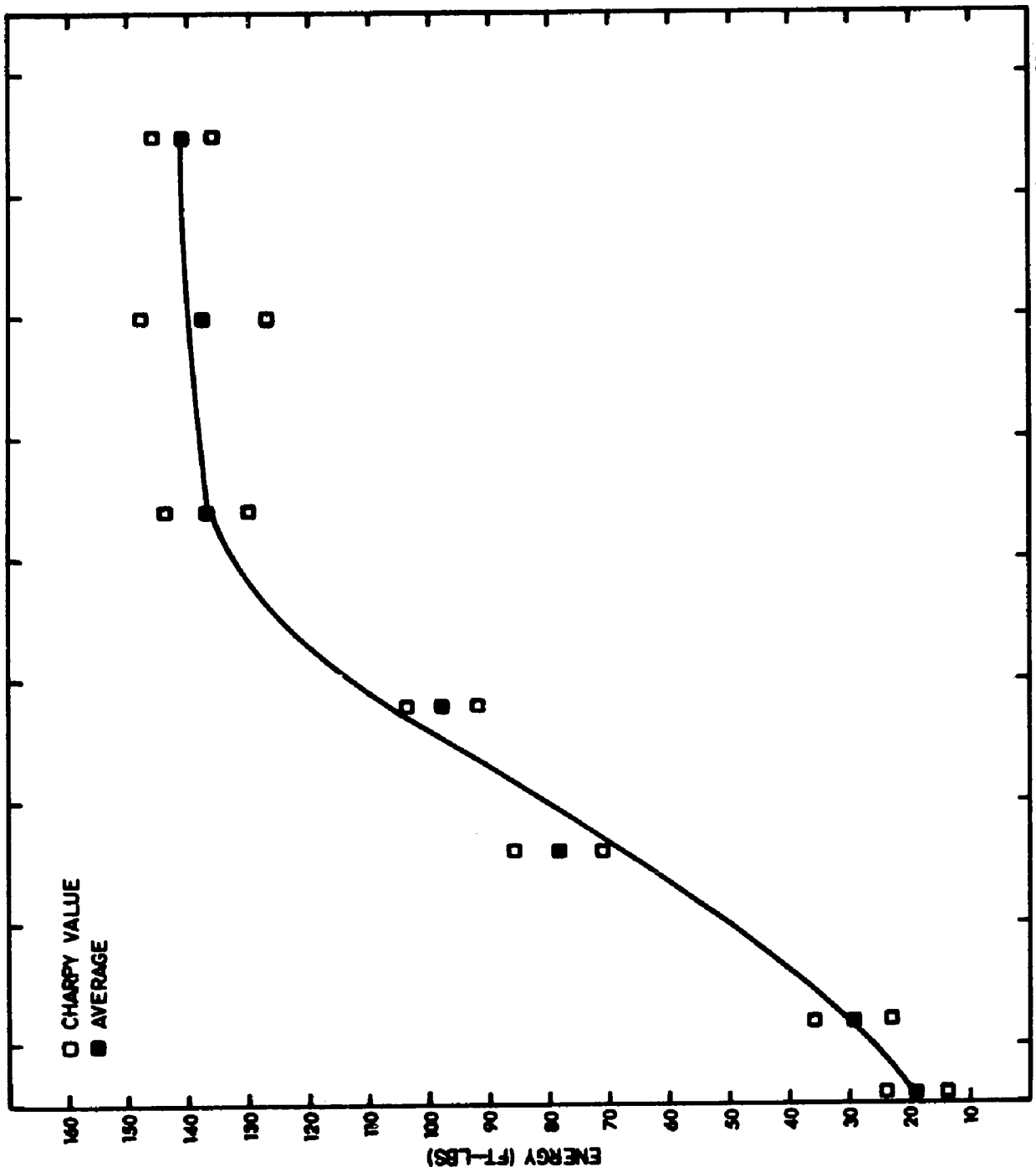

Figure 20 - Charpy V-notch energy-temperature curve.
3% Ni, GTA, pure argon shielding gas.

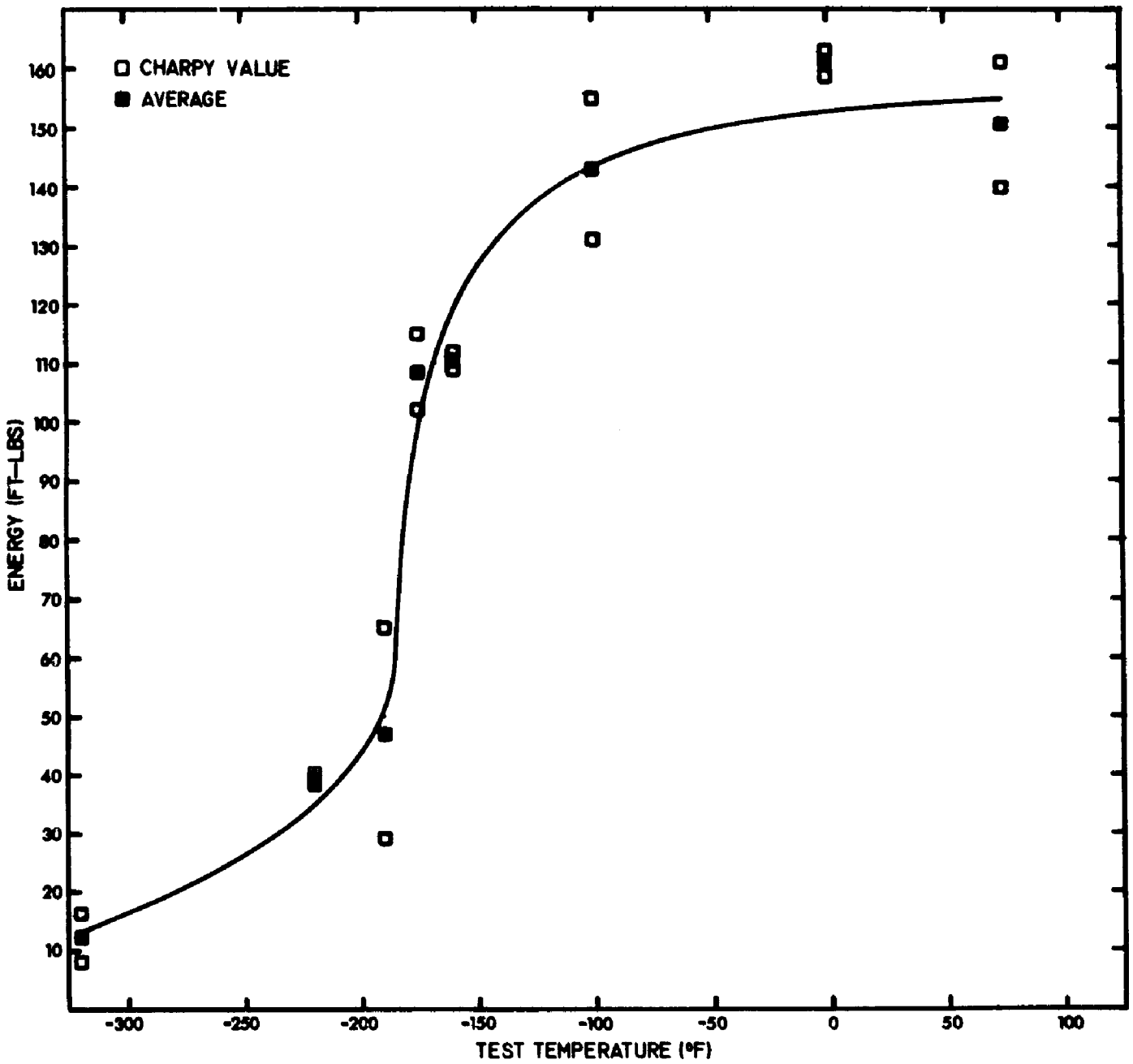

Figure 21 - Charpy V-notch energy-temperature curve.
3% Ni, GTA, argon-0.25% oxygen shielding gas.

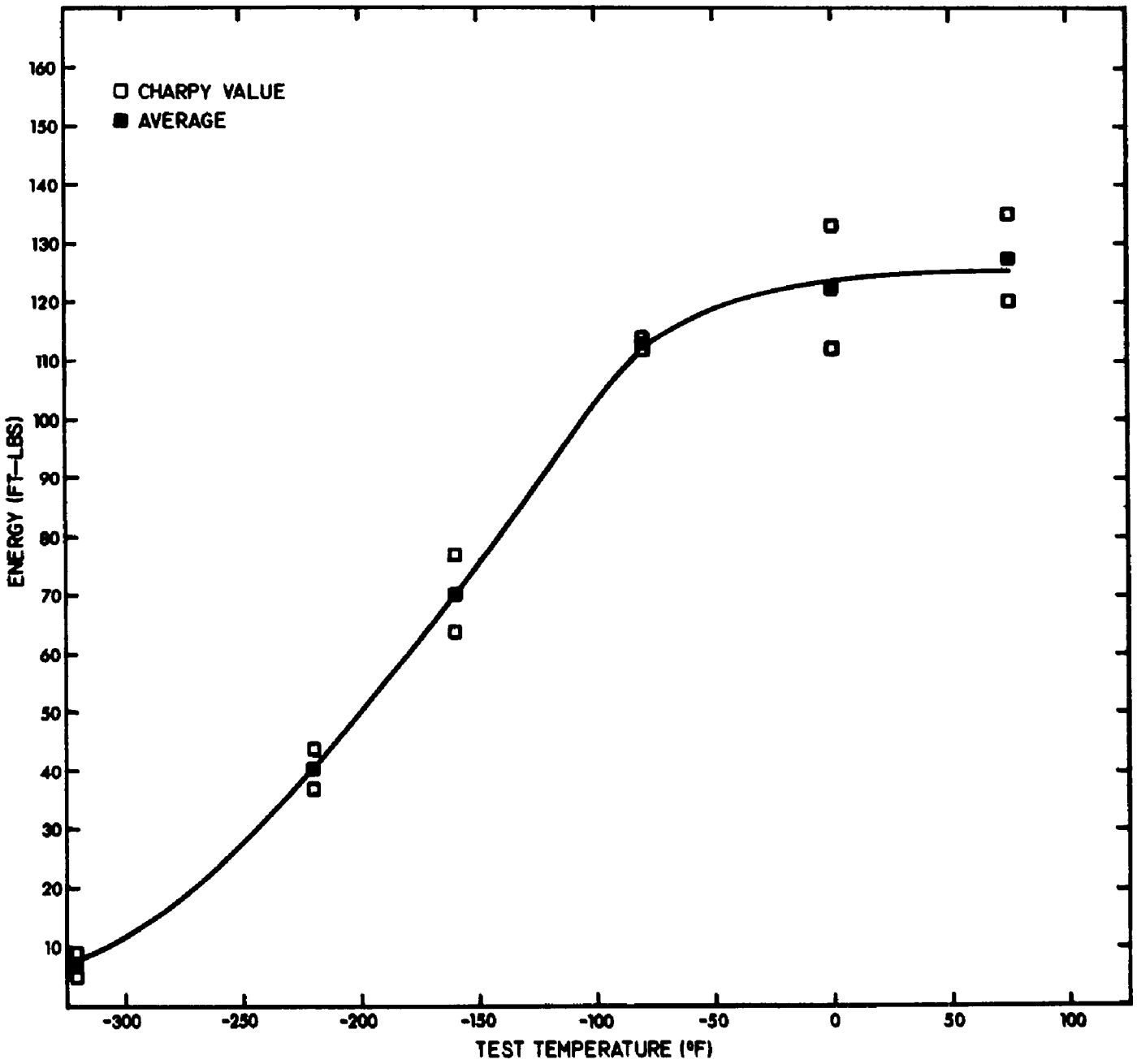

Figure 22 - Charpy V-notch energy-temperature curve.
3% Ni, GMA, pure argon shielding gas.

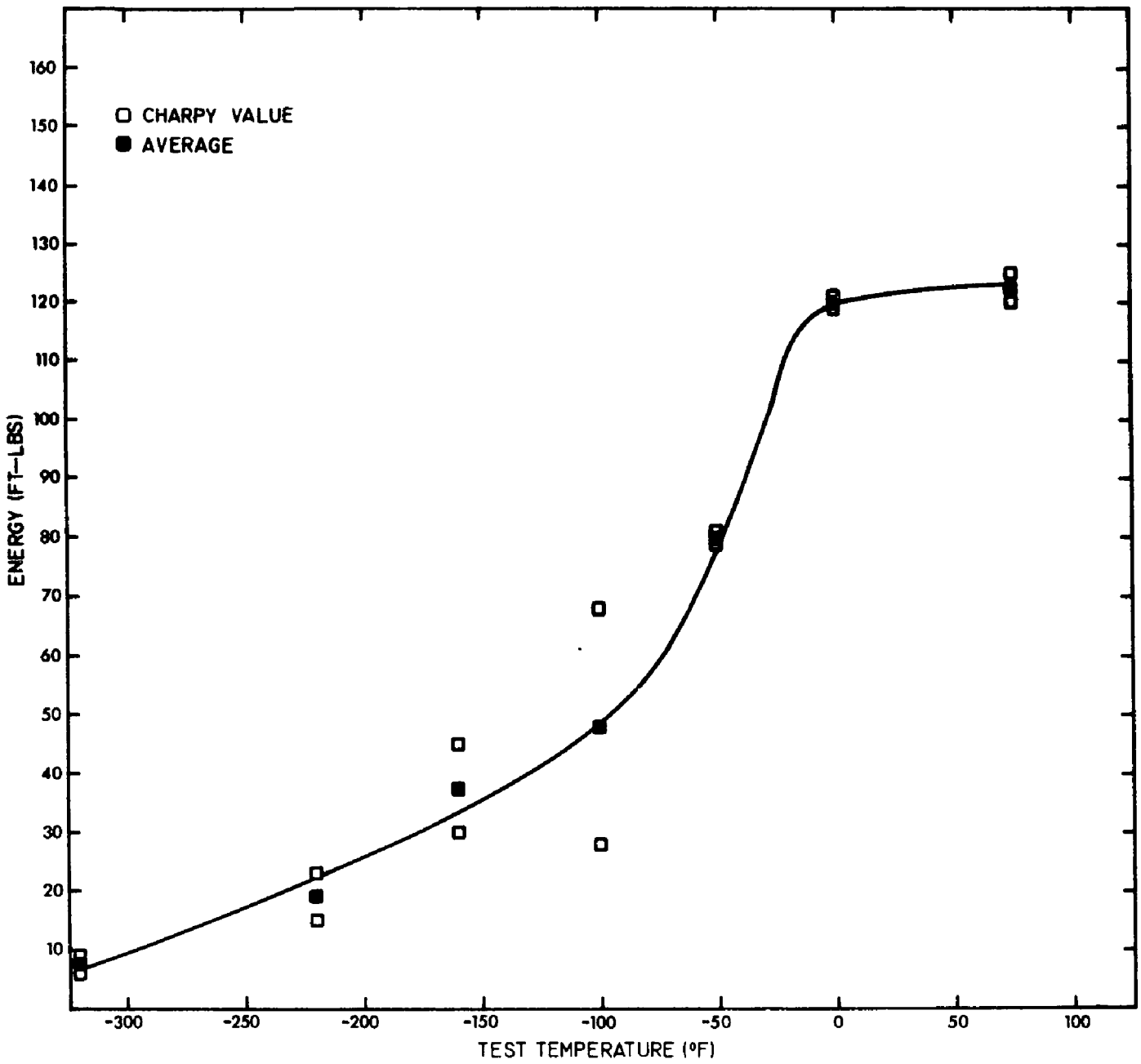

Figure 23 - Charpy V-notch energy-temperature curve.
3% Ni, GMA, argon-0.25% oxygen shielding gas.

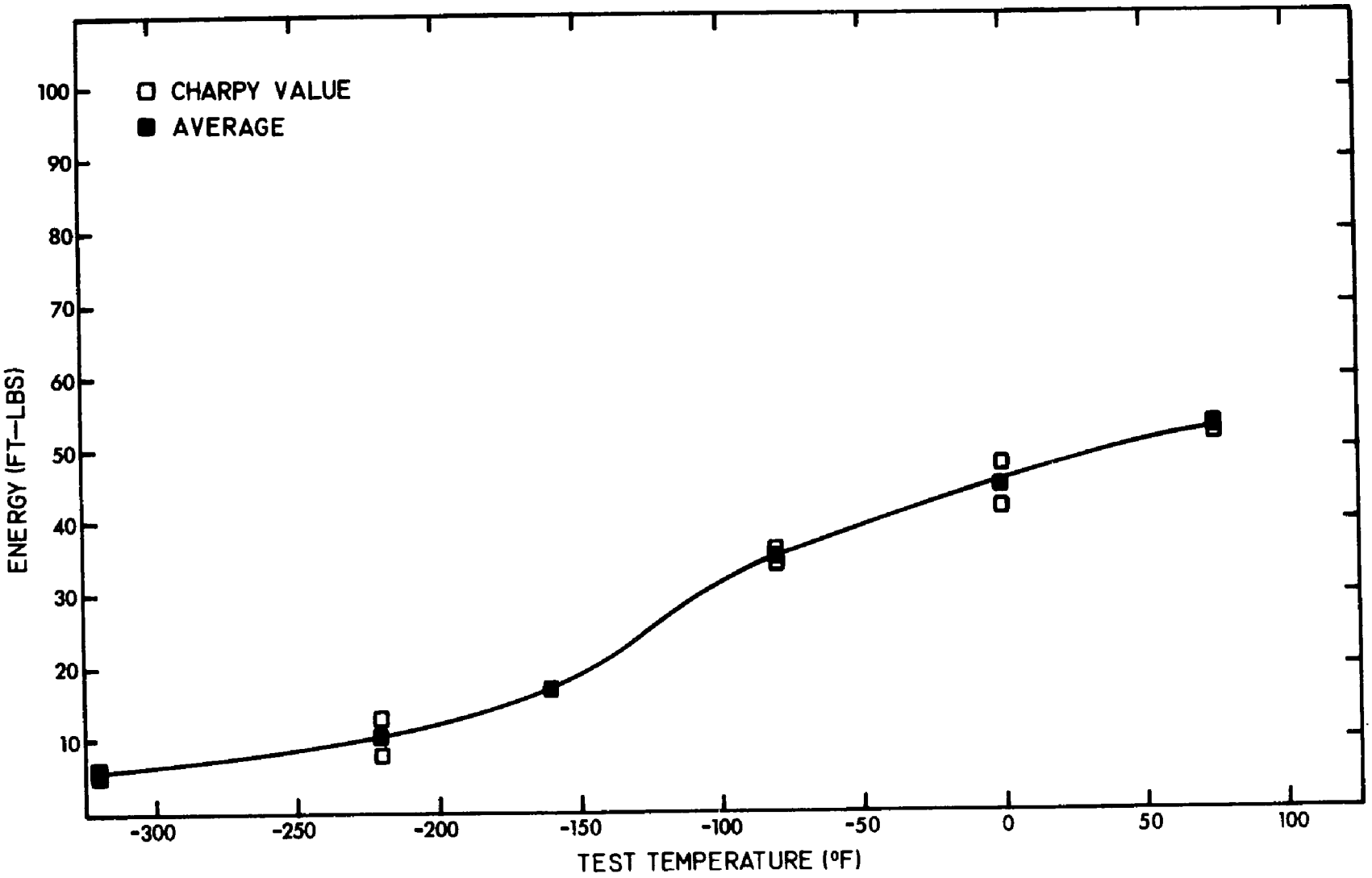

Figure 24 - Charpy V-notch energy-temperature curve.
3% Ni, GMA, argon-1.0% oxygen shielding gas.

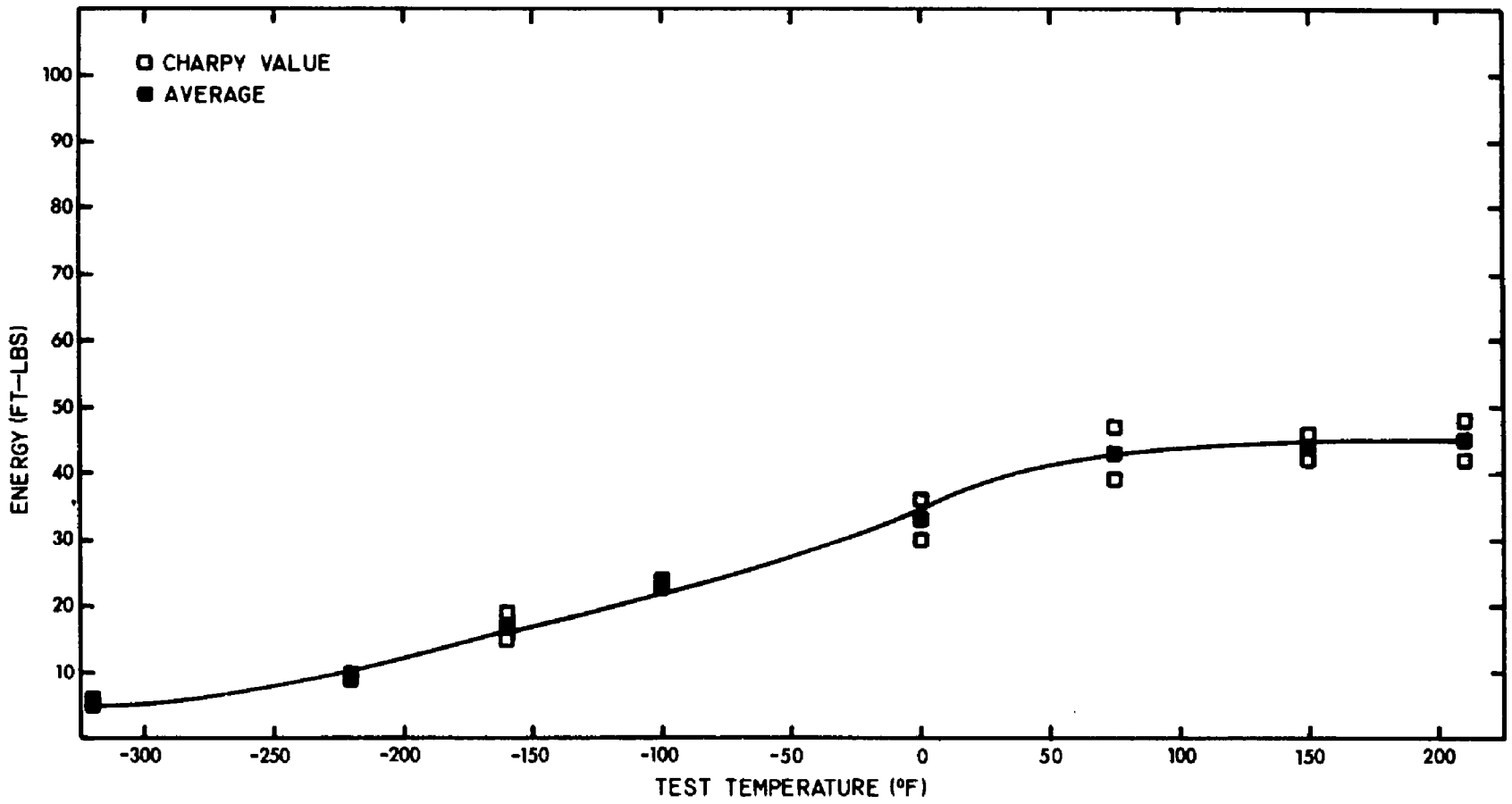

Figure 25 - Charpy V-notch energy-temperature curve.
3% Ni, GMA, argon-2.0% oxygen shielding gas.

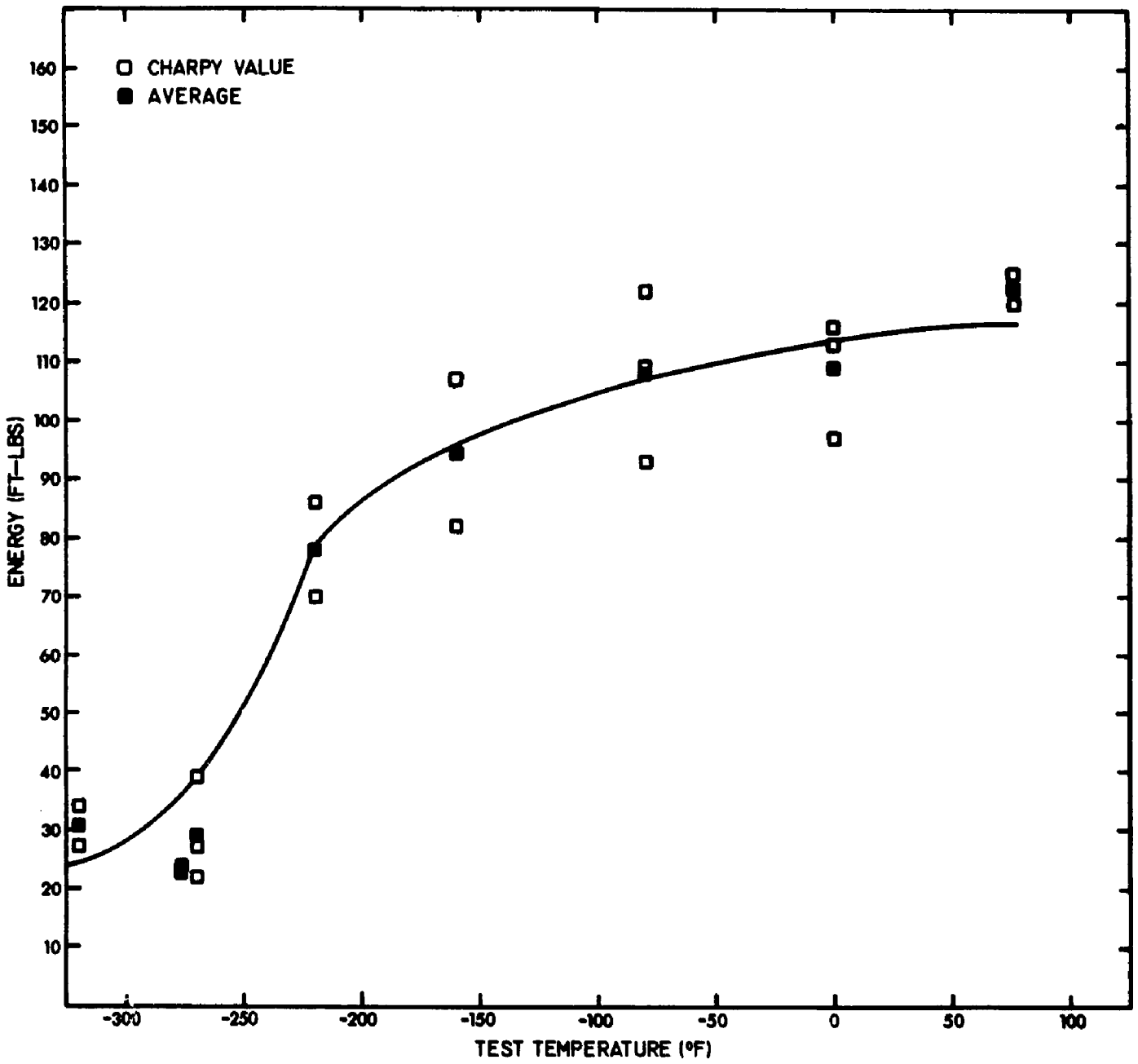

Figure 26 - Charpy V-notch energy-temperature curve.
5% Ni, GTA, pure argon shielding gas.

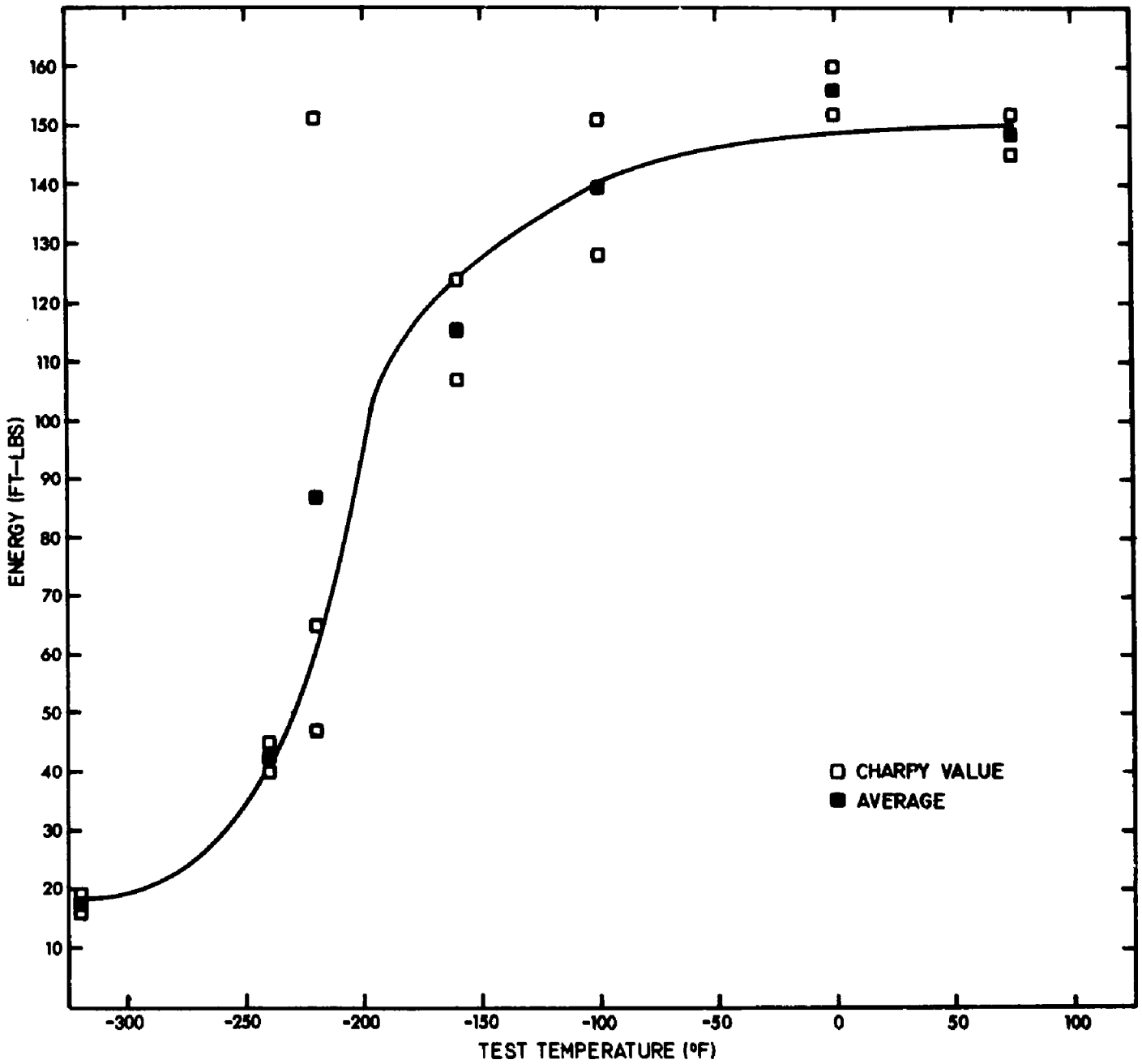

Figure 27 - Charpy V-notch energy-temperature curve.
5% Ni, GTA, argon-0.25% oxygen shielding gas.

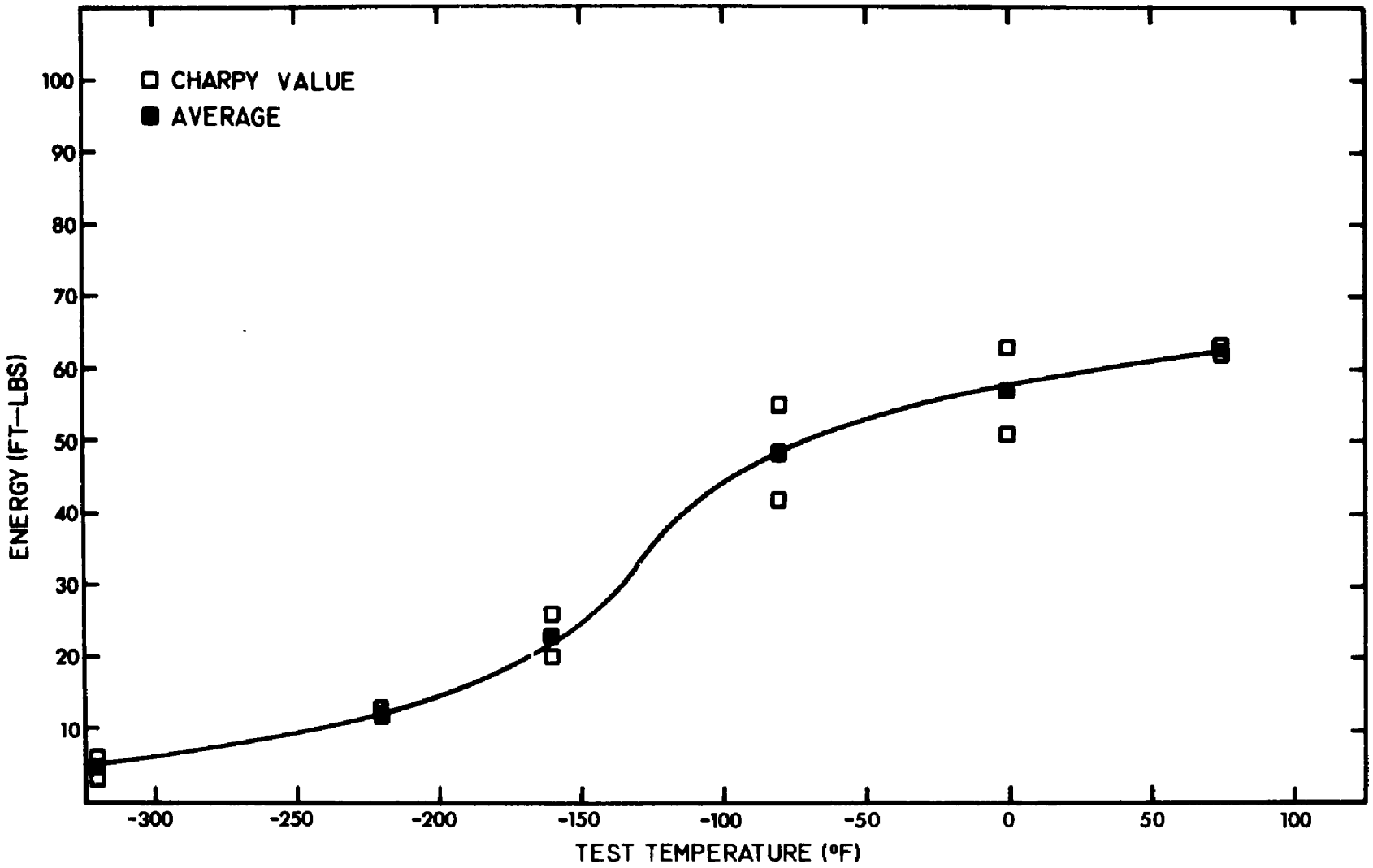

Figure 28 - Charpy V-notch energy-temperature curve.
5% Ni, GMA, pure argon shielding gas.

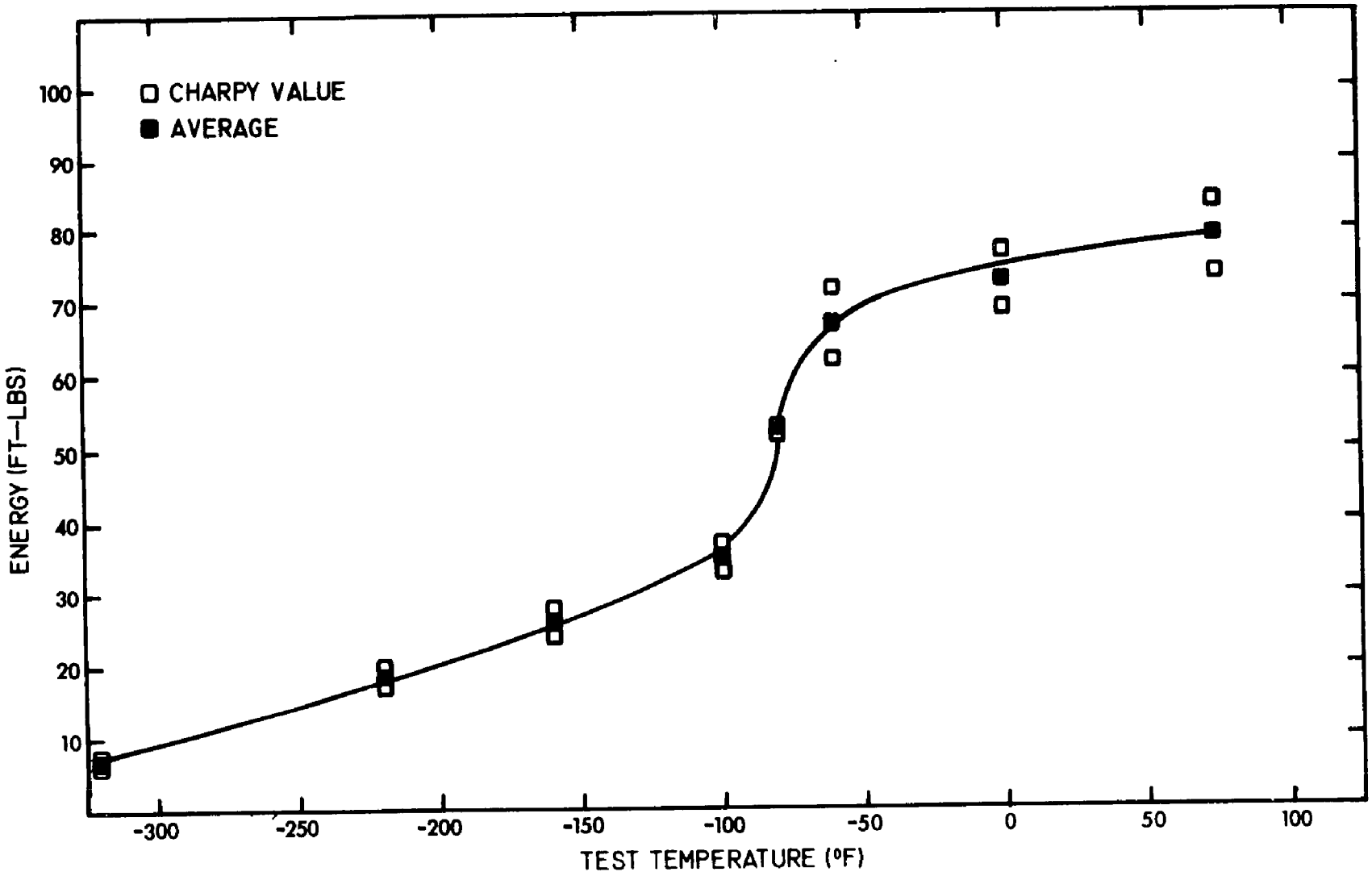

Figure 29 - Charpy V-notch energy-temperature curve.
5% Ni, GMA, argon-0.25% oxygen shielding gas.

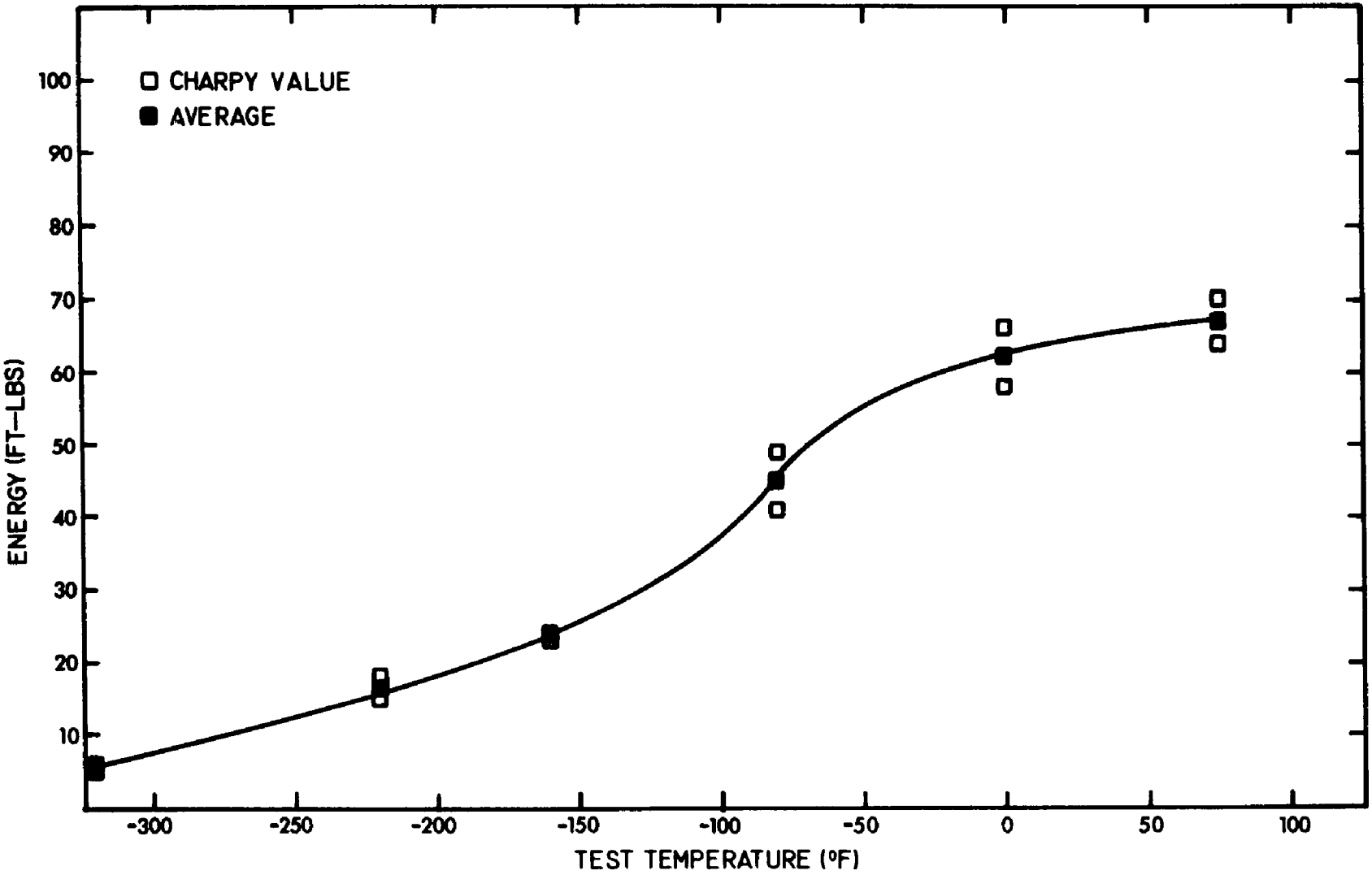

Figure 30 - Charpy V-notch energy-temperature curve.
5% Ni, GMA, argon-1.0% oxygen shielding gas.

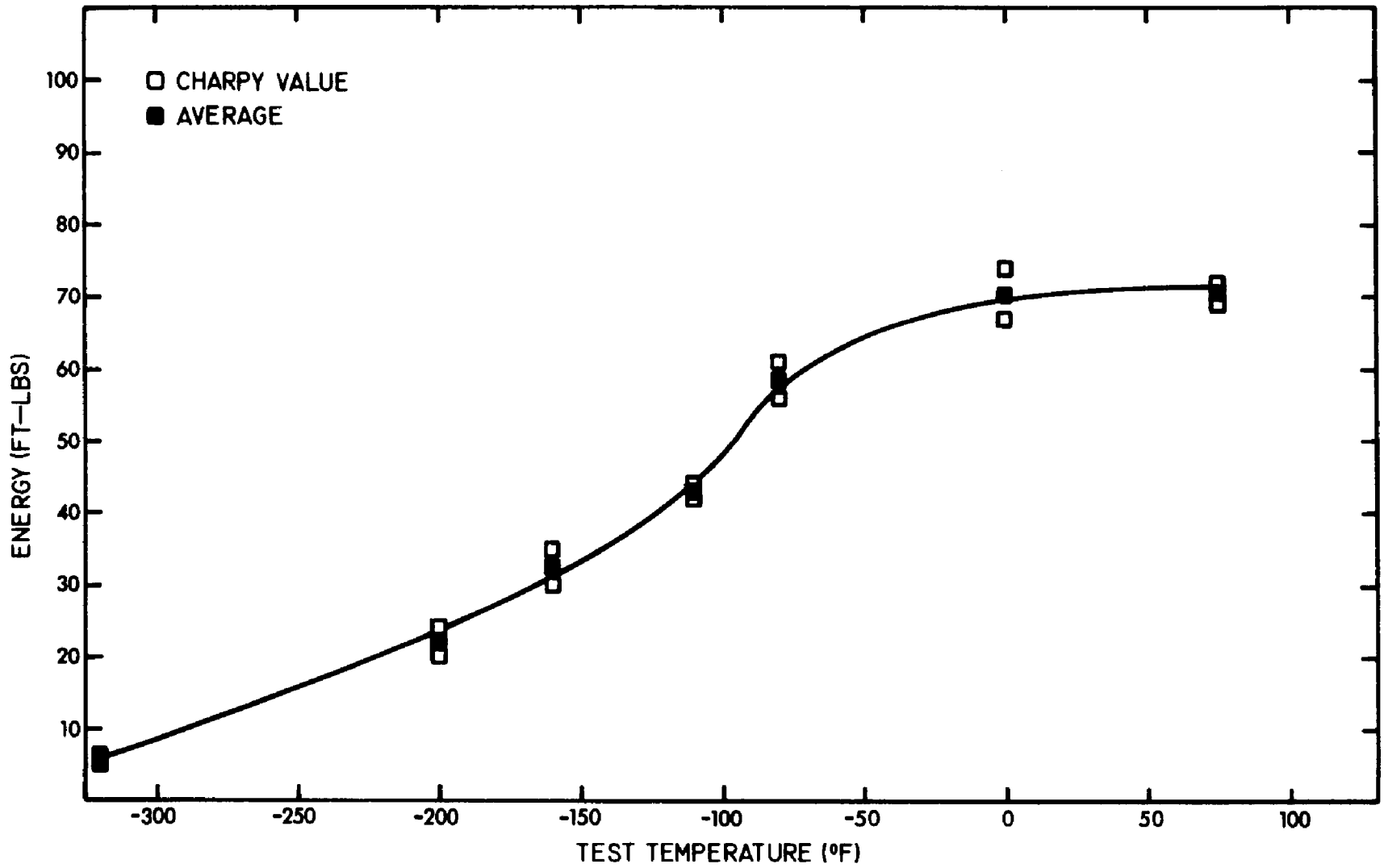

Figure 31 - Charpy V-notch energy-temperature curve.
5% Ni, hot wire GTA, argon-75% helium shielding gas.

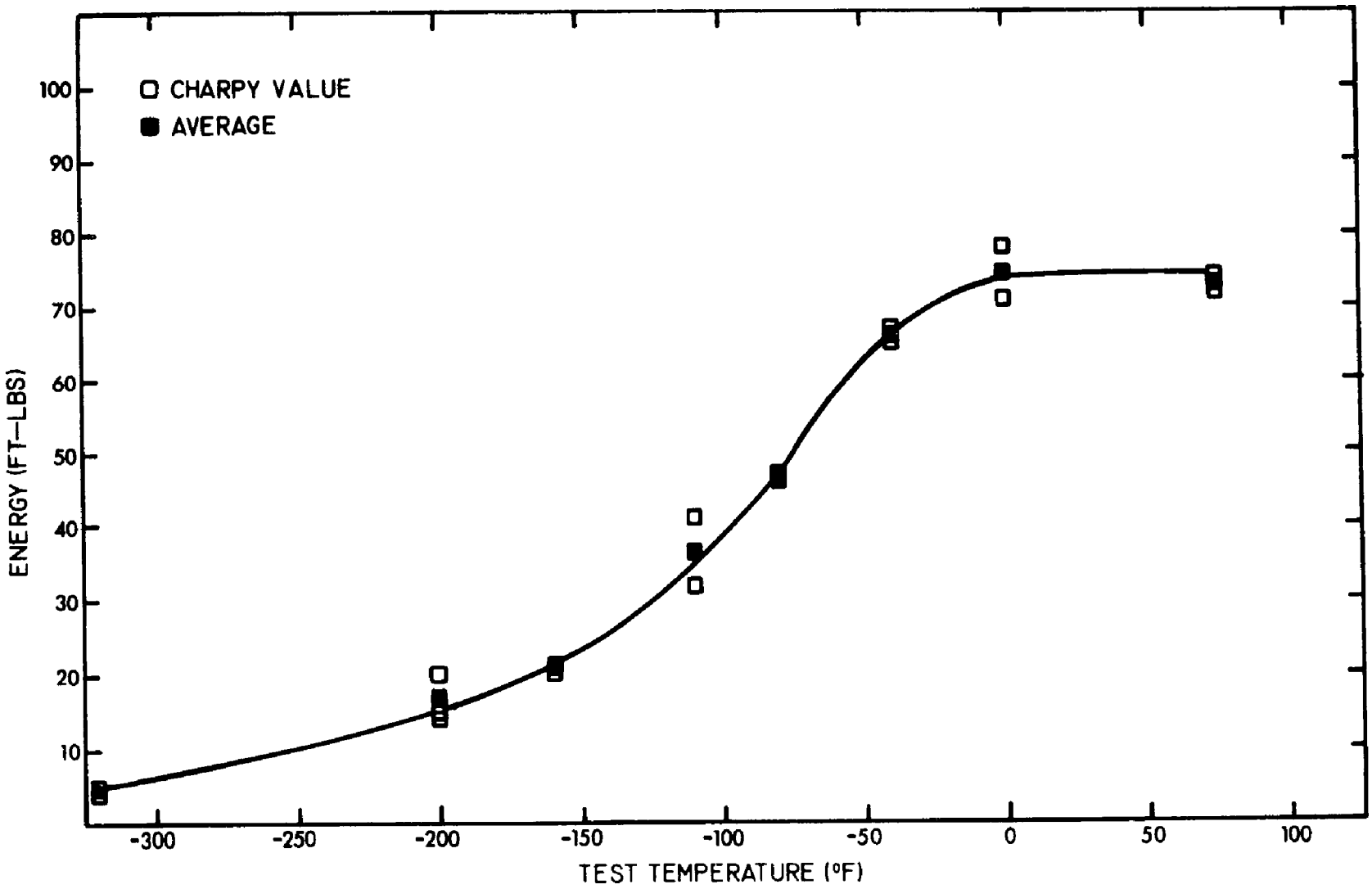

Figure 32 - Charpy V-notch energy-temperature curve.
5% Ni, hot wire GTA, argon-75% helium-0.5% oxygen shielding gas.

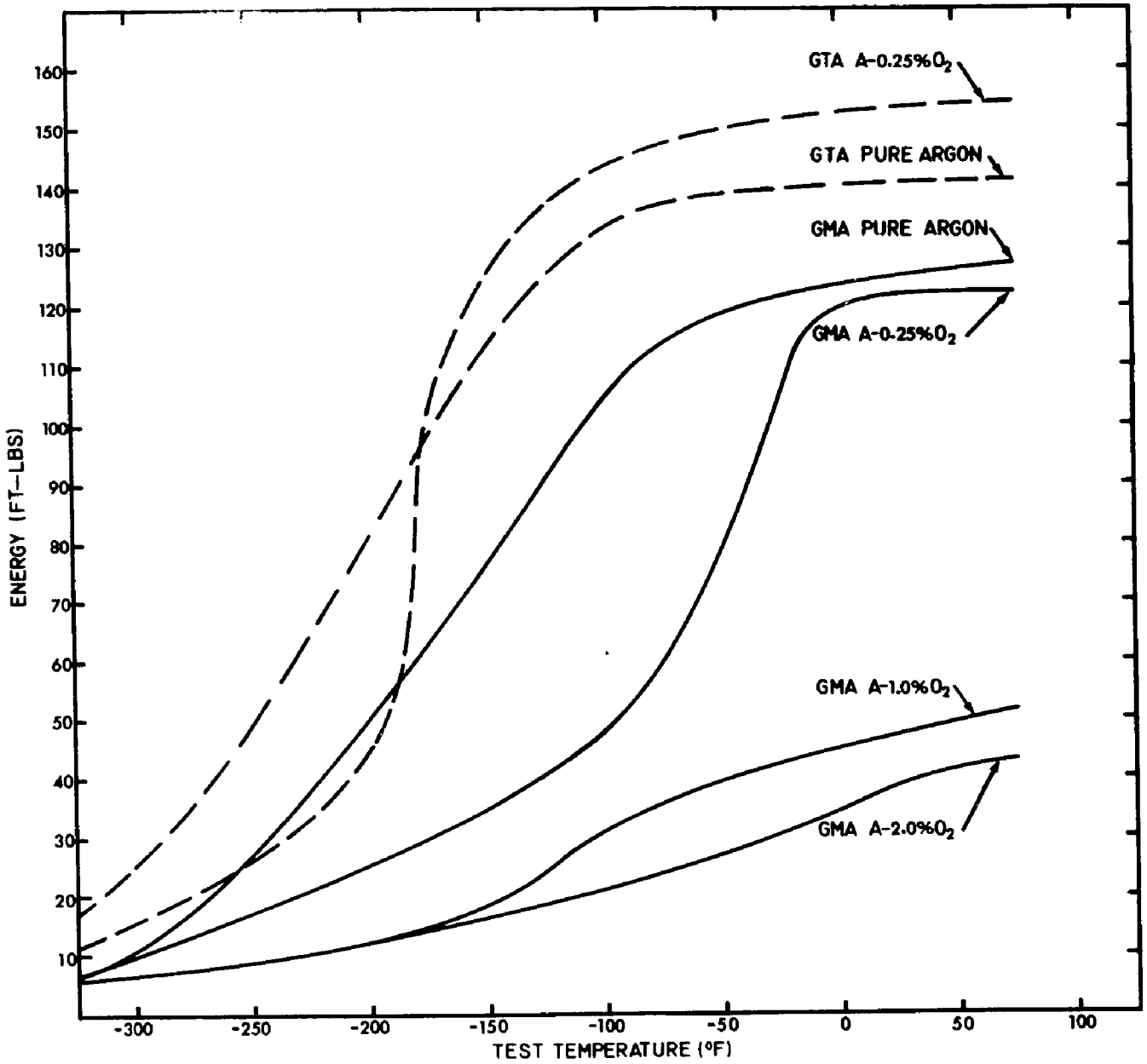

Figure 33 - Variation in Charpy V-notch energy-temperature curve as a function of weld shielding gas. 3% Ni welds.

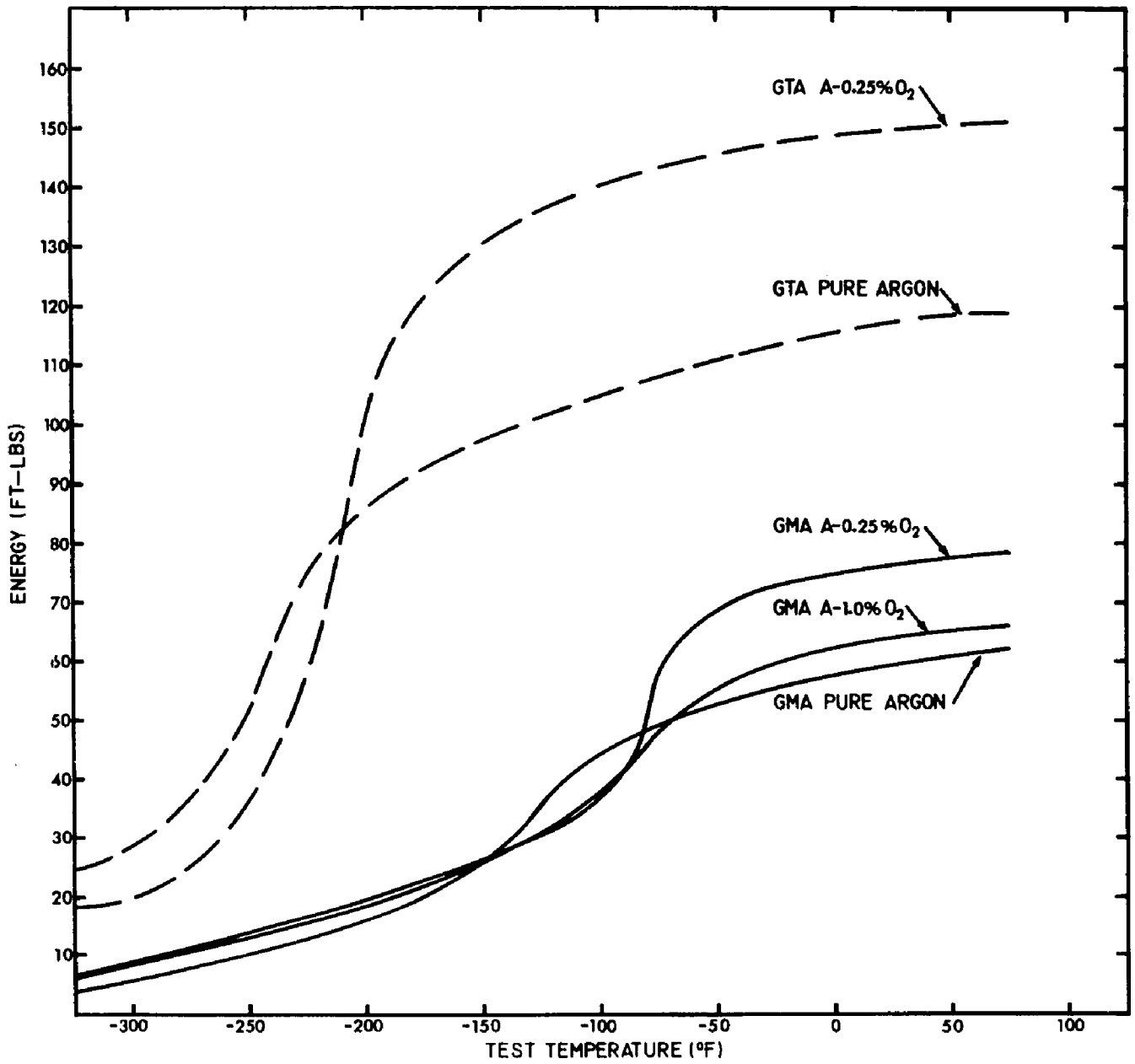

Figure 34 - Variation in Charpy V-notch energy-temperature curve as a function of weld shielding gas. 5% Ni GMA and GTA welds.

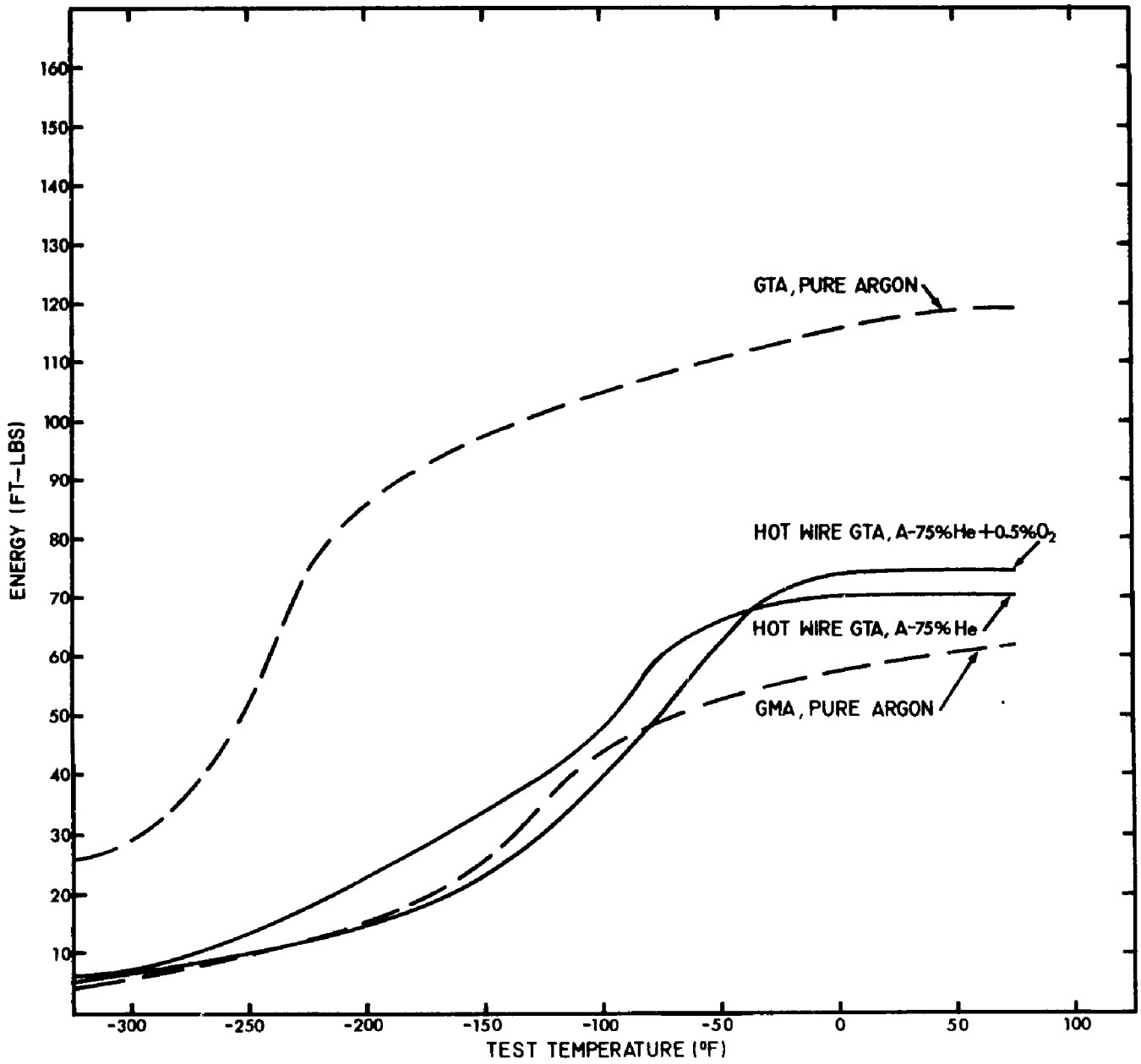

Figure 35 - Variation in Charpy V-notch energy-temperature curve as a function of weld shielding gas. 5% Ni hot wire GTA welds.

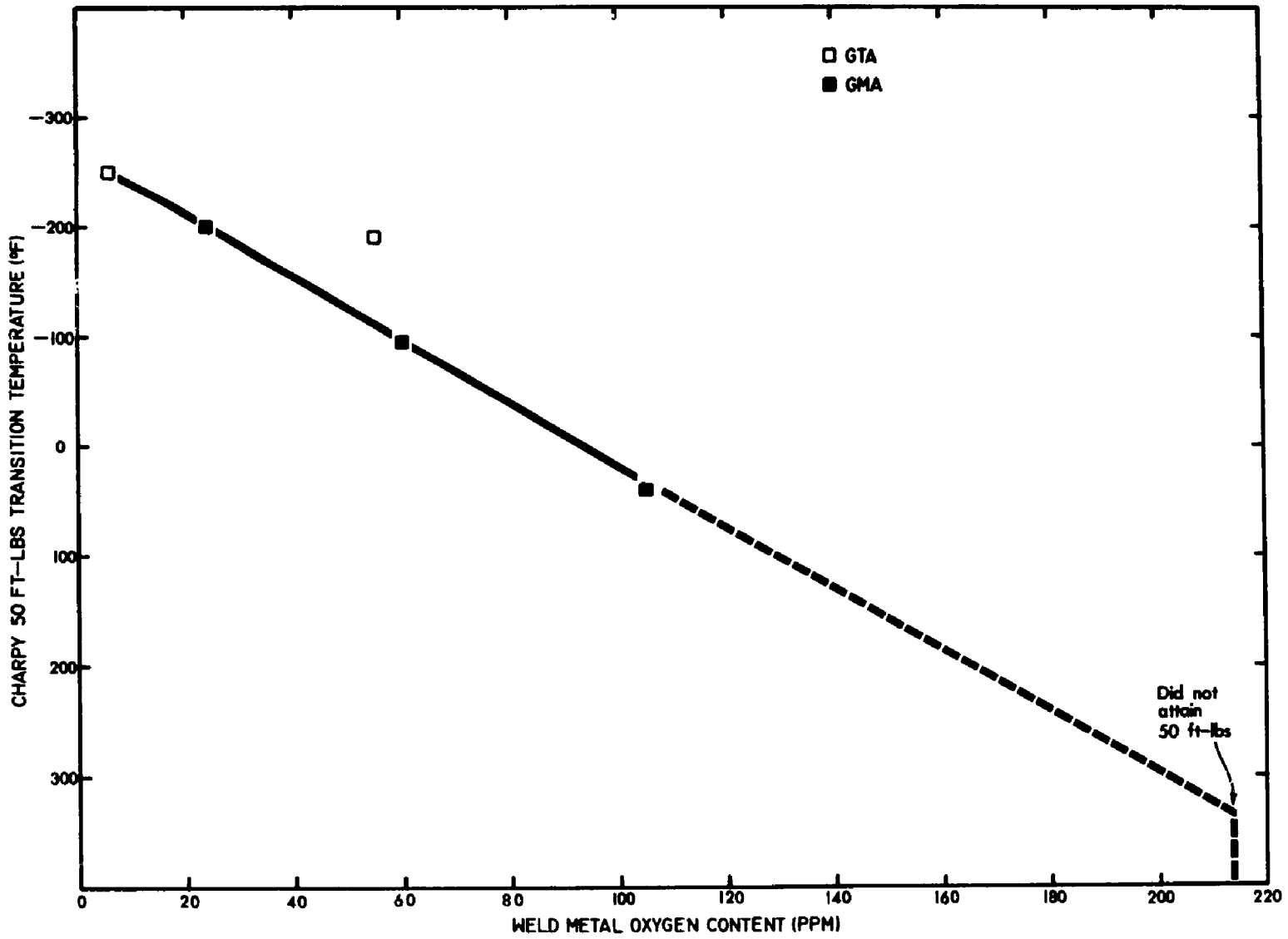

Figure 36 - Charpy V-notch 50 ft-lb transition temperature as a function of weld metal oxygen content. 3% Ni welds.

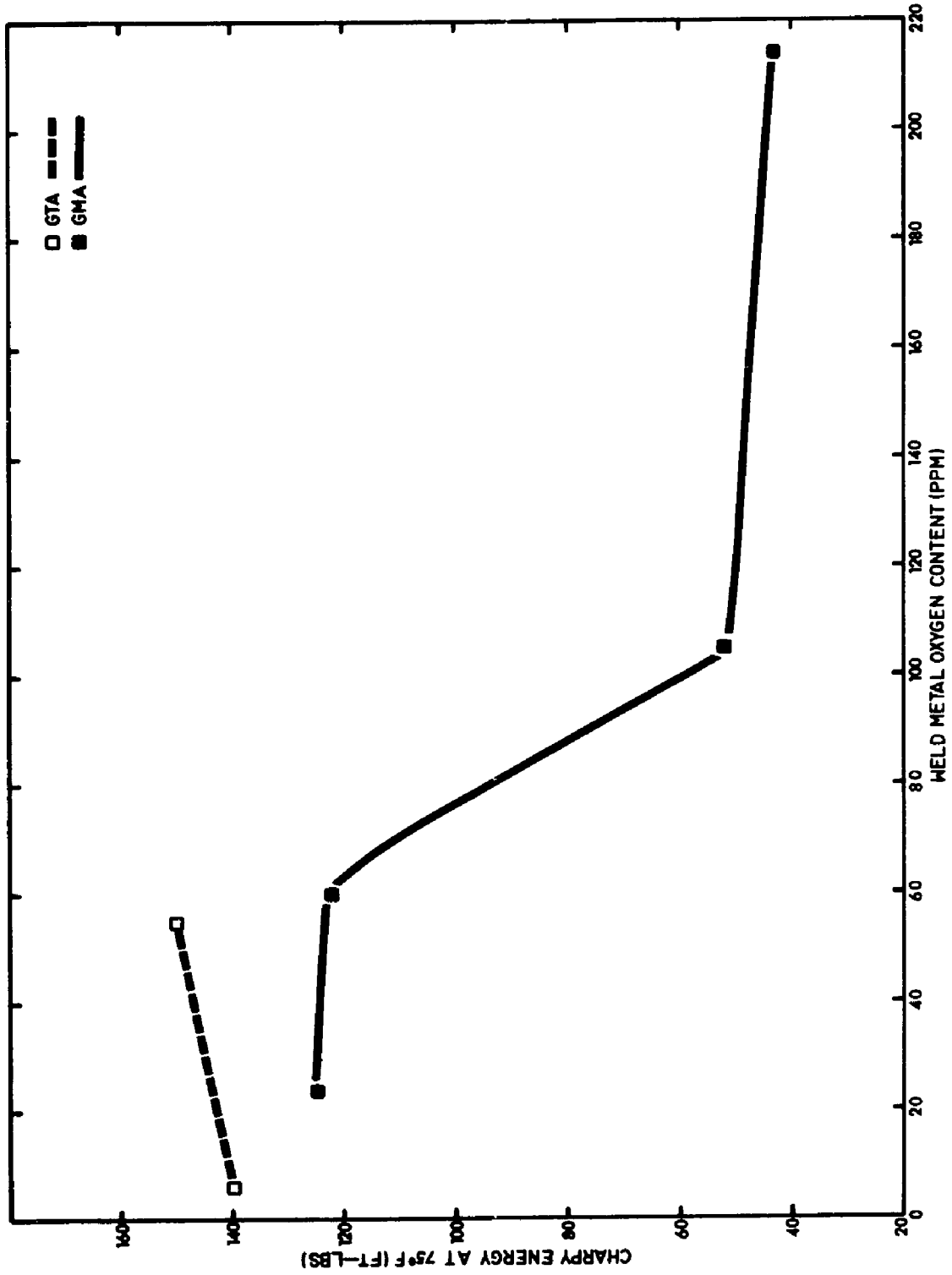

Figure 37 - Charpy V-notch energy at 75°F as a function of weld metal oxygen content. 3% Ni welds.

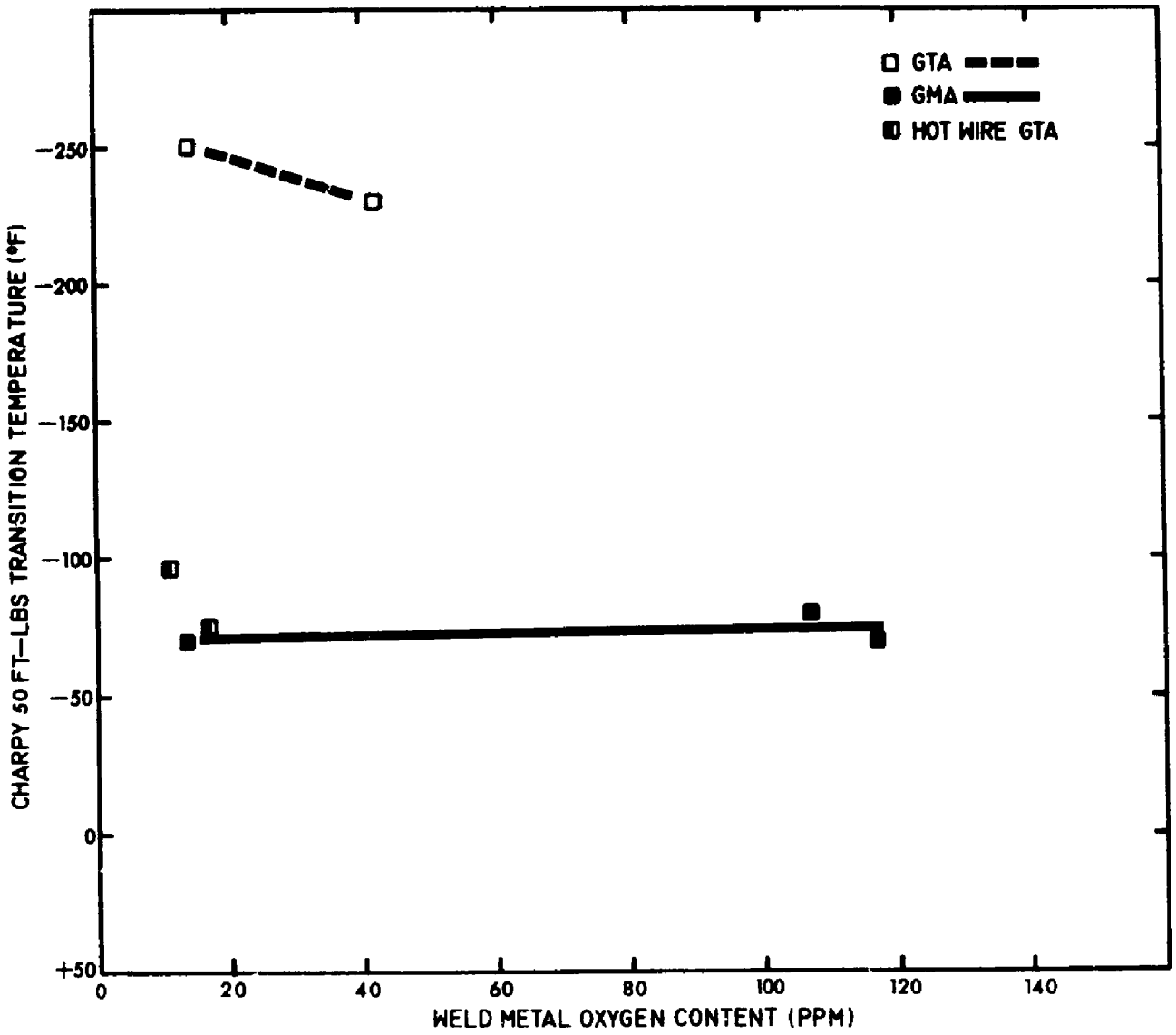

Figure 38 - Charpy V-notch 50 ft-lb transition temperature as a function of weld metal oxygen content. 5% Ni welds.

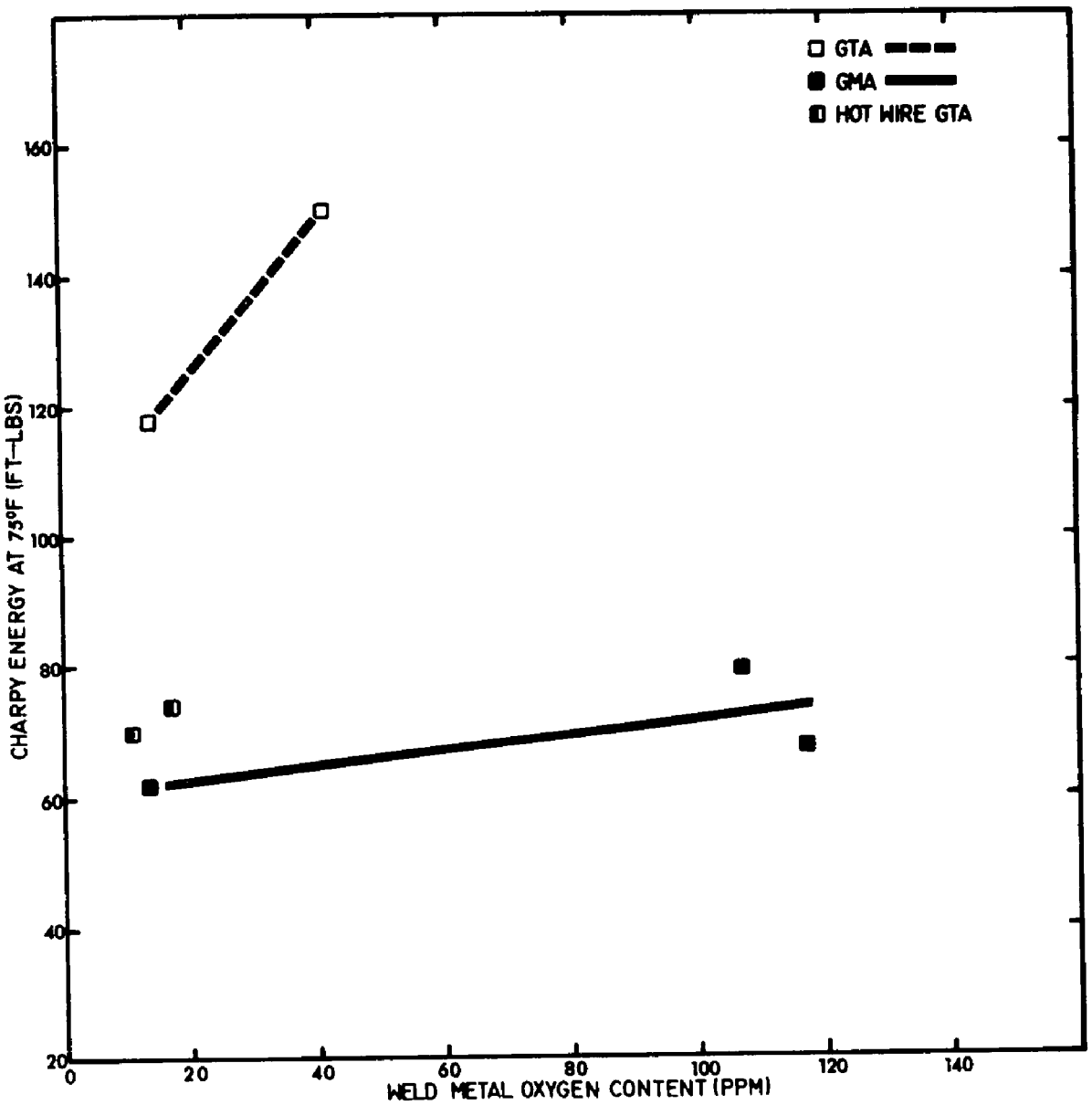

Figure 39 - Charpy V-notch energy at 75°F as a function of weld metal oxygen content. 5% Ni welds.

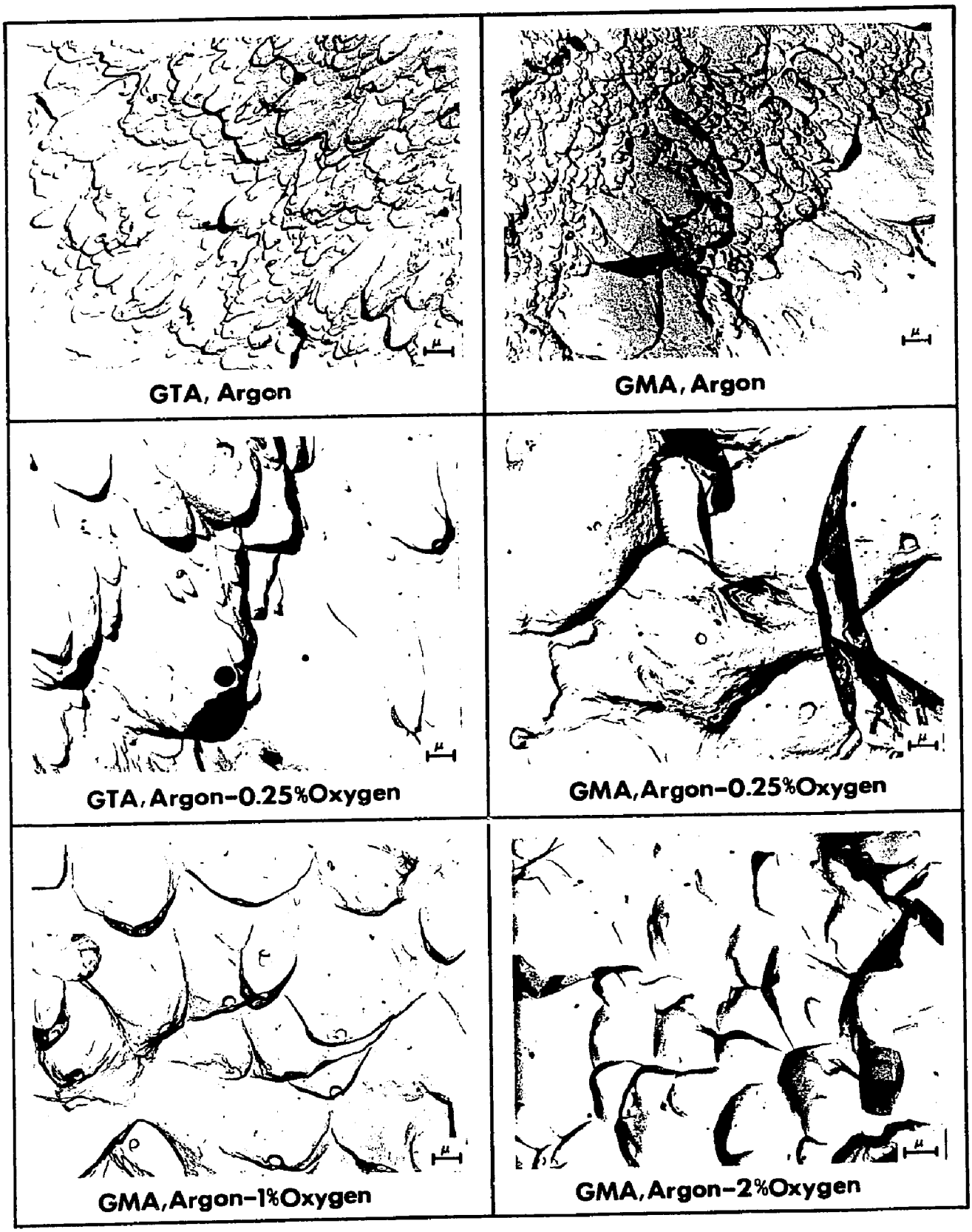

Figure 40 - Electron Fractographs of fractured Charpy specimens. 3% Ni welds.

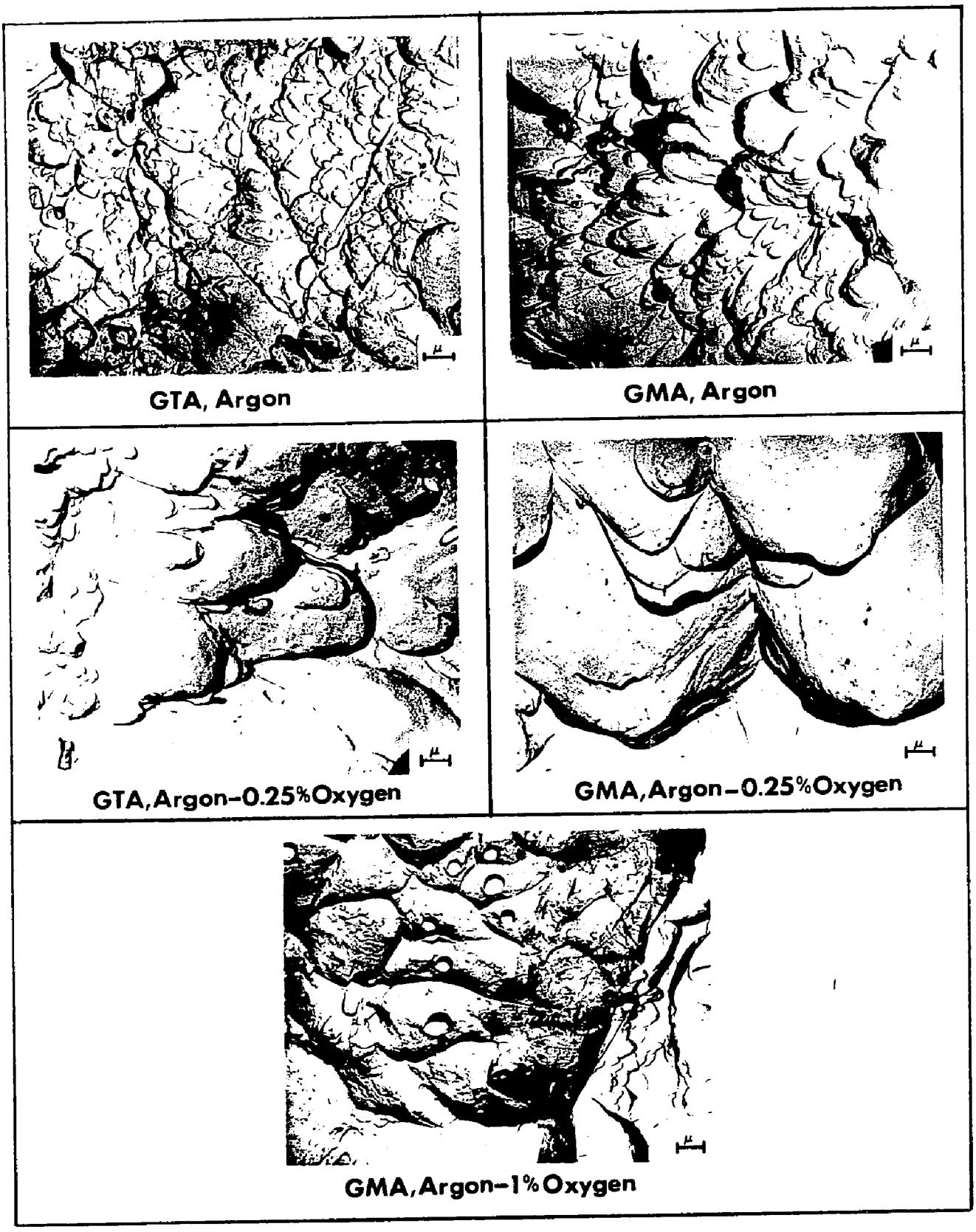

Figure 41 - Electron fractographs of fractured Charpy specimens. 5% Ni GMA and GTA welds.

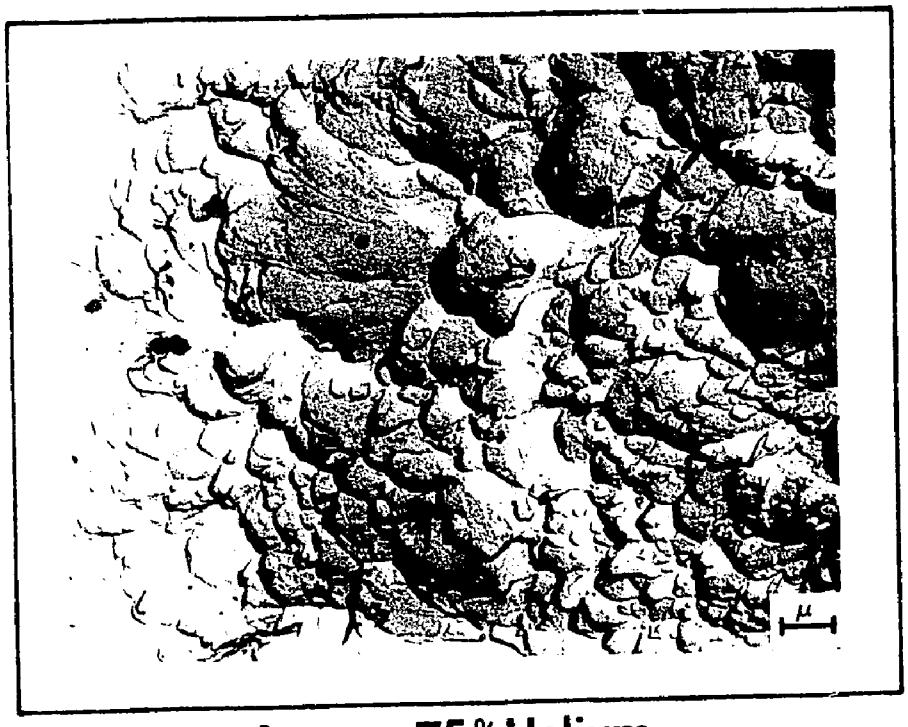

Argon-75%Helium

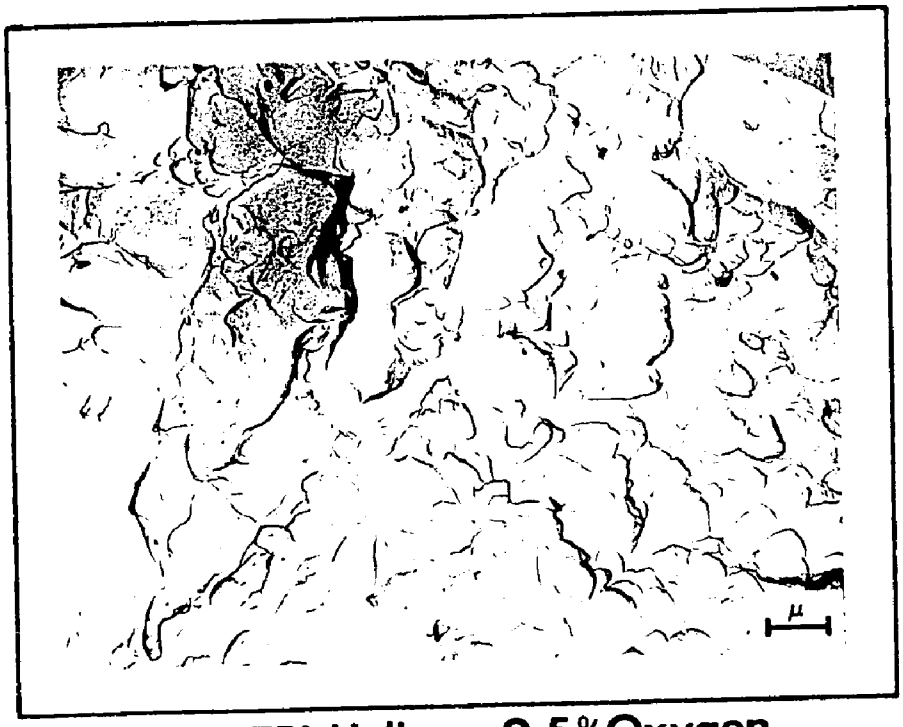

Argon-75%Helium-0.5%Oxygen

Figure 42 - Electron fractographs of fractured Charpy specimens. 5% Ni hot wire GTA welds.

TYPE A

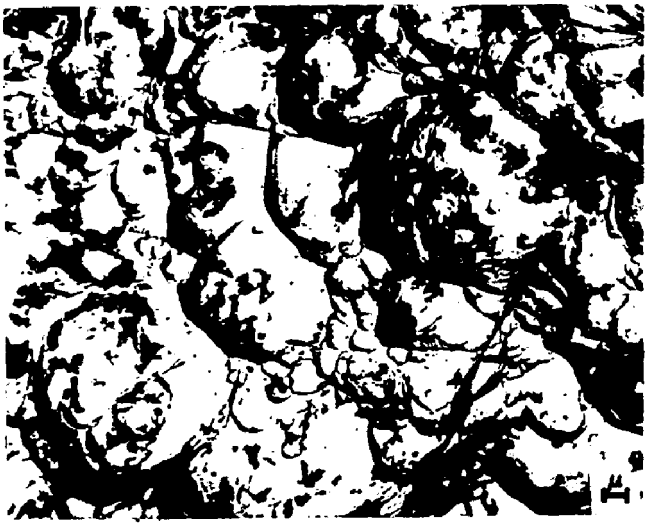

TYPE B

TYPE C

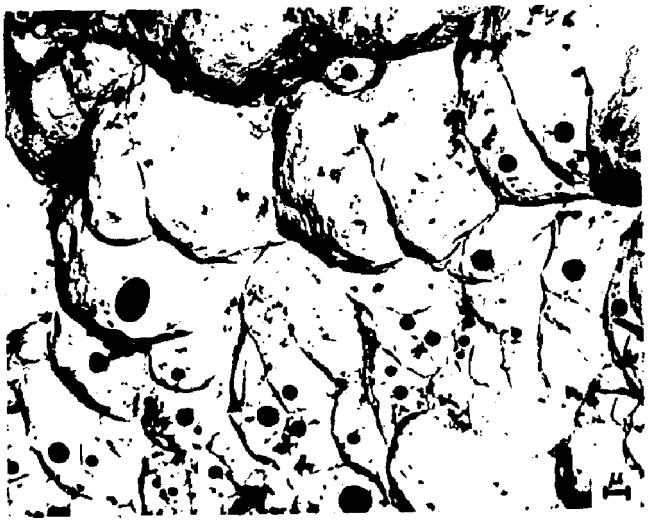

Figure 43 - Examples of particles extracted from the surface of fractured Charpy specimens.

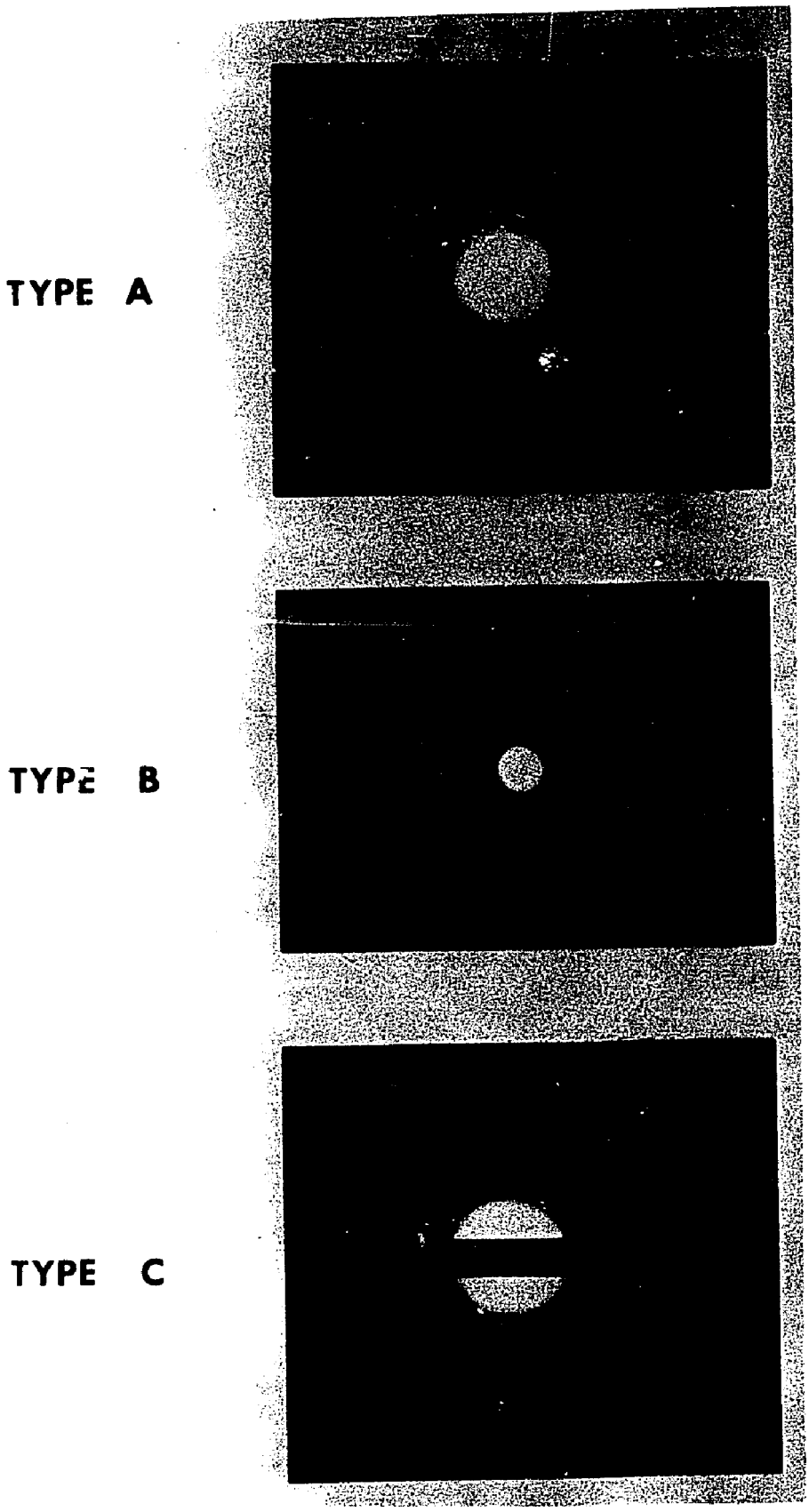

Figure 44 - Electron diffraction patterns from types A, B and C particles. Halos caused by printing mask.

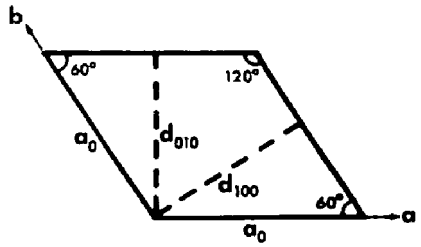

a. Hexagonal lattice–(001) plane

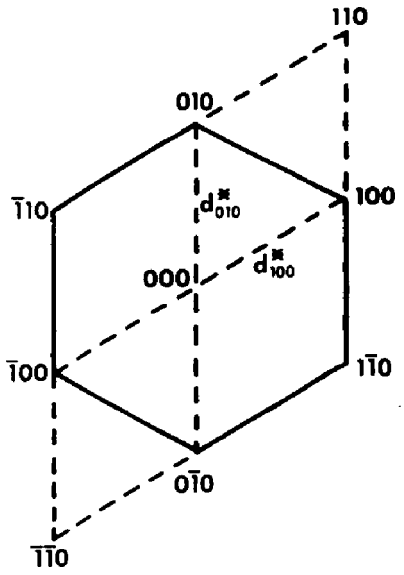

b. Reciprocal lattice

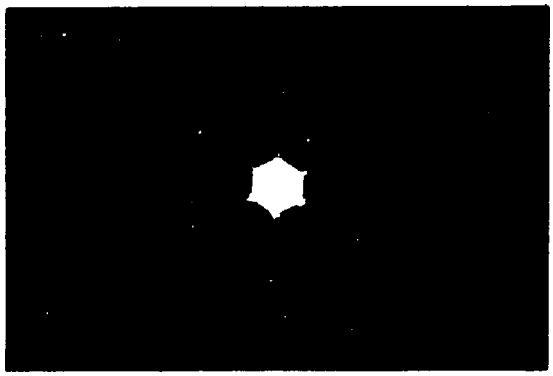

c. SiO_2 (β quartz) diffraction pattern

Figure 45 - Hexagonal lattice reciprocal lattice, and diffraction pattern of SiO_2 (beta quartz).

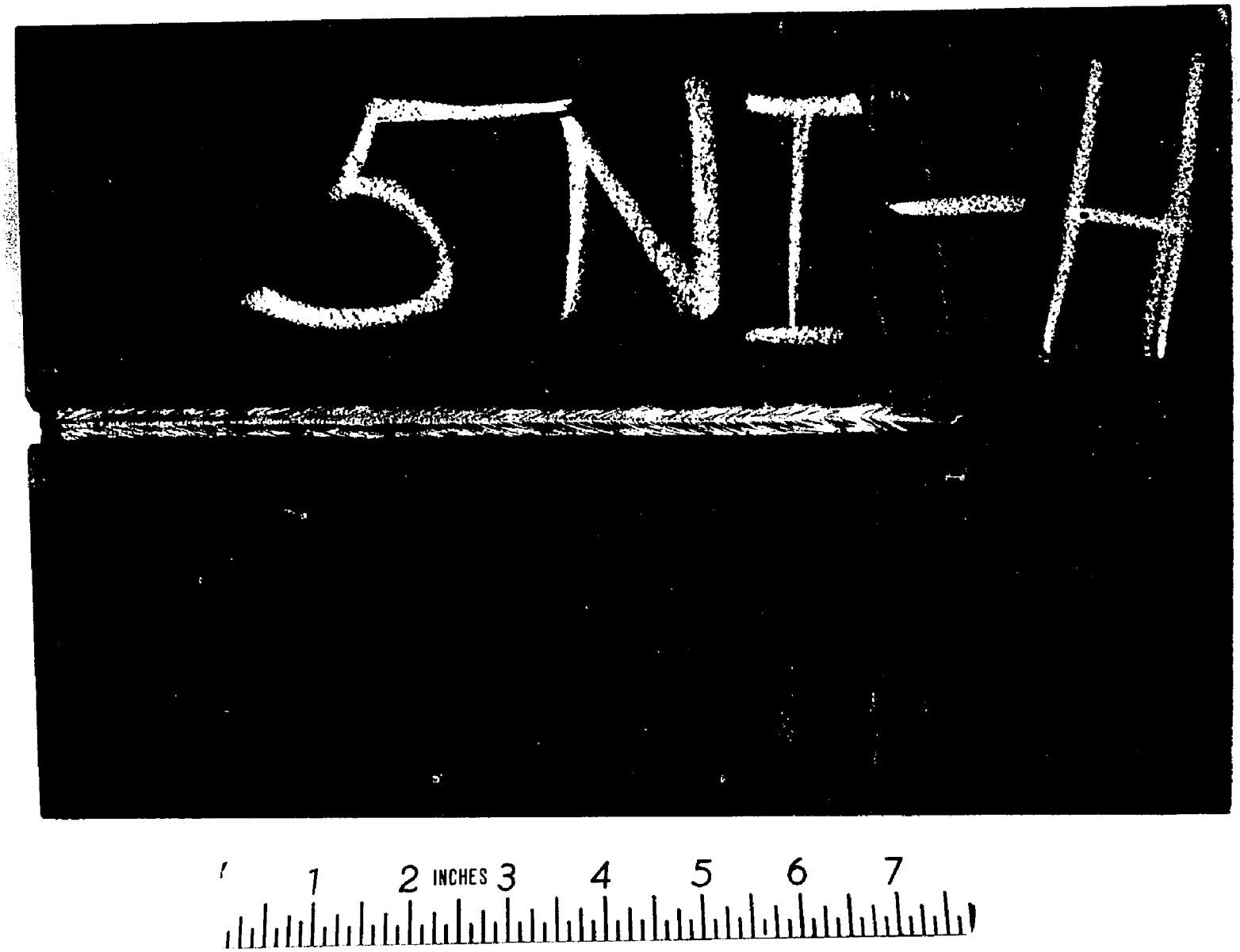

Figure 46 - Welded Keyhole specimen-uncracked.

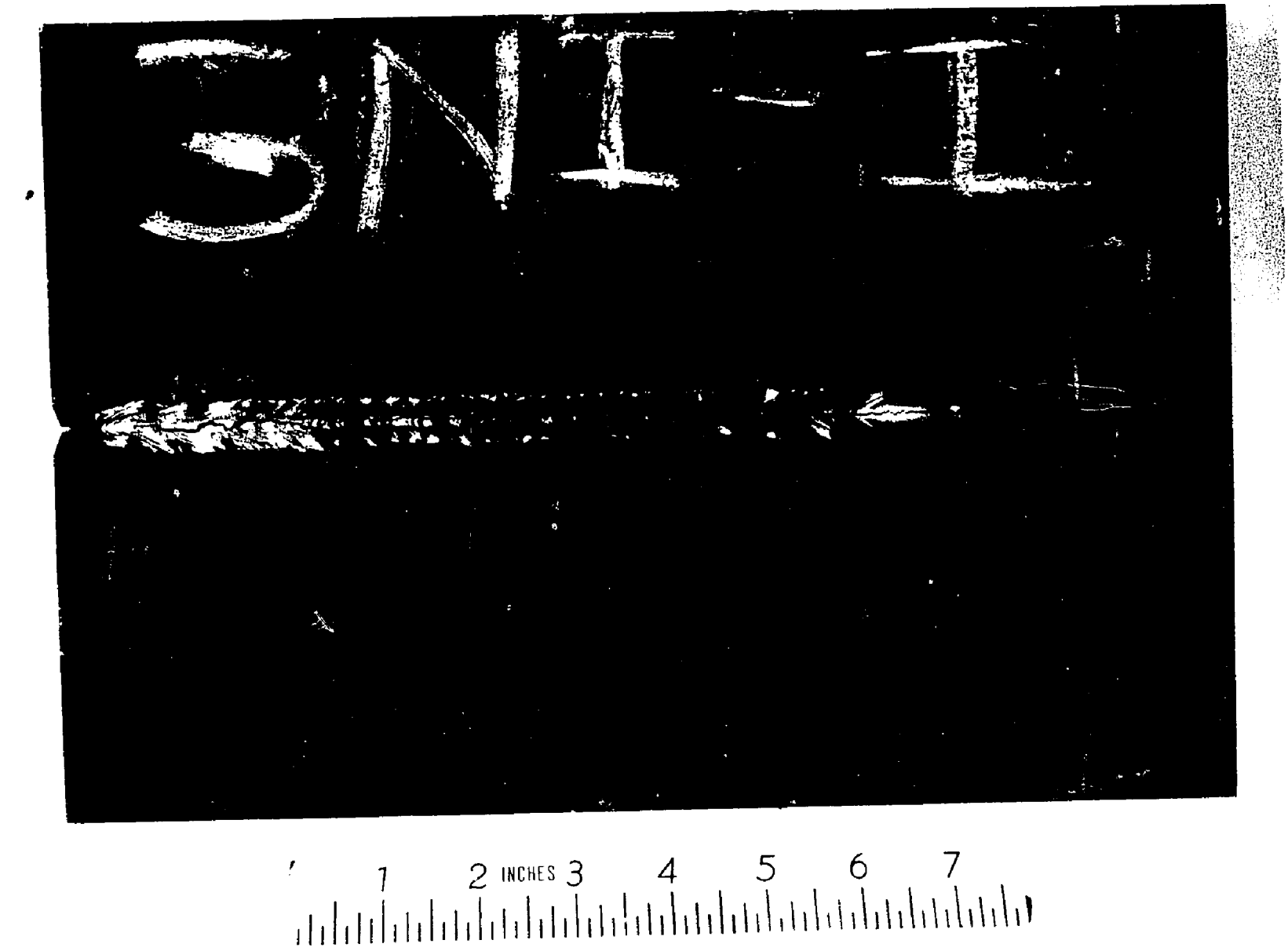

Figure 47 - Welded Keyhole specimen-cracked.

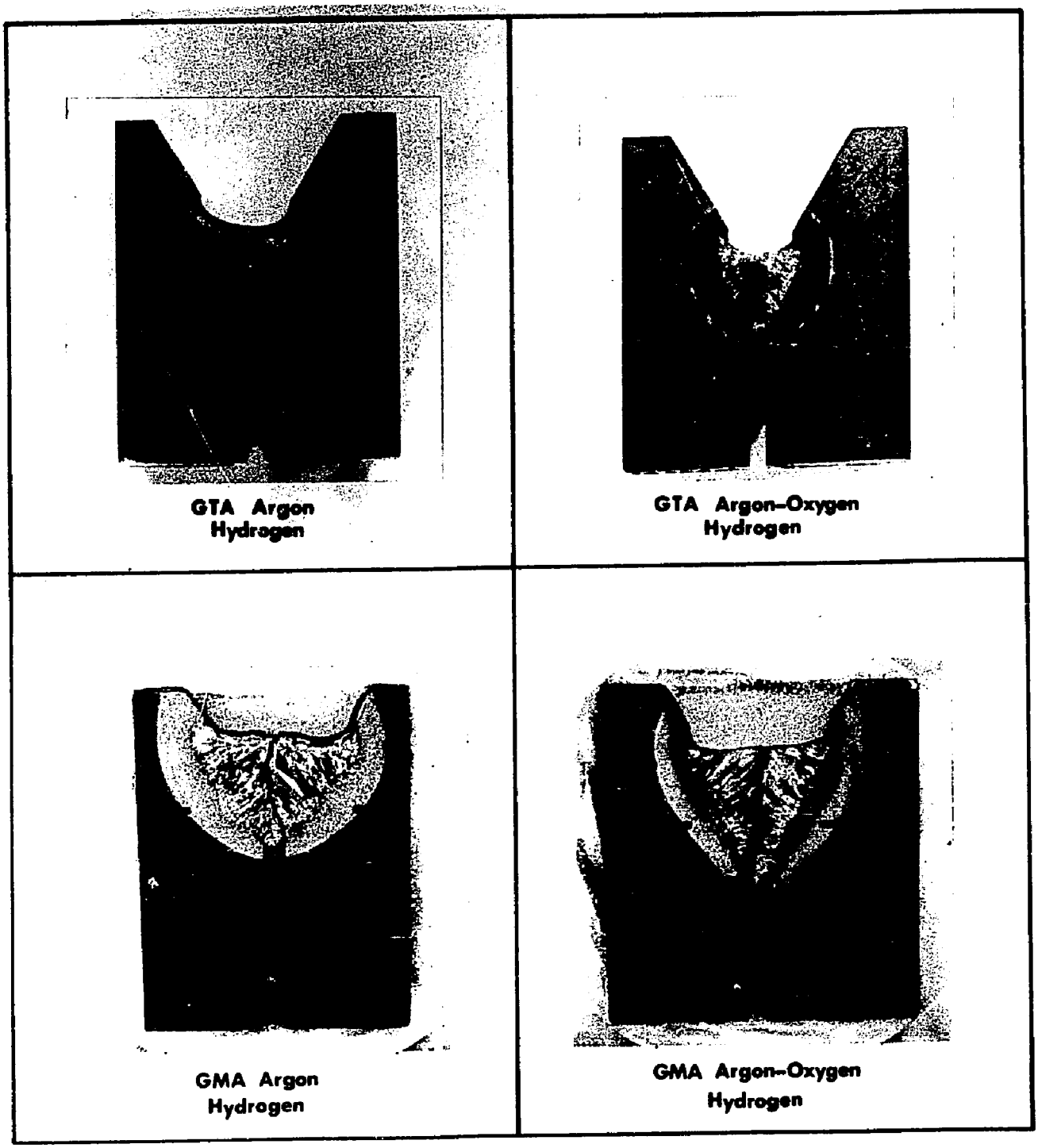

Figure 48 - Macrographs of Keyhole weld cross sections.
2% Nital etch, 2.1 diameters.

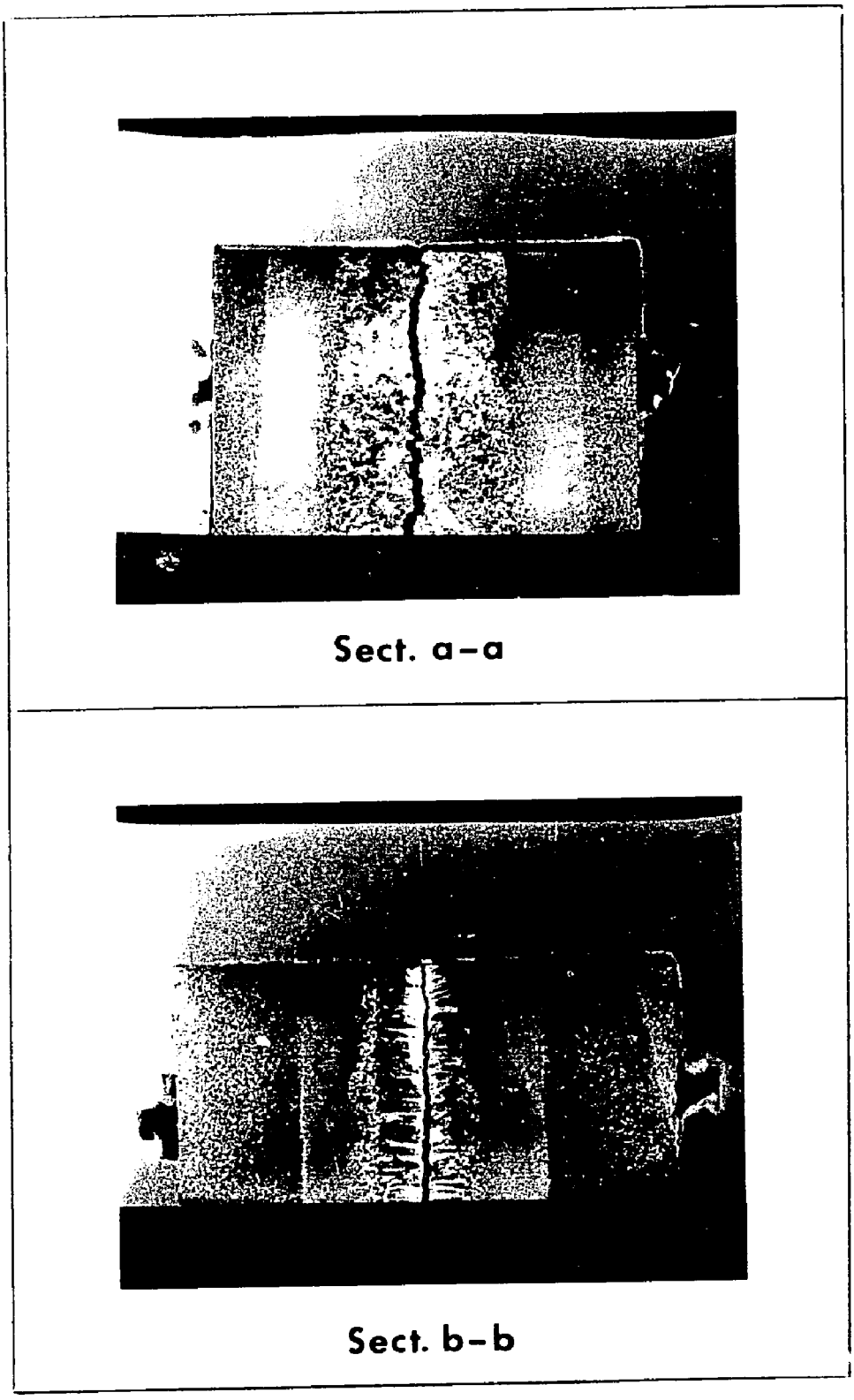

Figure 49 - Macrographs of Keyhole welds sectioned along the lines a-a and b-b in Figure 48.
2% Nital etch, 2.9 diameters.

Appendix A

Calculation of d_{hkl} Spacing for Various Planes in Iron Silicate

1. Structure[62] - Cubic (Face Centered)

$$a_o = 8.235\text{Å}$$

2. Relation Between d_{hkl} and h, k and l[64]

$$(1/d)^2 = \frac{h^2 + k^2 + l^2}{a^2}$$

Results of calculation of d_{hkl} for permitted values of $h^2 + k^2 + l^2$ between 1 and 107 are given on the following page.

Table A-1

Calculated d_{hkl} Spacings for Iron Silicate

$h^2 + k^2 + l^2$	{hkl}	d_{hkl} (Å)
3	111	4.7544
4	200	4.1175
8	220	2.9115
11	311	2.4829
12	222	2.3772
16	400	2.0587
19	331	1.8892
20	420	1.8414
24	422	1.6809
27	511,333	1.5848
32	440	1.4557
35	531	1.3919
36	600,442	1.3725
40	620	1.3020
43	533	1.2558
44	622	1.2414
48	444	1.1886
51	551,711	1.1531
52	640	1.1419
56	642	1.1004
59	731,553	1.0721
64	800	1.0293
67	733	1.0060
68	644,802	0.9986
72	660,822	0.9705
75	555,751	0.9508
76	662	0.9446
80	804	0.9207
83	753,911	0.9039
84	824	0.8985
88	646	0.8778
91	913	0.8632
96	844	0.8404
99	755,771,933	0.8276
100	860,1000	0.8235
104	826,1020	0.8075
107	773,591	0.7961

Appendix B

Calculation of d_{hkl} Spacings for Various Planes in Silicon Dioxide (Beta Quartz)

1. Structure[63] - Hexagonal

$c_o = 5.37\text{Å}$

$a_o = 5.11\text{Å}$

2. Relation Between d_{hkl} and h, k and l[64]

$$(1/d_{hkl})^2 = 4/3 \frac{(h^2 + hk + k^2)}{a^2} + l^2/c^2$$

Results of calculations of d_{hkl} for values of (hk) from (10) to (71) and values of l from 0 to 4 are given on the following page.

Table B-1

Calculated d_{hkl} Spacings for Silicon Dioxide (Beta Quartz)

	d_{hkl} (Å)				
hk	l=0	l=1	l=2	l=3	l=4
10	4.425471	3.415138	2.295547	1.659399	1.284693
11	2.554964	2.307125	1.850899	1.466014	1.188431
20	2.212681	2.045806	1.707569	1.391643	1.147766
21	1.672647	1.596967	1.419704	1.222123	1.046979
30	1.475125	1.422430	1.292859	1.138379	0.992876
22	1.277502	1.242816	1.153585	1.039840	0.925457
31	1.227386	1.196528	1.116284	1.012272	0.905862
40	1.106347	1.083588	1.022914	0.941099	0.853787
32	1.015257	0.997583	0.949637	0.883100	0.809773
41	0.965699	0.950451	0.908711	0.849902	0.783948
50	0.885077	0.873294	0.840585	0.793388	0.738940
33	0.851667	0.841153	0.811807	0.769055	0.719162
42	0.836320	0.826358	0.798483	0.757699	0.709850
51	0.794825	0.786259	0.762134	0.726430	0.683945
60	0.737564	0.730704	0.711218	0.681942	0.646431
43	0.727529	0.720942	0.702208	0.673986	0.639643
52	0.708630	0.702539	0.685169	0.658877	0.626685
61	0.674865	0.669598	0.654508	0.631476	0.602967
44	0.638750	0.634278	0.621408	0.601594	0.576792
70,53	0.632198	0.627862	0.615371	0.596112	0.571954
62	0.613690	0.609722	0.598263	0.580520	0.558140
71	0.586157	0.582695	0.572669	0.557050	0.537186

REFERENCES

1. Brown, B. F., "Metals and Corrosion," Machine Design, Volume 40, January 18, 1968, pp 165 to 173.

2. Gross, J. H. and Stout, R. D., "Steels for Hydrospace," Ocean Engineering, Volume 1, May, 1969, pp 395 to 413.

3. Woodland, B. T., "Deep Submergence Metal Structures," Machine Design, Volume 40, January 18, 1968, pp 159 to 164.

4. Kiernan, T. J. and Krenzke, M. A., "Future Pressure Hulls for Deep Submergence," SPE Journal, Volume 24, December, 1968, pp 56 to 62.

5. Pellini, W. S., "Status and Projections of Developments in Hull Structural Materials for Deep Ocean Vehicles and Fixed Bottom Installations," NRL Report 6167, November 4, 1964.

6. Stern, I. L., "Steels for Hydrospace," Ordinance, Volume L, January-February 1966, pp 432 to 435.

7. Dorschu, K. E. and Lesnewich, A., "Development of a Filler Metal for a High-Toughness Alloy Plate Steel with a Minimum Yield Strength of 140 ksi," Welding Journal, Volume 43, December 1964, pp 564-s to 576-s.

8. Gross, J. H., "The New Development of Steel Weldments," ibid, Volume 47, June 1968, pp 241-s to 270-s.

9. United States Steel Corporation Interim Technical Data Sheet, "HY-130(T) and HY-140(T)". Available through United States Steel Corporation, Pittsburgh, Pa. 15230.

10. Mangenello, S. J., Dabkowski, D. S., Porter, L. F. and Gross, J. H., "Development of a High Toughness Alloy Plate Steel with a Minimum Yield Strength of 140 ksi," Welding Journal, Volume 43, November, 1964, pp 514-s to 520-s.

11. Rathbone, A. M., Connor, L. P. and Gross, J. H., "Weldability of a High Toughness Alloy Plate Steel with a Minimum Yield Strength of 140 ksi," ibid, Volume 43, December, 1964, pp 551-s to 563-s.

12. Rolfe, S. T., Haak, R. P. and Gross, J. H., "Structural Suitability of a High Toughness Alloy Plate Weldment with a Minimum Yield Strength of 140 ksi," ibid, Volume 44, January 1965, pp 40-s to 48-s.

13. Stern, I. L. and Quattrone, R., "A Multiple Test Approach to the Prediction of Weldment Cracking," ibid, Volume 46, May, 1967, pp 203-s to 216-s.

14. "Comparative Weldability of Various 50,000 to 150,000 psi Yield Strength Steels - Controlled Thermal Severity (CTS) Test," Naval Applied Science Laboratory Project 9300-1, Technical Memorandum 29 of 1 April 1965.

15. Quattrone, R. and Stern, I. L., "Development of the NASL Circular Fillet Weldability (NCFW) Test," Naval Applied Science Laboratory Project 9300-1, Technical Memorandum 35 of 28 June 1965.

16. Enis, A. and Telford, R. T., "Gas Metal Arc Welding of HY-130(T) Steel," Welding Journal, Volume 47, June 1968, pp 271-s to 278-s.

17. Connor, L. P., Rathbone, A. M. and Gross, J. H., "Development of Procedures for Welding HY-130(T) Steel", ibid, Volume 46, July 1967, pp 309-s to 321-s.

18. Quattrone, R. and Stern, I. L., "Weldability of HY-130/150 Steel and MIG Filler Wires," Naval Applied Science Laboratory Project 9300-1, Progress Report 4 of 8 March 1966.

19. Quattrone, R. and Stern, I. L., "Weldability of HY-130/150 Steel Covered Electrodes," Naval Applied Science Laboratory Project 9300-1, Technical Memorandum 49 of 11 August 1966.

20. Schultz, B. L. and Stern, I. L., "Comparison of Weld Nugget Area with Heat Input Concepts for Control of HY-130 Weld Deposit Yield Strengths," Naval Applied Science Laboratory, Project 930-1, Progress Report 14 of 27 October 1967.

21. Schultz, B. L., "Application of the Weld Nugget Area Concept for Controlling HY-130 Weld Deposit Yield Strength," Master of Science Thesis, Ohio State University (to be published in the Welding Journal).

22. Telford, R. T. and Nelson, E. C., "Hardenability of Low Alloy Steel Weld Metal," Linde Division, Union Carbide Corporation Report L-1203, April 15, 1968.

23. "Material Probers Seek Keys to More Powerful Welds," Steel, Volume 162, March 25, 1968, pp 41-45.

24. Stout, R. D., Torok, T. E. and Podgurski, P. P., "Tensile Properties of High Purity Iron-Base Weld Metals," Welding Journal, Volume 42, September, 1963, pp 385-s to 391-s.

25. "Background for the Development of Materials to be Used in High Strength Steel Structural Weldments," DMIC Report 172, July 31, 1962, Battelle Memorial Institute.

26. Masubuchi, K., Monroe, R. E. and Martin, D. C., "Interpretative Report on Weld Metal Toughness," Ship Structure Committee Report SSC-169, July 1965.

27. Heuschkel, J., "Ultra-Tough, Steel Weld Metals," Westinghouse Research Laboratories Scientific Paper 65-1B4-MJCON-P2, September 14, 1965.

28. Heuschkel, J., "New Approach Produces Stronger Welds," Materials In Design Engineering, Volume 59, January, 1964, pp 87 to 91.

29. Heuschkel, J., "Composition Controlled, High-Strength, Ductile, Tough, Steel Weld Metals," Welding Journal, Volume 43, August, 1964, pp 361-s to 384-s.

30. Heuschkel, J., "Ultra Tough Steel Weld Metals," ibid, Volume 46, February, 1967, pp 74-s to 93-s.

31. Troiano, A. R., "The Role of Hydrogen and Other Interstitials in the Mechanical Behavior of Metals," Transactions of the ASM, Volume 52, 1960, pp 54-80.

32. Kammer, P. A., Masubuchi, K. and Monroe, R. E., "Cracking in High Strength Steel Weldments-A Critical Review," DMIC Report 197, February 7, 1964, Battelle Memorial Institute.

33. Interrante, C. G. and Stout, R. D., "Delayed Cracking in Steel Weldments," Welding Journal, Volume 43, April 1964, pp 145-s to 160-s.

34. Elsea, A. R. and Fletcher, E. E., "The Problem of Hydrogen in Steel," DMIC Memorandum 180, October 1, 1963, Battelle Memorial Institute.

35. Torok, T. E. and Stout, R. D., "Relation of Dilatometric Characteristics of Steels to Delayed Cracking in Welds," Welding Journal, Volume 44, December 1965, pp 529-s to 544-s.

36. Cottrell, C. L. M., "Austenite Transformation Characteristics in Relation to Hard-Zone Cracking in Welded Low Alloy Steels," Directorate of Weapon Research (Defence) Report W. R. (D) 2/53, May 1953. Available from Defense Documentation Center, AD No. 13035.

37. Granjon, H., "Information on Cracking Tests," Welding in the World, Volume 1, No. 2, 1963, pp 58-91.

38. Vagi, J. J., Meister, R. P., and Randall, M. D., "Weldment Evaluation Methods," DMIC Report 244, August, 1968, Battelle Memorial Institute.

39. White, S. S., Moffatt, W. G. and Adams, Jr., C. M., "Dynamic Measurement of Stress Associated with Weld Cracking," Welding Journal, Volume 37, April, 1958, pp 185-s to 192-s.

40. Quattrone, R., "Comparison of Cracking Tests for Assessing Weldability," Master of Science Report, Polytechnic Institute of Brooklyn, June, 1966.

41. "Standard Methods for Notched Bar Impact Testing of Metallic Materials," ASTM Standards, Part 30, May, 1966.

42. Kay, D. H., Techniques for Electron Microscopy, Second Edition, F. A. Davis Company, Philadelphia, Pa., 1965.

43. Birkle, A. J., Dabkowski, D. S., Paulina, J. P. and Porter, L. F., "A Metallographic Investigation of the Factors Affecting the Notch Toughness of Maraging Steels," United States Steel Corporation Applied Research Laboratory Project 40.018-002(19), July 1, 1964.

44. Class, I., "Present State of Knowledge in Respect to the Properties of Steels Resistant to Hydrogen Under Pressure," Stahl und Eisen, volume 80, August 18, 1960, pp 1117 to 1135.

45. Marder, A.R. and Krauss, G., "The Morphology of Martensite in Iron-Carbon Alloys," Transactions Quarterly, Volume 60, December, 1967, pp 651 to 660.

46. The Welding Handbook, Fifth Edition, Section 1, "Fundamentals of Welding," American Welding Society, 1962.

47. Stout, R. D. and Doty, W. D., The Weldability of Steels, Welding Research Council, 1953.

48. Irvine, K. J. and Pickering, F. B., "Relationship Between Microstructure and Mechanical Properties of Mild Steel Weld Deposits," British Welding Journal, Volume 7, May, 1960, pp 353 to 364.

49. Honeycombe, R. W. K., "Some Strengthening Mechanisms in Alloy Steels," in "Metallurgical Developments in High Alloy Steels," ISI Special Report 86.

50. Roberts, M. J. and Owens, W. S., "Solid Solution Hardening by Carbon and Nitrogen in Ferrous Martensites," in Physical Properties of Martensite and Bainite, Special Report 93, The Iron and Steel Institute, Percy Lund, Humphries and Co., Ltd., 1965.

51. Irvine, K. J., and Pickering, F. B., "The Effects of Composition on the Structure and Properties of Martensite," Journal of the Iron and Steel Institute, Volume 196, September, 1960, pp 66 to 81.

52. Grant, N. J., "Dispersed Phase Strengthening," in Strengthening of Metals, D. Peckner, Ed., Reinbold, 1964.

53. Rees, W. P. and Hopkins, B. E., "Intergranular Brittleness in Iron-Oxygen Alloys," Journal of the Iron and Steel Institute, Volume 171, December, 1952, pp 403 to 409.

54. Marschall, C. W., "The Factors Influencing the Fracture Characteristics of High Strength Steels," DMIC Report 147, February 6, 1961, Battelle Memorial Institute.

55. Linnert, G. E., Welding Metallurgy, Volume 2, American Welding Society, 1967.

56. Gross, J. H. and Stout, R. D., "The Effect of Microstructure on Notch Toughness-Part III," Welding Journal, Volume 35, February, 1956, pp 72-s to 76-s.

57. Gurland, J. and Plateau, J., "The Mechanism of Ductile Rupture of Metals Containing Inclusions," Transactions of the ASM, Volume 56, 1963, pp 442 to 454.

58. Brother, A. J. and Yukawa, S., "Engineering Applications of Fractography," in Electron Fractography, ASTM STP 436, ASTM, 1968.

59. Philips, A., Kerlins, V. and Whiteson, B. V., "Electron Fractography Handbook," Air Force Material Laboratory Report ML-TDR-64-416, Wright Patterson AFB, January 31, 1965.

60. Beachem, C. D. and Pelloux, P. M. N., "Electron Fractography-A Tool for the Study of Micromechanisms of Fracturing Processes," in Fracture Toughness Testing, ASTM STP 381, ASTM, 1965.

61. Crussard, C., Plateau, J., Tamhankar, R., Henry, G. and Lajeunesse, D., "A Comparison of Ductile and Fatigue Fractures," in Fracture, Averback, B. L., Felbeck, D. K., Hahn, G. T. and Thomas, D. A., Editors, J. Wiley and Sons, 1959.

62. ASTM X-Ray Powder Data File Card Number 12-284, Fe_2SiO_4, Iron Silicate.

63. ASTM X-Ray Powder Data File Card Number 7-346, SiO_2, Silicon Dioxide, Beta Quartz.

64. Culity, B. D., Elements of X-Ray Diffraction, Addison-Wesley, 1959.

65. Chalmers, B., Principles of Solidification, John Wiley & Sons, 1964.

66. Johnson, H. H., Morlet, J. G. and Troiano, A. R., "Hydrogen, Crack Initiation and Delayed Failure in Steel," Transactions of the AIME, Volume 215, August, 1958, pp 528 to 536.

67. Fletcher, E. E. and Elsea, A. R., "Hydrogen Induced, Delayed Brittle Fracture of High Strength Steel," DMIC Report 196, January 20, 1964, Battelle Memorial Institute.

68. Travis, R. E., Barry, J. M., Moffatt, W. G. and Adams Jr., C. M., "Weld Cracking Under Hindered Contraction: Comparison of Welding Processes," Welding Journal, Volume 43, November, 1964, pp 504-s to 513-s.

69. Smith, N. and Bagnall, B. I., "The Influence of Sulphur on Heat-Affected Zone Cracking of Carbon-Manganese Steel Welds," British Welding Journal, Volume 15, February, 1968, pp 63 to 69.

70. Fletcher, E. E. and Elsea, A. R., "Hydrogen Movement in Steel-Entry, Diffusion and Elimination," DMIC Report 219, June 30, 1965, Battelle Memorial Institute.

Vita

Robert Quattrone, one of two sons of Mr. and Mrs. Nicholas Quattrone, was born on March 31, 1940, in Bronx, New York. He attended grammer school in the Bronx, and junior and senior high school in Hicksville, Long Island, New York, graduating in 1957. Mr. Quattrone attended the Polytechnic Institute of Brooklyn on the Naval Applied Science Laboratory's Co-op Student Trainee Program, graduating in 1962 with the degree of Bachelor of Metallurgical Engineering and soon afterward marrying the former Miss Anita Mazzocchi. While an undergraduate, he was elected to the national honorary engineering fraternity, Tau Beta Pi and was a charter member of the New York Beta Section of the national honorary metallurgy fraternity, Alpha Sigma Mu. Working as a welding engineer in the Naval Applied Science Laboratory he earned the degree of Master of Science in Metallurgical Engineering on an evening program from the Polytechnic Institute of Brooklyn in 1966. It was during this time that his son, Scott, was born in 1963. Mr. Quattrone attended Lehigh University on a sabbatical during 1966-1967, completing his dissertation in abstentia. In 1967, he was elected to the Research Society of America. In 1969, he was appointed Chief of the Metallurgy Branch of the U.S. Army Construction Engineering Research Laboratory.